

**ION/ION REACTION FACILITATED MASS SPECTROMETRY AND
FRONT-END METHOD DEVELOPMENT**

by
Nan Wang

A Dissertation

*Submitted to the Faculty of Purdue University
In Partial Fulfillment of the Requirements for the degree of*

Doctor of Philosophy



Department of Chemistry
West Lafayette, Indiana
May 2019

**THE PURDUE UNIVERSITY GRADUATE SCHOOL
STATEMENT OF COMMITTEE APPROVAL**

Dr. Scott A. McLuckey, Chair

Department of Chemistry

Dr. Hilikka I. Kenttämää

Department of Chemistry

Dr. Garth J. Simpson

Department of Chemistry

Dr. Peter T. Kissinger

Department of Chemistry

Approved by:

Dr. Christine A. Hrycyna

Head of the Graduate Program

*To my family and friends
Thank you for all your love and support*

ACKNOWLEDGMENTS

In my graduate years, I would like to thank so many people who have guided and supported me along the way. First and foremost, I would like to thank my advisor, Scott McLuckey. Thank you for your invaluable help and guidance that support me through the graduate years. You are not only a great research advisor, who has so many ideas for the students to test on and who gives valuable suggestions when the projects got stuck. You also taught me on a variety of non-research-related aspects with your actions, such as communication skills, diligence and hardworking, more encouragement and less criticism towards other people, regular exercise, self-discipline, and lab management with the right amount of freedom and encouragement to let each lab member grow.

I would also like to express my gratitude toward my lab mates. To my mentors, Christine Fisher, Josh Gilbert, Alice Pilo, Jiexun Bu, and Chunfen Jin, thank you for sharing your knowledge and experiences with me, and guiding me through my early years in the lab. It was great fun talking about research and life with you. To Zhou Peng, Stella Betancourt, Eric Dziekonski, Corinne Demuth, Andrew DeBlase, Nicole Redwine, and Carl Luongo, thank you for all your help – big and small – and those interesting small talks we had on topics besides research. To Feifei Zhao and Mack Shih, I'm very lucky to join the group with you two and thank you for all the precious days we had. To David Foreman, Josh Johnson, Chris Harrilal, Kenny Lee, Caitlin Randolph, Anthony Pitts-McCoy, John Lawler, Elissia Franklin, Sarju Adhikari, Hsi-Chun Chao, Abdirahman Abdillahi, Jay Bhanot, De'Shavon Shenault and Ian Carrick, I've learnt a lot from you guys and it's a great pleasure to discuss all kinds of stuff with you along with research.

To Jim Hager, Larry Campbell and Frank Londry, thank you for being such great collaborators at SCIEX and gave us tremendous help on instrument maintenance and experiment

guidance. I learnt a lot from you, not only the knowledge related to mass spectrometry, but also the qualities of expertise, patience and clear communications in each one of you.

To my friends Zhengtian Song, Yiyang Zhou, Zhe Li, Mingzhe Li, Jiawen Yu, Jing Yang, Changqin Ding, Siyu Wu, Fengyuan Deng, Shijie Zhang, Yun Yang, and many others, it's been great to have known you and experience new things together with you.

Finally, I'd like to thank my parents and my husband for all your support. Even though physically we are so far apart, you are always by my side.

TABLE OF CONTENTS

LIST OF FIGURES	10
LIST OF SCHEMES.....	14
LIST OF TABLES	15
LIST OF ABBREVIATIONS.....	16
ABSTRACT.....	18
CHAPTER 1. INTRODUCTION	21
1.1 Mass Spectrometry.....	21
1.1.1 Principles	22
1.1.2 Ion Source: Electrospray Ionization (ESI).....	23
1.1.2.1 ESI Source Setup	24
1.1.2.2 Mechanism.....	24
1.1.2.2.1 Ion Evaporation Model (IEM).....	26
1.1.2.2.2 Charge Residue Model (CRM)	26
1.1.2.2.3 Chain Ejection Model (CEM)	27
1.1.3 Mass Analyzer: Quadrupole and Linear Quadrupole Ion Trap (LQIT)	28
1.1.4 Mass Analyzer: Time of Flight (TOF).....	30
1.2 Tandem Mass Spectrometry	31
1.2.1 Collision Induced Dissociation (CID)	32
1.2.1.1 In-Trap Resonant Collision Induced Dissociation.....	33
1.2.1.2 Dipolar Direct Current (DDC) Collision Induced Dissociation (CID).....	34
1.2.1.3 Beam-Type Collision Induced Dissociation.....	35
1.2.2 Ultraviolet Photodissociation (UVPD).....	36
1.2.3 Peptide and Protein Fragmentation.....	36
1.3 Ion/Ion Reactions in Gas Phase	37
1.3.1 Instrumentation for Ion/Ion Reaction	39
1.3.2 Thermodynamics and Kinetics of Ion/Ion Reactions	40
1.3.3 Charge Transfer Reactions	42
1.3.4 Gas-Phase Covalent Modification Reactions	42
1.4 Ion Mobility: Differential Mobility Spectrometry (DMS).....	43

1.4.1	Configuration of the DMS Interface.....	44
1.4.2	Separation Mechanism.....	45
1.4.3	Effect of Modifier in Analyte Separation	46
1.5	Conclusions.....	47
1.6	References.....	48
CHAPTER 2. GAS-PHASE REARRANGEMENT REACTION OF SCHIFF-BASE-MODIFIED PEPTIDE IONS.....		67
2.1	Introduction.....	67
2.2	Experimental.....	69
2.2.1	Materials.....	69
2.2.2	Mass Spectrometry.....	69
2.3	Results and Discussion	70
2.3.1	Novel Fragmentation Pathway from Schiff-Base-Modified Lysine-Containing Peptides.....	70
2.3.2	Proposed Reaction and Mechanism.....	73
2.3.3	Reactivity of Histidine- or Arginine-Containing Schiff-Base-Modified Peptides. ...	75
2.4	Conclusions.....	78
2.5	References.....	79
CHAPTER 3. DISTINCTION OF NON-SPECIFIC AGGREGATION IN ESI FROM SOLUTION-PHASE AGGREGATION: THEORETICAL CONSIDERATIONS		95
3.1	Introduction.....	95
3.2	Experimental.....	97
3.2.1	Materials	97
3.2.2	Mass Spectrometry	97
3.2.3	Data Analysis.....	98
3.2.4	MATLAB Simulations	98
3.2.4.1	Droplet Size Distribution.....	98
3.2.4.2	Concentration Error	99
3.2.4.3	Aggregation in Droplet-Size-Measurement Solution	99
3.3	Results and Discussion	100
3.3.1	Issue of Droplet-Induced Non-specific Aggregation in ESI-MS	100

3.3.2	Theory for Model.....	100
3.3.2.1	Poisson Statistics and Its Relationship with ESI Process	100
3.3.2.2	Qualitative Application of Poisson Statistics to Aggregation Detection.....	101
3.3.2.3	Quantitative Application of Poisson Statistics to Aggregation Detection.....	102
3.3.3	Factors that Affect Droplet Size Determination (MATLAB Simulations)	104
3.3.3.1	Droplet Size Distribution.....	104
3.3.3.2	Concentration Error	105
3.3.3.3	Aggregation in the Droplet-Size-Measurement Solution	107
3.4	Conclusions.....	108
3.5	References.....	109
CHAPTER 4. EARLY DETECTION OF SOLUTION-PHASE AGGREGATION OF SMALL PEPTIDES AND PROTEINS.....		121
4.1	Introduction.....	121
4.2	Experimental.....	122
4.2.1	Materials	122
4.2.2	Mass Spectrometry	123
4.2.3	Data Analysis.....	123
4.2.4	Mass Spectrum Overlap Correction.....	124
4.2.5	Size-Exclusion Chromatography (SEC) Protocol	125
4.2.6	Insulin Stress Conditions	125
4.3	Results and Discussion	125
4.3.1	Peak Overlap Reduced or Eliminated by Ion/Ion Reaction.....	125
4.3.2	Differentiation between Solution-Phase and Droplet-Induced Aggregation.....	126
4.3.2.1	Non-Specific Aggregation in ESI-MS.....	126
4.3.2.2	Poisson-Statistics Based Model to Analyze Solution-Phase Aggregation	127
4.3.2.3	Experimental Droplet Size Determination	128
4.3.2.4	Application of Model on Stressed Insulin System	129
4.3.2.5	Application of Model on Concentration Recovery from ESI-MS Spectra.....	131
4.4	Conclusions.....	132
4.5	References.....	134

CHAPTER 5. FACILITATED ISOMER DETECTION WITH DIFFERENTIAL MOBILITY SPECTROSCOPY AND ION-ION REACTION.....	141
5.1 Introduction.....	141
5.2 Experimental.....	144
5.2.1 Materials	144
5.2.2 Mass Spectrometry	144
5.3 Results and Discussion	145
5.3.1 Setup of DMS-Ion/Ion Scan Function	145
5.3.2 Application of 1D DMS-Ion/Ion Method to a Model Peptide Isomer System.....	148
5.3.2.1 Exploration on Isomer Identification by CID Only	148
5.3.2.2 Exploration on Isomer Identification by Ion/Ion Reaction.....	150
5.3.2.3 Exploration on Isomer Identification with DMS Only	151
5.3.2.4 Exploration on Isomer Identification with 1D DMS-Ion/Ion.....	152
5.3.3 Application of 1.5D DMS-Ion/Ion Method to a Peptide Mixture System	153
5.4 Conclusions.....	155
5.5 References.....	157
PUBLICATION.....	166

LIST OF FIGURES

- Figure 1.1 Cartoon schematics for different ESI setups. (a) conventional ESI, (b) ESI with auxiliary gas and heat, (c) nano-electrospray ionization (nESI), (d) inductive nESI. The abbreviation “+kV” is short for “positive kilovolts”. “GND” is abbreviated for “Ground”. 60
- Figure 1.2 Schematic drawings for the general process and the three main models for ionization mechanism in ESI. (a) General fissioning process of ESI charged droplet; (b) Ion Evaporation Model (IEM); (c) Charge Residue Model (CRM); (d) Chain Ejection Model (CEM). The circle is the droplet; the pink filled circle or chain is the analyte; the plus signs are the positive charges. 61
- Figure 1.3 Schematics for quadrupole and quadrupole ion trap. (a) Cartoon of quadrupole. (b) Mathieu stability diagram, with the darker shade meaning more unstable region of the ions. (c) Cartoon of the 2D quadrupole ion trap. 62
- Figure 1.4 Nomenclature of common peptide backbone cleavages and structures of their corresponding fragment ions. 63
- Figure 1.5 Instrument schematics for the ion/ion reactions in the dissertation. (a) QTRAP 4000 (SCIEX, Concord, Canada), modified for ion/ion reactions. (b) TripleTOF 5600 (SCIEX, Concord, Canada), modified for ion/ion reactions. 64
- Figure 1.6 Generic energy diagram for (a) ion/ion proton transfer reaction and (b) ion/molecule proton transfer reaction. 65
- Figure 1.7 Schematic for (a) DMS setup with detailed gas flow, (b) DMS mechanism explanation, and (c) three general shapes of alpha curves. OR is short for orifice. SV is abbreviated for Separation Voltage. CV is abbreviated for Compensation Voltage. 66
- Figure 2.1 Spectra illustrating the gas-phase Schiff base modification of KAKAKAA with FBDSA and its special fragmentation pathway. Positive mode (a) ion/ion reaction between doubly protonated peptide cation $[M+2H]^{2+}$ and singly deprotonated FBDSA $[FBDSA-H]^{-}$, (b) CID of the ion/ion complex $[M+FBDSA+H]^{+}$ forming a Schiff-base-modified peptide $[M+H+\blacklozenge]^{+}$, (c) Ion-trap CID of $[M+H+\blacklozenge]^{+}$. Negative mode (d) ion/ion reaction between singly protonated peptide cation $[M+H]^{+}$ and doubly deprotonated FBDSA $[FBDSA-2H]^{2-}$, (e) CID of the ion/ion complex $[M+FBDSA-H]^{-}$ forming a Schiff-base-modified peptide $[M-H+\blacklozenge]^{-}$, (f) ion-trap CID of $[M-H+\blacklozenge]^{-}$. Degree symbols ($^{\circ}$) denote water losses (-18 Da). Asterisks (*) denote ammonia losses (-17 Da). Solid diamonds (\blacklozenge) denote ion mass shift with Schiff base modification (+248 Da). Hollow diamonds (\blacklozenge) denote the special fragmentation products (-19 Da) and all products in the special fragmentation pathway are labeled in red. 82

Figure 2.2 Spectra illustrating the gas-phase Schiff base modification and rearrangement reaction of KAKAKAA with FBMSA ((a) and (b)) and KGAGGKGAGGKL with FBDSA ((c) and (d)). KAKAKAA and FBMSA in positive mode: (a) ion/ion reaction between doubly protonated KAKAKAA, $[M+2H]^{2+}$, and singly deprotonated FBMSA $[FBMSA-H]^-$, (b) Ion trap CID of the Schiff-base-modified peptide $[M+H+\blacklozenge]^+$. KGAGGKGAGGKL and FBDSA in both modes: ion trap CID of (c) the Schiff-base-modified peptide $[M+H+\blacklozenge]^+$ in positive mode and (d) the Schiff-base-modified peptide $[M-H+\blacklozenge]^-$ in negative mode. Degree symbols ($^{\circ}$) denote water losses (-18 Da). Asterisks (*) denote ammonia losses (-17 Da). Solid diamonds (\blacklozenge) denote ion mass shift with Schiff base ($\blacklozenge=+168$ Da for FBMSA, $\blacklozenge=+248$ Da for FBDSA). Hollow diamonds (\diamond) denote peptide rearrangement products (-19 Da) and all products in rearrangement pathway are labeled in red. 83

Figure 2.3 Ion trap activation of the ions generated via rearrangement for Schiff-base-modified KAKAKAA and KGAGGKGAGGKL, including (a) $[M+H+\diamond]^+$ generated from CID of Schiff-base-modified KAKAKAA cation $[M+FBDSA+H-H_2O]^+$, (b) $[M+H+\diamond]^+$ generated from CID of Schiff-base-modified KAKAKAA cation $[M+FBMSA+H-H_2O]^+$, (c) $[NL-H]^-$ generated from CID of Schiff-base-modified KAKAKAA anion $[M+FBDSA-H-H_2O]^-$, (d) $[M+H+\diamond]^+$ generated from CID of Schiff-base-modified KGAGGKGAGGKL cation $[M+FBDSA+H-H_2O]^+$, and (e) $[M-H+\diamond]^-$ generated from CID of Schiff-base-modified KGAGGKGAGGKL anion $[M+FBDSA-H-H_2O]^-$ (spectrum y-axis zoomed in 10 times to reduce the noise peak). Degree symbols ($^{\circ}$) denote water losses (-18 Da). Asterisks (*) denote ammonia losses (-17 Da). Hollow diamonds (\diamond) denote peptide rearrangement products (-19 Da) and all products in rearrangement pathway are labeled in red. The peak labeled with an orange solid circle (581 Da) is proposed to be a ring cleavage fragment (proposed structure in Scheme 2.7). 84

Figure 2.4 Ion trap CID of the gas-phase Schiff-base-modified peptide ions formed using deprotonated FBDSA and doubly protonated AKAAAKA. Degree symbols ($^{\circ}$) denote water losses (-18 Da). Black solid diamonds (\blacklozenge) denote ions with Schiff base modification (+248 Da). Hollow diamonds (\diamond) denote peptide rearrangement products (-19 Da) and all rearrangement products are labeled in red. 85

Figure 2.5 Ion trap CID of the gas-phase Schiff-base-modified peptides formed using (a) singly deprotonated FBDSA and doubly protonated RARARAA, (b) doubly deprotonated FBDSA and singly protonated RARARAA, (c) singly deprotonated FBDSA and doubly protonated HAHAHAA, and (d) doubly deprotonated FBDSA and singly protonated HAHAHAA. Degree symbols ($^{\circ}$) denote water losses (-18 Da). Asterisks (*) denote ammonia losses (-17 Da). Black solid diamonds (\blacklozenge) denote ions with Schiff base modification (+248 Da). Solid squares (\blacksquare) denote the arginine side chain methanediimine ($H_2N=C=NH_2$) losses to form ornithine (-42Da). Solid hearts (\heartsuit) denote carbon dioxide losses (-44 Da). Hollow diamonds (\diamond) denote peptide rearrangement products (-19 Da) with the formation of the AMBDSA neutral loss. Solid spades (\spadesuit) denote histidine-specific rearrangement products (-82 Da) with the formation of the 330 Da neutral loss. All rearrangement related products are labeled in red. 86

- Figure 2.6 Ion trap CID of the gas-phase Schiff-base-modified peptide ions formed using deprotonated FBDSA and doubly protonated AHAAAHA. Degree symbols ($^{\circ}$) denote water losses (-18 Da). Asterisks (*) denote ammonia losses (-17 Da). Black solid diamonds (\blacklozenge) denote ions with Schiff base modification ($+248$ Da). Hollow diamonds (\lozenge) denote peptide rearrangement products (-19 Da) and all rearrangement products are labeled in red. The water losses in parentheses denote that the peaks could be assigned both ways and it is not determined which one is the more accurate assignment. 87
- Figure 3.1 Mass spectrum of $5 \mu\text{M}$ insulin in an aqueous solvent with $20 \mu\text{M}$ $\text{Zn}(\text{OAc})_2$, $10 \mu\text{M}$ NH_4Cl , 5 mM phenol and 300 mM NH_4OAc adjusted to a pH of 7.4 to show the non-Poisson distribution of monomer, dimer and hexamer. The inset is a zoomed-in mass spectrum for the m/z range of $1500 - 4000$ to show that no intermediate oligomer sizes (i.e., trimer, tetramer or pentamer) were observed on the spectrum. 112
- Figure 3.2 Poisson distributions at different μ values. 113
- Figure 3.3 The relationship between the spread of droplet size distribution and the error of the calculated diameter. μG denotes the average droplet diameter for the Gaussian distribution of droplet size. $(d_0 - \mu G)$ denotes the error of the calculated diameter from the true average droplet diameter. σG refers to the standard deviation of the Gaussian droplet diameter distribution. 114
- Figure 3.4. Relationship between relative error of concentration ($errc\%$) and that of droplet diameter measurement ($errd\%$). The curve was plotted from Equation 3.8. 115
- Figure 3.5 Simulated measured droplet diameter when 1% and 10% monomers aggregated into (a) dimers or (b) trimers. The analytical concentration of the solution is $1000\mu\text{M}$, $500\mu\text{M}$ and $100\mu\text{M}$ respectively. The measured droplet sizes with the same monomer concentration error but no aggregation are listed on the left to show how aggregation-caused concentration change affects the measured droplet size. 116
- Figure 4.1 Zoomed-in mass spectrum of $196 \mu\text{M}$ insulin solution. The region in blue shading has overlap peaks of 1^{3+} (oligomer size^{charge}) and 2^{6+} , with the non-overlap isotopic peaks of 2^{6+} labelled in number. The region in yellow shading has 2^{6+} adduct peaks only. 136
- Figure 4.2 Comparison between mass spectra before and after ion-ion reaction. (a) mass spectrum of peptide NNQQNY not subjected to ion-ion reaction with PFO, with the peak assignment labeled as (oligomer size)^{charge}; (b) zoomed-in mass spectrum of the shaded labeled peak in spectrum (a) to show how overlap peaks are assigned based on isotope spacing; (c) mass spectrum of peptide NNQQNY subjected to ion-ion reaction with PFO, with an inset showing the zoomed-in spectrum for m/z range 5000 to 15000 137

- Figure 4.3 SEC separation of 3.4 mg/mL insulin in mobile phase and its corresponding MS spectra of the SEC fractions. (a) SEC separation of insulin (zoomed-out). (b) Zoomed-in SEC chromatogram highlighting the main insulin fraction at 17.8 min and the small covalent insulin dimer fraction at 16.2 min. (c) MS spectrum of the 17.8-min fraction, with only monomers at different charge states observed. (d) MS spectrum of the 16.2-min fraction, with a tiny peak of covalent dimer (2^{6+} -NH₃) observed. (e) Zoomed-in spectrum of the monomer at 3+ charge state from spectrum (c). (f) Zoomed-in spectrum of the covalent dimer at 6+ charge state from spectrum (d), with the peak position of the noncovalent insulin dimer labeled by the red dash line. 138
- Figure 5.1 CID on $[M+2H]^{2+}$ and $[M+H]^+$ of K(AG)₄K and KAGK(AG)₃. Top: K(AG)₄K; Bottom: KAGK(AG)₃; Left: CID of $[M+2H]^{2+}$; Right: CID of $[M+H]^+$. The red dot labels the unique peaks that distinguish the two peptides..... 160
- Figure 5.2 CID spectra of FBDSA-modified (a) K(AG)₄K and (b) KAGK(AG)₃. Degree symbols (°) denote water losses (-18 Da). Asterisks (*) denote ammonia losses (-17 Da). Solid diamonds (◆) denote ion mass shift with Schiff base modification (+248 Da) and all Schiff-base modified ions are labeled in blue. Hollow diamonds (◇) denote the rearrangement products (-19 Da) and all products in the Schiff base rearrangement pathway are labeled in green. The red dot labels the unique peaks that distinguish the two peptides. 161
- Figure 5.3 Compensation Voltage (CV) of $[M+2H]^{2+}$ ion in a DMS CV scan. Solution: a) K(AG)₄K, b) KAGK(AG)₃, and c) mixture of the two peptides. 162
- Figure 5.4 CID on Schiff bases formed by K(AG)₄K and KAGK(AG)₃ with FBDSA. a) K(AG)₄K, CV=20.3V. b) KAGK(AG)₃, CV=27.7V. c) Mixture, CV=20.0. d) Mixture, CV=28.0. Degree symbols (°) denote water losses (-18 Da). Solid diamonds (◆) denote ion mass shift with Schiff base modification (+248 Da) and all Schiff-base modified ions are labeled in blue. Hollow diamonds (◇) denote the rearrangement products (-19 Da) and all products in the Schiff base rearrangement pathway are labeled in green. The red dot labels the unique peaks that distinguish the two peptides..... 163
- Figure 5.5 The application of 1.5D DMS-Ion/Ion method on the peptide mixture of ARAAKA, AHAAHA, GRGMGRGMGRL, and K(AG)₄K. (a) Averaged mass Spectrum of direct spray of the peptide mixture with a DMS CV ramp of -5V to 35V. (b) Extracted CV ionograms of the doubly protonated peptides, with their corresponding climax CV voltage labeled with the same color coding as the legend in panel (a). (c) Mass spectrum of the periodate ion with a DMS CV ramp of -25V to 5V. (d) Extracted CV ionogram of the periodate ion. (e)-(h) Post-ion/ion and DDC-CID (35V DDC) mass spectra at the respective climax CV voltage for each analyte peptide ion, with their climax CV voltages labeled using the same color coding as the legend in panel (a). All the DMS experiments are done with an SV setting of 4000V and at a DMS temperature of 150°C. The x-axis of DMS CV ionograms are shown in time (min) due to the software limitation of recording CV voltages in the DMS-Ion/Ion mode, but the CV voltages can be converted from the time using the CV voltage ramp range. 164

LIST OF SCHEMES

- Scheme 2.1 Reactions for Schiff base modification and fragmentation in (a) positive mode and (b) negative mode with FBDSA as an example. (c) Structures of Schiff base modification reagents (FBDSA, FBMSA) and proposed neutral loss structures (AMBDSA and AMBMSA). Solid diamonds (\blacklozenge) denote ion mass shift with Schiff base modification (+248 Da for FBDSA). Hollow diamonds (\blacklozenge) denote the mass shift of the special fragmentation products (-19 Da). 88
- Scheme 2.2 Proposed mechanisms for the formation of the 249 Da peak from the fragmentation of the neutral losses, or from the fragmentation of the Schiff-base-modified peptide itself. N-terminal Schiff base modification was shown here as an example. 89
- Scheme 2.3 Proposed mechanism for the rearrangement of the lysine-containing Schiff-base-modified peptides between an amino group and (a) a neutral imine group, or (b) a protonated imine group. N-terminal lysine residue is used here as an example. 90
- Scheme 2.4 Proposed mechanism for rearrangement reaction of arginine-containing Schiff-base-modified peptides between an imine group and a) a neutral guanidine group or b) a protonated guanidinium group. N-terminal arginine residue is used here as an example. 91
- Scheme 2.5 Proposed mechanism for rearrangement reaction of histidine-containing Schiff-base-modified peptides between an imine group and a neutral imidazole group. N-terminal histidine residue is used here as an example. 92
- Scheme 2.6 Proposed mechanism for rearrangement reaction of Schiff-base-modified peptides between an amide group and (a) an imine group, or (b) a protonated imine group. Imine formed on the N-terminus is used here as an example. 93
- Scheme 2.7 Proposed cleavage site of the rearrangement peptide product to form the orange dot labeled ambiguous peak in Figure 2.3. The top part with the negative charge would be the peak with 581 Da mass and one negative charge. 94
- Scheme 3.1 A demonstration of solution-phase aggregation and droplet-induced aggregation. Each black dot in the scheme denotes one analyte molecule. The charges on the droplet or the analytes are not drawn for simplicity. 117
- Scheme 3.2 Flow chart of the quantitative approach of solution-phase aggregation detection. μ and c are the average number of analytes per droplet and the analyte concentration (no subscript: non-aggregating solution; subscript s: sample solution). V_{drop} is the droplet volume for the ESI-MS method. 118

LIST OF TABLES

Table 3.1 List of symbols and abbreviations and their definitions	119
Table 4.1 Droplet size measurement results summary for insulin and glucagon	139
Table 4.2 List of symbols and abbreviations and their definitions	140
Table 5.1 Fragment ion mass of $KAGK(AG)_3$ and $K(AG)_4K$	165

LIST OF ABBREVIATIONS

AC	Alternating Current
AFM	Atomic Force Microscopy
AMBDSA	4-(Aminomethyl)benzene-1,3-Disulfonic Acid
AMBMSA	2-(Aminomethyl)benzene(mono)sulfonic Acid
CID	Collision Induced Dissociation
CRM	Charge Residue Model
CEM	Chain Ejection Model
CV	Compensation Voltage
DC	Direct Current
DDC	Dipolar Direct Current
DMS	Differential Mobility Spectrometry
DTIMS	Drift Tube Ion Mobility Spectrometry
ECD	Electron Capture Dissociation
ESI	Electrospray Ionization
ETD	Electron Transfer Dissociation
FAIMS	High Field Asymmetric Waveform Ion Mobility Spectrometry
FBDSA	4-Formyl-1,3-Benzenedisulfonic Acid
FBMSA	2-Formyl-Benzene(mono)sulfonic Acid
GC	Gas Chromatography
HPLC	High Pressure Liquid Chromatography
IEM	Ion Evaporation Model
IMS	Ion Mobility Spectrometry

IRMPD	Infrared Multiphoton Photodissociation
IVR	Intramolecular Vibrational Energy Redistribution
LC	Liquid Chromatography
LQIT	Linear Quadrupole Ion Trap
MALDI	Matrix Assisted Laser Desorption Ionization
MS	Mass Spectrometry
MS/MS	Tandem Mass Spectrometry
MS ⁿ	N-Stage Tandem Mass Spectrometry
MSAE	Mass-Selective Axial ejection
nESI	Nanoelectrospray Ionization
NHS	N-Hydroxysuccinimide
NL	Neutral Loss
PFO	2,2,3,3,4,4,5,5,6,6,7,7,8,8,8-Pentadecafluoro-1-Octanol
RF	Radio Frequency
SEC	Size Exclusion Chromatography
SV	Separation Voltage
TEM	Transmission Electron Microscopy
TIMS	Trapped Ion Mobility Spectrometry
TOF	Time-of-Flight
TWIMS	Travelling Wave Ion Mobility Spectrometry
UV	Ultraviolet
UVPD	Ultraviolet Photodissociation

ABSTRACT

Author: Wang, Nan. PhD

Institution: Purdue University

Degree Received: May 2019

Title: Ion/Ion Reaction Facilitated Mass Spectrometry and Front-End Method Development

Committee Chair: Scott McLuckey

Mass spectrometry is a versatile analytical tool for chemical and biomolecule identification, quantitation, and structural analysis. Tandem mass spectrometry further expands the applications of mass spectrometry, making it more than a mere detector. With tandem mass spectrometry, the mass spectrometer is capable of probing reaction mechanisms, monitoring reaction processes, and performing fast analysis on complex samples. In tandem mass spectrometry, after activation the precursor ions fragment into small fragment ions through one or more pathways, which are affected by the ion's inherent property, the ion type, and the activation method. To obtain complementary information, one can alter the fragmentation pathway by changing the ion via ion charge manipulation and covalent modification to the ion. Gas-phase ion/ion reactions provide an easy approach to changing ion type and facile modification to the analyte ions. It has been extensively used for spectrum simplification and analyte structural studies. In this dissertation, ion/ion reaction facilitated mass spectrometry methods are studied, and explorations into the method development involving front-end mass spectrometer are discussed.

The first work demonstrates a special rearrangement reaction for gas-phase Schiff-base-modified peptides. Gas-phase Schiff-base modification of peptides has been applied to facilitate the primary structural characterization via tandem mass spectrometry. A major or minor fragment pathway related to the novel rearrangement reaction was observed upon in-trap collisional activation of the gas-phase Schiff-base-modified peptides. The rearrangement reaction involves

the imine of the Schiff base and a nucleophile present in the polypeptide. The occurrence of the rearrangement reaction is affected by several factors, such as ion polarity, identity of the nucleophile in the peptide (e.g., side chains of lysine, histidine, and arginine), and the position of the nucleophile relative to the imine. The rearrangement reaction does not affect the amount of structural information that can be obtained by collisional activation of the Schiff-base-modified peptide, but when the rearrangement reaction is dominant, it can siphon away signal from the structurally diagnostic processes.

Efforts have also been put into the method development of peptide and protein aggregation detection via electrospray ionization mass spectrometry (ESI-MS). People have studied peptide and protein aggregation processes to understand the mechanism of amyloid-related diseases and to control the quality of the peptide and protein pharmaceuticals. ESI-MS is suitable for solution aggregation studies because of its compatibility with solution samples and the straightforward result of the analyte's oligomeric state on the mass spectrum. However, peak overlap issue and nonspecific aggregation in the ESI process can obscure the result. Here, the application of proton transfer ion/ion reaction to the analyte has been found useful to reduce or eliminate the peak overlap issue. A statistical model based on Poisson statistics has been proposed to deal with the ESI-induced nonspecific aggregation in the droplet and to differentiate the solution-phase aggregation from the droplet-induced aggregation. Factors that affect the accuracy of the statistical model have been discussed with MATLAB simulations.

In the era of biological system studies, sample complexity is a challenge every analytical chemist has to face. The analysis of complex sample can be facilitated by the combination of separation techniques outside the mass spectrometer (such as differential mobility spectrometry (DMS)) and ion structure probing techniques inside the mass spectrometer (such as tandem mass

spectrometry and gas-phase ion/ion reactions). Here the coupling method between DMS and ion/ion reaction is developed and tested with model peptide systems to demonstrate its possible application in complex sample characterization such as isomer identification.

CHAPTER 1. INTRODUCTION

1.1 Mass Spectrometry

Nowadays the chemical identification and quantitation, which analytical chemistry mainly deals with, plays an important role in everyday life and scientific discoveries. [1, 2] Among all the analytical chemistry techniques, mass spectrometry stands out due to its merits of high sensitivity, low detection limit, fast analysis speed and diversity of its applications. [3, 4]

Since the first mass spectrometer, the cathode ray tube invented by J. J. Thomson in the 1897, [5] the instrumentation and application of mass spectrometry has evolved tremendously. While mass spectrometers were mostly used for small particle and small molecule analysis for almost a century, [6] the advent of new ionization methods like electrospray ionization (ESI) [7, 8] and matrix assisted laser desorption ionization (MALDI) [9] in the late 1980s has empowered mass spectrometers with a broader sample compatibility. At the moment the mass spectrometry has been applied more to large molecule detection and structural analysis, [10] especially biomolecules such as peptides and proteins, [11] carbohydrates, [12] oligosaccharides, [13] and even viruses. [14-16]

Another trend in the development of mass spectrometry is the coupling (or hyphenation) between mass spectrometry and other analytical techniques. [17] The advantage is obvious: by coupling two or more analytical techniques together, the functions of all the techniques coupled together are utilized at the same time and more complex samples can be analyzed. One example is the hyphenation between mass spectrometry and chromatography. In the early 1950s people first built gas chromatography – mass spectrometry (GC-MS) instruments. [18] Later as GC-MS was developed more, liquid chromatography – mass spectrometry (LC-MS) coupling started to arise. [19] In the beginning of the 21st century, LC-MS and GC-MS has become two mature analytical

methods widely used in the pharmaceutical, clinical, and environmental areas. [19] Another coupling example is between the ion mobility spectrometry (IMS) and mass spectrometry (MS). Unlike GC and LC, which separate analytes by their different fractionation in the stationary phase and the mobile phase, [19] IMS uses the different gas-phase ion mobility to separate the analytes. [20] Currently IMS-MS has been used a lot in the structural studies of large biomolecules. [21, 22]

1.1.1 Principles

Mass spectrometer is an analytical instrument that measures the mass-to-charge ratio (m/z) of ions. [4] It can be considered as a “molecular balance” because mass of the analyte molecule can be calculated from the m/z of the analyte ions detected by the mass spectrometer. [23]

Generally, mass spectrometers consist of three parts: an ion source that generates ions from the sample, a mass analyzer that measures the m/z of the ions, and a detection and data collection system that collects the mass spectrum. [24] The ion source determines what analytes can be ionized from the sample (e.g., small molecules with molecular weight less than 500, large molecules like proteins, etc.) and their ion type (e.g., singly protonated, doubly deprotonated, radical with one electron loss, etc.). [3] It also determines how efficiently the analytes are turned into ions, which is directly related to the sensitivity of the method. [25] The mass analyzer determines how accurately the m/z is measured (accuracy), the m/z range of the ions that can be detected (mass range), and how well different ions can be resolved (resolution). [26] Some analyzers can be used by itself or in sequence with other mass analyzers to achieve multiple stages of mass spectrometry (tandem mass spectrometry), where structural information of the analyte ions could be obtained through ion fragmentation. [3, 27-28] The detection and data collection system, though not discussed in detail in this dissertation, is very important since it is related to

several of the instrument's figures of merit, such as sensitivity, resolution and the speed of detection. [29]

There is a huge variety of ion sources, analyzers and detectors, [3] but only ion sources and analyzers related to this dissertation shall be introduced in detail to let the readers better understand the content of the dissertation.

1.1.2 Ion Source: Electrospray Ionization (ESI)

Electrospray Ionization (ESI) is an ionization method that generates ions from the solution. [3] The idea was proposed by Dole in 1968, [30] but it was first successfully established on mass spectrometers in the John Fenn group in 1984 [7] and four years later, when they presented results showing the application of ESI to large protein ionization on the ASMS annual conference, [8, 31] ESI was rapidly welcomed by the whole mass spectrometry world. [6] It is now widely used in biomolecule analysis, not only because it efficiently and softly generates ions directly from the solution, where most biomolecules exist in the nature, [32] but also due to its ability to generate multiply charged ions, which lowers the m/z range requirement of mass analyzers for the detection of high-mass biomolecules. [25] Furthermore, the analyte ion series with multiple charges on the spectrum help people to obtain an accurate molecular weight of the unknown analyte, either by solving the two unknown variables (charge z and molecular weight MW) from the multiple equations for the m/z ratios of the ion series, or by mass spectrum deconvolution. [33]

Even though the development of the ESI source went from solvated cations [7] and anions, [34] to small molecules and peptides, [35] to medium-size polymers, [36] and finally to large proteins, [8] when ESI first drew people's great attention in 1988, most people immediately recognize its value in large protein molecule ionization [37] and in online coupling interface of MS with other techniques such as capillary zone electrophoresis [38] and liquid chromatography.

[35] For now ESI has been applied to a lot of sample types [3] and to reaction monitoring. [39] It is also an important online HPLC/MS interface and is widely used in plenty of areas such as pharmaceutical quantitation [40] and clinical disease screening. [41]

1.1.2.1 ESI Source Setup

Electrospray is generally operated by applying a high voltage (a few kilovolts relative to the inlet of mass spectrometer) to the solution flowing through a capillary (Figure 1.1(a)). [3] One problem ESI could have is the difficulty in releasing the ions from the charged droplet. To assist the ion generation process, multiple modifications have been developed. For example, nebulizer gas [42] and heat [43, 44] has been applied to speed up the solvent evaporation process (Figure 1.1(b)). [45] Capillaries with smaller inner diameter (i.d.) have been utilized to generate smaller droplets, which helps in salt reduction and analyte ion release. [46] Compared to a typical ESI capillary i.d. of 100 μm , [47] the tip size has been further reduced with nano-electrospray ionization (nESI, Figure 1.1(c)), which uses μm to sub- μm tips to generate even smaller droplets. [48] The smaller droplets produced by nESI greatly increase the sensitivity for non-surface-active compounds such as oligosaccharides and glycoproteins. [48] Unlike conventional ESI, nESI normally doesn't require a back pressure on the sample to get a constant spray. [48] Another issue ESI may have is the electrochemical reaction (redox reaction) caused by the high voltage applied to the solution. To reduce the solution redox reactions, inductive nESI (Figure 1.1(d)) has been developed to induce electric field inside the borosilicate capillary to spray samples. [49, 50]

1.1.2.2 Mechanism

The description below is a widely accepted general explanation on how the droplets turn into ions (Figure 1.2(a)). [3, 25, 51-53] When a high electric field is applied to the sample solution in the ESI source, charges of the same polarity as the electric field will be driven to the tip of the

ESI capillary. As the charge accumulates, when the Coulomb repulsion exceeds the solution's surface tension, a Taylor cone would form and charged droplets are generated from the tip of the Taylor cone. Due to Coulomb repulsion, all the excess charge would spread on the surface of the droplet. The solvent of the charged droplets would be evaporated on its way to the mass spectrometer, which makes the charged droplets shrink in volume. As the volume decreases, the charge density on the surface increases, which makes the Coulomb repulsion on the surface increase to a point when it equals to the surface tension of the droplet. At this point, which is called the Rayleigh limit, the number z_R of charges on the droplet follows the equation below:

$$z_R = \frac{8\pi}{e} \sqrt{\varepsilon_0 \gamma R^3} \quad (1.1)$$

where e is the elementary charge, ε_0 is the vacuum permittivity, γ is the surface tension, and R is the droplet radius. [54, 55] To relieve the tension caused by the Coulomb repulsion, the charged droplet reduces its surface charge by either fissioning into smaller charged droplets, or ejection of the ions on the droplet surface. By repeating the evaporation / fission or evaporation / ejection process, ions are generated and finally enter the mass spectrometer.

Even though the general explanation on how the droplets turn into ions is widely accepted, however, in terms of the detailed ion release process, multiple theories have been proposed and supported by different experimental observations. Up to now, there are three main models for ionization mechanism of ESI (Figure 1.2(b)-(d) [56]): Ion Evaporation Model (IEM), [57] Charge Residue Model (CRM) [30, 58] and Chain Ejection Model (CEM). [59, 60] Although generally they apply to different scenarios, a lot of times it's hard to tell for sure by what mechanistic model the ions of interest are ionized. [56] Therefore, when explaining experimental results by ESI mechanisms, it's very important to consider the three models collectively.

1.1.2.2.1 Ion Evaporation Model (IEM)

Ion Evaporation Model (IEM, Figure 1.2(b)) was proposed by Iribarne and Thomson in 1976. [57] In the IEM, the ions are formed by evaporation from the droplet surface. That requires a large Coulomb repulsion on the droplet surface, which only exists for very small droplets. Generally, when the charged droplets are below 10 nm in diameter, the ion formation mechanism is considered to be IEM, and ion evaporation would happen before another Rayleigh fission occurs. Another important factor for the IEM mechanism is the size or molecular weight of the ions, as only solvated low mass ions (such as Na^+ and Cl^-) could be ejected from the surface.

Experimentally, Iribarne and Thomson found that the spray-produced ions must be singly charged small ions based on their mobility spectra and the diffusion coefficient, which supports the IEM picture of the evaporation of one charge surrounded by some solvent molecules. [57] They later used a mass spectrometer with an atmospheric pressure source to confirm that the ions are coming from the electrolyte sample droplets via IEM mechanism. [61] Besides, de la Mora group experimentally measured the charge and size of the solid residue after complete evaporation of the solvent in the electrospray process, whose results support the IEM theory. [62]

In summary, the IEM works well for small ions, but it does not apply to large molecules like proteins. For large molecules like proteins, the Charge Residue Model (CRM) is more suitable.

1.1.2.2.2 Charge Residue Model (CRM)

Charge Residue Model (CRM, Figure 1.2(c)) was first proposed by Dole in 1968. [30] In CRM, the analyte molecules stay in the droplet as the droplet go through the solvent evaporation and Rayleigh fission process. As the droplet fissions into smaller droplets, the analyte molecules are also distributed in the smaller droplets, resulting in one or a couple of analyte molecule(s) per small droplet depending on the analyte concentration. When all the solvent is evaporated, the

charges and the salt in the droplet condense onto the analyte and thus the analyte ion forms. It is widely accepted that large molecules go through the CRM mechanism, such as proteins with a molecular weight larger than 10 kDa. [63] Theoretically, the solvation energy of large globular molecules is so large that it's impossible for the large molecules to overcome the energy barrier and get evaporated from the droplet surface.

CRM has been supported by a lot of experimental evidence. According to CRM, the droplets should only fission near or at the Rayleigh limit, which means the charge state of the CRM-formed analyte ions should follow the Rayleigh limit equation (Equation 1.1). The speculation of the relationship between protein charge state and the theoretical charge state calculated from Rayleigh limit is confirmed by the data summary and analysis from the de la Mora group. [64] Moreover, theoretically large protein ions formed by CRM should have salt adduction, because all the salt in the final droplet should condense onto the analyte ion. Experimentally salt adduction is often observed on the mass spectrum for proteins using ESI-MS. [65] To reduce the salt adduction phenomenon, volatile salts such as ammonium acetate are favored in the ESI spray of large proteins. [66, 67]

1.1.2.2.3 Chain Ejection Model (CEM)

Chain Ejection Model (CEM, Figure 1.2(d)) was proposed by the Konermann group in 2012 based on the molecular dynamics simulations and experimental data. [59, 60] Like CRM this model also applies to large molecules, but unlike CRM where the analytes stay in the compact globular form, CEM mainly discuss about analytes that extend like a chain, such as linear polymers and unfolded proteins. In the CEM, to relieve the Coulomb repulsion in the droplet, the analyte unfolds and gets ejected as a chain full of charges from the droplet. Two driving forces may exist in the chain ejection process. Electrostatically, if we think of the droplet as a smooth sphere, the

ends of the chain-shaped analyte would serve as a sharp point on the surface, where charges are most likely to be concentrated and released. Another possible driving force for the chain ejection is the hydrophobicity of the exposed unfolded parts in the chain (like in the case of unfolded protein). The hydrophobic parts of the unfolded analyte can cause the analyte being repelled to the droplet surface, and the subsequent release of the unfolded analyte can be entropically favored.

Experimentally the CEM theory is supported by the striking signal difference between protein sprayed in the native condition (pH=7) and denatured condition (pH=2) [59] and the charge state distribution of the proteins under denatured condition. [60] The analogies between the CEM picture and the well-recognized charge partition in the dissociation of multiprotein assemblies back up the CEM theory as well. [56, 60]

1.1.3 Mass Analyzer: Quadrupole and Linear Quadrupole Ion Trap (LQIT)

Quadrupole and quadrupole ion traps are very important mass analyzers for the analysis of small to medium size molecules. The mass range of quadrupole can go up to a couple of thousands and it provides unit resolution. [3] Because of quadrupole's robustness, ease in manufacture process, and flexibility in tandem mass spectrometry, quadrupole is widely used in commercial instruments. [68, 69]

Quadrupole, as its name indicates, is composed of four rods (Figure 1.3(a)). The rods can be hyperbolic or circular in shape, but they have to be parallel. Two out-of-phase RF waveforms (and two opposite DC voltages if necessary) are applied to the two pairs of opposing rods to create a quadrupolar field. [3] By solving the ion motion equations for the quadrupole, a Mathieu stability diagram (Figure 1.3(b) [70]) can be plotted for the parameters a_u and q_u :

$$a_u = \frac{8zeU}{m\Omega^2 r_0^2} \quad (1.2)$$

$$q_u = \frac{4zeV}{m\Omega^2r_0^2} \quad (1.3)$$

where z is the number of charges, e is the elementary charge, U is the potential for the applied DC voltage, V is the zero-to-peak potential for the RF voltage, m is the mass of the ion, Ω is the driving RF frequency, and r_0 is the effective radius between electrodes. The ions would be stable in the quadrupole's u axis (u stands for x or y) if its calculated a_u and q_u values are within the stable region (unshaded region in Figure 1.3(b)). When two DC potentials with the same polarity as the ions are applied to the lenses on both ends of the quadrupole (L1 and L2 in Figure 1.3(c)), the quadrupole with the lenses is considered as a linear quadrupole ion trap (LQIT), because ions are trapped both in the x - y dimensions by the driving RF and in the z dimension by the two DC potentials. [71] Because 3D quadrupole ion trap [72] is not used in the projects in this dissertation, only the linear ion trap will be introduced here.

When doing mass analysis with LQIT, ions with different m/z ratios are ejected from the LQIT at different time to get detected by the detector. There are two common ways to eject the ions by moving the ions out of the stable region on the Mathieu stability diagram, which are frequently used in 3D quadrupole ion trap. [73] One way, called boundary ejection, is to simply ramp the driving RF amplitude V to make the q_u of each ion reach the instable region one by one across the boundary of the Mathieu stability diagram. The other way, called resonance ejection, is to have a supplemental AC waveform on the rods with the driving RF amplitude ramp. When the ion's secular frequency matches with the supplemental AC frequency, the ion would absorb the energy from the AC waveform, move with a large displacement from the center on the x - y dimensions, and get ejected in the end. With resonance ejection, the ions are being ejected faster and usually it leads to higher resolution due to faster ejection. As for the ion ejection from LQIT, two modes have been developed with resonance ejection: mass selective axial ejection (MSAE)

[74] and radial ejection. [71] In MSAE, AC waveforms are applied to the quadrupole rods and the exit lens, and ions close to the exit lens are ejected axially by the fringe field. In radial ejection, two slits are cut in two opposite rods, and the AC waveform applied onto the cut rods would eject the ions through the slits.

Quadrupole is also capable of ion isolation via ejecting out the ions of no interest, either by having a suitable RF-DC combination to push the a_u and q_u of the ion of interest to the climax of the Mathieu stability diagram, [70] or by resonance ejection of all the irrelevant ions. [75, 76] Ions could also be excited in the quadrupole by the supplemental AC waveform as described above, [73] which is why quadrupole is often used for ion activation and dissociation. The feature of ion isolation and activation in the quadrupole is very beneficial for tandem mass spectrometry.

1.1.4 Mass Analyzer: Time of Flight (TOF)

Time of flight (TOF) is a mass analyzer that has high speed, high resolution, great mass accuracy and theoretically no upper m/z limit. [77] It pulses the ions at the same time with the same voltage V to give the ions initial kinetic energy and measures the arrival time of each ion species at the detector. The relationship between the m/z of the ions and the arrival time t is

$$\frac{m}{z} = \left(\frac{2eV}{L^2} \right) t^2 \quad (1.4)$$

where m is the mass of the ion, z is the number of charges, e is the elementary charge, V is the pulsing voltage, L is the length of the TOF ion path. [78] Since a higher m/z of the ion leads to a lower initial velocity of the ion, and thus a longer arrival time (also see Equation 1.4), the large ions can be detected as long as the wait time is long enough and the detector is sensitive enough. The resolution of TOF is directly related to its ion traveling length L . Therefore, to elongate the ion traveling length for resolution purposes and to reduce instrument size at the same time,

different TOF geometries have been designed, including but not limited to straight tube, [78] V-shape geometry, [79] W-shape geometry [80] and multi-turn geometry. [81] In the curved TOF geometries, reflectrons are commonly used to reflect the ions along another direction without interfering with the ions' arrival time. [79, 80] Electrostatic sectors are another choice for building curved TOF geometries. [81, 82]

TOF is widely used in high mass ion detection, such as native mass spectrometry where large proteins are analyzed. [83] Typically, TOF has a much higher resolution than quadrupole, [77] so when the experiment requires the differentiation of isobaric ions or exact mass measurement, it's better to do it on a TOF instrument than a quadrupole mass spectrometer.

1.2 Tandem Mass Spectrometry

Tandem mass spectrometry (MS/MS, or MS^n , where n is the number of MS events) is developed to further study the structure of analytes. [84, 3] In the first stage MS, intact mass of the analyte ion is obtained. In the sequential n stages of MS, as the ions are fragmented in the mass spectrometer, the fragment ions would tell us the connections of different moieties in the molecule or complex, which can be used for structural analysis, analyte identification and quantification.

Usually the tandem mass spectrometry starts with an m/z scan of the sample, where the first stage MS spectrum is collected. Then the ion of interest is isolated, activated by the method of choice, and the product ions of the activation are detected to generate the second stage MS spectrum. Similarly, if the n^{th} stage of MS is performed, the ion of interest in the $(n-1)^{\text{th}}$ stage MS would be isolated, activated and its product ions being detected.

In a fragmentation event, the ion that's being fragmented is called the precursor ion, and the fragments are called product ions. The fragmentation pattern or pathway of the precursor ion is determined by three factors: the nature of the precursor ion, the form of the precursor ion, and

the activation method. [85] By nature, each molecule has its own strong bonds and weak bonds. The weak bonds are the places where fragmentation is more likely to happen. The same analyte with different ion types (e.g., protonated, deprotonated, metallated, radical) can have different fragmentation patterns, [85] because different charge types and locations would weaken different bonds and activate different pathways. The activation method changes how much, how fast and in what way the energy is input into the system, which determines the structure of the activated ion and its fragmentation pathway. Therefore, in order to probe the analyte structure comprehensively, people have utilized various methods to give complementary structural information, such as change of analyte chemical nature by chemical modification, [86] change of the ion type and number of charges, [87, 88] and change of the activation method. [89]

A large amount of activation methods has been developed, such as collision induced dissociation (CID), electron transfer dissociation (ETD) and electron capture dissociation (ECD), and photodissociation (ultraviolet photodissociation (UVPD) or infrared multiphoton photodissociation (IRMPD)). [85] CID will be discussed in detail in this section because of its extensive usage in this dissertation. A brief introduction of UVPD is also provided for the readers to better understand the material in the following chapters. Since most of the tandem mass spectrometry used in the following chapters are about peptides and proteins, the common fragmentation patterns of peptides and proteins are also explained.

1.2.1 Collision Induced Dissociation (CID)

Collision induced dissociation (CID) is currently the most common activation method. [3, 90] It is achieved by the collisions between accelerated analyte ions and neutral molecules. When the ions are having collisions with the neutrals, some of the translational energy is converted into internal energy, until eventually the internal energy reaches the energy barrier for complex

dissociation or bond breakage. [91] CID does not change ion type during the activation process. Based on how the analyte ions are accelerated, CID can be categorized into three types: in-trap resonance CID, dipolar direct current CID, and beam-type CID.

1.2.1.1 In-Trap Resonant Collision Induced Dissociation

In the in-trap resonant CID, ions are trapped in the ion trap, usually in an LQIT. An excitation AC waveform at a frequency in resonance with the ions of interest is applied to the apparatus. Since the frequency of the ion and the AC waveform are in resonance, ions would absorb the energy from the excitation AC waveform and move with larger displacement from the trap center. [92] The increased “RF-heating” with larger off-center displacement leads to more collisions between the ions and the neutrals, which eventually causes ion fragmentation. [93,94] Generally, in-trap resonance CID is a slow-heating process and the ion has time to redistribute the energy and change its conformation. [95]

To reach the resonant frequency, the frequency of the applied AC waveform should be the same as the ion motion secular frequency $\omega_{0,u}$, which is defined by Equation 1.5 in the case of dipolar excitation (which is more commonly used for in-trap resonant CID):

$$\omega_{0,u} = \frac{\beta_u \Omega}{2} \quad (1.5)$$

where β is a stability related parameter, u is the axis of interest, and Ω is the driving RF frequency. [72] Parameter β_u can be calculated from the Mathieu stability diagram parameters a_u and q_u , using the following approximation equation (for $q_u < 0.4$)

$$\beta_u \cong \sqrt{a_u + \frac{q_u^2}{2}} \quad (1.6)$$

For precise β_u calculation without approximation, the calculation equation for β_u is a continued fraction expression and can be found in the literature. [72, 96]

In-trap resonant CID is especially useful for fragmentation of a single ion species. because the frequency of the excitation AC waveform and the voltage of the driving RF are usually fixed, which can only excite ions of a certain m/z . This is also beneficial as the product ions are not excited with the precursor ion. Of course, there are ways that can do a broadband excitation with in-trap resonant CID, either by ramping the driving RF amplitude or by ramping the excitation AC waveform frequency, [97, 98] but they are not that frequently used compared to single ion excitation.

1.2.1.2 Dipolar Direct Current (DDC) Collision Induced Dissociation (CID)

Different from in-trap resonant CID, dipolar direct current (DDC) CID is usually a broadband excitation method. [99, 100] By applying a dipolar DC on the opposing rods of a quadrupole, the entire ion cloud in the quadrupole ion trap can feel the electric force from the dipolar DC field and is shifted off-center in the x-y plane of the trap. When the ions are off-center, they pick up the energy from the stronger RF field and higher order fields (if exist) inside the quadrupole ion trap and experience more RF heating there. Thus, more collisions between the ions and the neutrals in the trap are induced and finally result in ion fragmentation. DDC CID is still a slow-heating process, where ions can redistribute the energy obtained and change their conformation before their dissociation. [99-101]

When ions undergo DDC CID, their elevated temperature in a linear quadrupole ion trap is given by:

$$\Delta T_k = \frac{m_g \Omega^2 r_0^2}{24k_b} \left(\frac{V_{DDC}}{V_{RF}} \right)^2 \quad (1.7)$$

where m_g is the mass of the neutral, Ω is the drive RF frequency, r_0 is the effective radius between electrodes, k_b is the Boltzmann constant, V_{DDC} is the dipolar DC voltage, and the V_{RF} is the drive RF zero-to-peak amplitude. [100-102] From the equation we can see that when the instrument condition remains the same, a higher DDC voltage relative to the drive RF amplitude would lead to a higher elevated temperature.

The advantages of DDC CID are the broadband activation and its ease of use compared to in-trap resonant CID (no frequency calculation is required). It's very useful in cases where broadband activation is needed, such as the salt removal process by a little activation. [102] Recently the combination of DDC and electron transfer process has been developed to further dissociate the ETnoD products, which enhances the protein identification. However, this technique introduces a high-mass cutoff. Upon the application of DDC CID, the approximate average displacement r_e of the ion from the center of the LQIT is proportional to the m/z of the ion: [100, 102]

$$r_e = \frac{r_0^3 \Omega^2 m V_{DDC}}{4e z V_{RF}^2} \quad (1.8)$$

and the limit is reached when $r_e = r_0$. Therefore, to extend the high-mass cutoff from DDC, one should have a higher driving RF amplitude to decrease the r_e for the high m/z ions, and apply a higher DDC voltage to reach the same elevated temperature.

1.2.1.3 Beam-Type Collision Induced Dissociation

Beam-type CID is another broadband excitation method, which utilizes the potential difference between two MS elements. [103, 104] A high potential difference along the ion path speeds up the entire ion cloud and high-speed ions get fragmented by the collisions with neutrals. It is a transmission CID method and does not require the ions being trapped in the ion trap.

Compared to in-trap resonant CID and DDC CID, beam-type CID is the fastest activation and dissociation method among the three CID techniques. [105]

1.2.2 Ultraviolet Photodissociation (UVPD)

Photodissociation is a way to activate ions by the application of photons. When the energy of one photon or multiple photons matches with the energy difference between the ions' vibrational or electronic states, the ions would absorb the photon(s), gain energy, and release the energy by direct fragmentation, fragmentation after intramolecular vibrational energy redistribution (IVR), or other relaxation processes like fluorescence. [106-108]

Ultraviolet photodissociation (UVPD) specifically uses UV photons to fragment ions. Except for high-absorption density UV wavelengths such as 193 nm and 157 nm, UVPD usually requires the ions to have light-absorbing moieties or functionalities at the specific UV wavelength. [109] For example, at 266nm only tryptophan- and tyrosine-containing peptides exhibit some absorption, and at 355 nm chromophore is required to show any absorption. Since UV photons have a very high energy, UVPD events are usually single photon events. This makes the UVPD process very fast and gives no room for the excited ion to change its conformation. [106, 109] Therefore, UVPD is especially useful to probe analyte with its original conformation. The fragmentation pattern of UVPD is usually different from that of CID, so people often use UVPD as a complementary method to CID. [106-110]

1.2.3 Peptide and Protein Fragmentation

Tandem mass spectrometry has been extensively applied to peptide and protein analysis. For peptides, because their structure is comparably simple, direct sequence analysis can be done by tandem mass spectrometry. [111] For proteins, due to its complexity, three types of structural analysis have been developed: bottom-up, top-down and middle-down. [112, 113] Bottom-up

proteomics use complete enzyme digestion to hydrolyze the proteins into small peptides, and then use tandem mass spectrometry to sequence the protein. Top-down proteomics directly use tandem mass spectrometry on intact proteins, and structural information is obtained by fragmentation of proteins in the gas phase. Middle-down methods use enzymes to partially digest the proteins, and then use tandem mass spectrometry to the partially digested protein moieties to gain both sequence and structural information.

When peptides and proteins are fragmented in the mass spectrometer, there are backbone cleavages, side-chain losses, and small neutral losses such as water and ammonia. [114] Three commonly observed types of backbone cleavage and their fragmentation nomenclature are shown in Figure 1.4. [115] The letter a/b/c/x/y/z refers to the cleavage bond type and which ion is generated at the cleavage site. The subscript n refers to the position of the cleavage site relative to the N- or C-terminus. Proposed structures of each type of fragment ions for peptide and protein cations are listed in Figure 1.4 as well. There is a debate on the structure of b ions, [116, 117] but only one of them is shown here. The b ions are found to go through a process called “peptide scrambling” by the formation of a ring structure on the two ends of b ions. [118] Therefore, the subsequent fragment ions of the b ion could have a “scrambled” sequence compared to the original peptide or protein. Oftentimes b/y ions are generated by CID and IRMPD, a/x ions by UVPD, and c/z ions by ECD or ETD, but the type of fragment ion is also related to the nature of the ion itself. [115]

1.3 Ion/Ion Reactions in Gas Phase

The nature of ion and ion type is very important in the ion fragmentation process, as discussed in Section 1.2. Different structural information can be obtained through chemical modification of the ion structure or change of the ion type. An example of the chemical

modification is the crosslinking of the target functional group (e.g., amine) on proteins. Fragmentation of the crosslinked protein gives us the spatial relationship between different lysine residues, which helps to shed light on the 3D structure of the protein. [119] As for the example of ion type change, cations and anions of the same peptide oftentimes breaks at different bond locations after CID, which is good for peptide sequencing. [85]

People have used solution-phase methods to modify the analyte or change the ion type. [120, 121] However, due to the solvation of reactants in the solution, reactions usually need to overcome a high reaction barrier, which greatly affects the reaction rate. [122] The reduced yield of the solution-phase reactions or methods due to solvent-involved side reactions may be an issue, and further purification is usually required as the reaction solvent conditions may not be MS compatible.

Ion/ion reaction is very useful to change the ion type or to chemically modify the analyte ion. [123] As gas-phase reactions, ion/ion reaction shares the advantage with ion/molecule reactions that there is no solvent in the gas phase, so the collisions between the reactants are easier to happen and requires less energy. [124] Due to the electrostatic attraction between cations and anions, they tend to come together and form a complex, which creates an environment for ion/ion reaction. The energy released by the complex formation is an autogenous energy source for the reaction to happen. A low-energy ion/ion reaction, such as proton transfer reaction, can happen without external excitation of the electrostatic complex, while for some more complicated reactions, such as gas-phase covalent modification reactions, they often require a supplemental energy input to help overcome the reaction energy barrier. [125]

1.3.1 Instrumentation for Ion/Ion Reaction

The instrumentation for ion/ion reaction has two requirements: 1. Two ion sources that can generate both polarities of ions; 2. An MS element that ions with both polarities can stay. The ion source is usually not the problem, because the ion source is the element outside the vacuum.

The first ion/ion reaction inside the vacuum was performed on a 3D quadrupole ion trap system. [126] The 3D trap is usually operated by keeping the end caps at ground and having a driving rf on the ring electrode, which inherently is an operation mode that can trap ions of both polarities. [72] However, 3D trap has low trapping efficiency, limited trapping capacity and is more prone to the space charge issue. [127] Linear quadrupole ion trap has better trapping efficiency and capacity than 3D trap, but unlike 3D trap, linear quadrupole ion traps trap ions by the DC potential on the two lenses outside the quadrupole (Section 1.1.3), which can trap only one polarity along the z axis. [128] The other polarity ions would be attracted to the end lenses and get ejected. Later people find that when AC waveforms are added to the end lenses, ions of each polarity are trapped by half of the AC waveform at the same polarity. [129, 130] Since the AC waveform is changing the polarity of the potential rapidly, ions of both polarities can be trapped.

Besides the instrumentation for trapping ions of both polarities, another way to do ion/ion reaction is the transmission ion/ion reaction. [131] This only needs one polarity of ions being trapped when the ions of the other polarity pass through the trapped ions and react. Proton transfer and electron transfer ion/ion reactions have been done with transmission ion/ion reaction. [131-133] However, in transmission mode the time of reaction is very short and is hard to control. Therefore, instrument configurations for trapping mode ion/ion reaction are preferred for most ion/ion reaction studies.

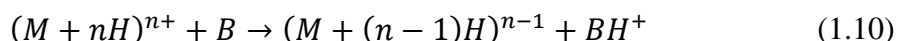
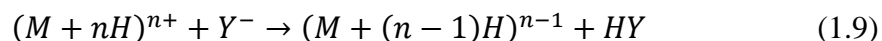
The instruments for the ion/ion reactions in the following chapters are modified QqQ and QqTOF systems, as shown in Figure 1.5. [129, 134] Two AC waveforms are added on the end

lenses IQ2 and IQ3 of q2, where ions of both polarities are mutually stored and reacted. The generation of ions of both polarities are achieved with two standalone nESI sources, placed at an angle in front of the mass spectrometer. The injection of cation or anion into q2 is performed by sequential injection.

1.3.2 Thermodynamics and Kinetics of Ion/Ion Reactions

Before the development of ion/ion reactions, ion/molecule reactions were more prevalent, while thermodynamically and kinetically ion/ion reaction is more favorable than ion/molecule reaction. [135, 136] Therefore, the thermodynamics and kinetics of ion/ion reaction is discussed here in comparison with the ion/molecule reactions.

Proton transfer reaction is used here as an example to compare ion/ion reaction and ion/molecule reaction for multiply charged ions. The ion/ion and ion/molecule reactions are listed in Equations 1.9 and 1.10:



where B represents a strong neutral gaseous base. The generic energy diagram for the two reactions are shown in Figure 1.6, with the reaction coordinate proceeding from left to right. [135, 136] For ion/ion proton transfer reaction, the entrance channel is dominated by the long-range electrostatic attraction between the cation and the anion, while the exit channel is dominated by short-range ion-dipole and ion-induced dipole potentials since the products are an ion and a neutral. For ion/molecule proton transfer reaction, the entrance channel is dominated by short-range attractive polarization force, while the exit channel is dominated by long-range electrostatic repulsion from the two same-charge product ions. The Coulomb repulsion in the ion/molecule reaction exit channel raises an energy barrier and makes ion/molecule reaction less efficient than ion/ion

reaction. From the enthalpy change of the two reactions, we can see that ion/ion reaction is more exothermic and favored thermodynamically.

Kinetically, for the dependence of reaction rate on the charge state of multiply charge ion/ion reaction, a model [135, 136] has been proposed based on the following assumptions: 1. The rate constant for reaction is the same as the rate constant for forming a stable orbiting complex k_c ; 2. The cation and anion will react immediately when they form a complex due to the high exothermicity of the ion/ion reaction; 3. The long-range interaction between the cation and the anion is Coulomb attraction only. If the assumptions above are met, the rate constant for reaction (complex formation) is

$$k_c = v\pi \left[\frac{Z_1 Z_2 e^2}{\mu v^2} \right]^2 \quad (1.11)$$

where v is the relative velocity of the oppositely charged ions, μ is the reduced mass of the collision partners, Z_1 and Z_2 are the charges of the oppositely charged ions, and e is the elementary charge.

Although this model is not perfect because it doesn't consider the distance limit required for an ion/ion reaction to happen, the charge-squared dependence of the ion/ion reaction rate has been experimentally confirmed by reaction rates measured under pseudo-first order kinetics conditions. The charge-squared relationship indicates that ions at higher charge states react much faster than ions at lower charge states. Compared to ion/molecule reaction, where the reaction rate decreases much faster for lower charge state ions, ion/ion reaction is more suitable for the reaction of ions at low charge states. It is also worth mentioning that due to the charge-squared dependence of the ion/ion reaction rate, ions of very different initial charge states can be neutralized in a similar time frame for proton transfer reactions. [137]

1.3.3 Charge Transfer Reactions

Charge transfer reactions are a common type of ion/ion reactions that involves the transfer of small charged particles (proton, electron, metal ion, etc.). Such reactions may happen via two possible mechanisms. [136, 138] One mechanism is that the particle “hops” onto the other reactant ion when the two reactant ions fly by each other without the formation of a long-lived complex. The other is that the two reactant ions form a long-lived complex and during that time the particle transfers among them. Based on the charges of the reactants and products, charge transfer reactions can be categorized into charge reduction reactions and charge inversion reactions. In the charge reduction reactions, the charges of the analyte ion of interest are reduced by the reagent. In the charge inversion reactions, the polarity of the analyte ion is inverted by the reagent.

Proton transfer reaction is analogous to acid/base reaction in solution. It has been widely used for spectrum simplification, [139] reactant ion concentration via ion parking, [140] optimized protein identification and structural analysis at specific charge states, [88] and molecular weight measurement for large biomolecules. [141] Electron transfer reaction is similar to the redox reactions in solution. It's mostly used for complimentary structural information of the analyte and detection of the post translational modification sites such as phosphorylation. [142] Metal transfer reaction and metal switching reaction is often applied to generate metallated analyte ion, which gives special cleavage sites and fragmentation pathways. [143]

1.3.4 Gas-Phase Covalent Modification Reactions

Ion/ion reaction can also achieve gas-phase covalent modification on the analyte ions. [85, 123, 136] This type of reaction usually requires the formation of electrostatic complex and external energy input so that the reactants have enough proximity and energy to go through a reaction. The

efficiency of the covalent modification via ion/ion reaction is affected by competing reactions like proton transfer reactions and metal transfer reactions.

Gas-phase covalent modification reactions are developed mostly for the purpose of providing more structural information, either by gas-phase labeling of specific functional group, or by altering the fragmentation pattern after the covalent modification. Up to now multiple covalent modification reactions via ion/ion reaction have been developed. Examples of gas-phase covalent modification reactions include the reactions between N-hydroxysuccinimide (NHS) esters and nucleophiles like primary amines, [144] guanidine groups [145] and carboxylates; [146] Schiff base formation between formyl-benzenesulfonic acids and primary amines; [147] carboxylic acid group labelling with carbodiimide reagents; [148] and gas-phase oxidation of peptides with periodate or persulfate derivatives. [149, 150]

1.4 Ion Mobility: Differential Mobility Spectrometry (DMS)

Ion mobility spectrometry (IMS) devices are instruments that separate ions by their mobility in the carrier gas. Since both MS and IMS are studying ions in the gas phase, the hyphenation of the two techniques has given people more insights to gas-phase ion structures. According to their working mechanism, currently IMS devices can be categorized into the following four types: drift tube IMS (DTIMS), travelling wave IMS (TWIMS), trapped IMS (TIMS), and differential mobility spectrometry (DMS). [151] Compared to other IMS techniques, DMS has the advantages of its application in ambient environment and small device size. Though due to the complexity of the influencing factors in DMS separations, structural information like collisional cross section cannot be obtained from DMS results, DMS is more widely used in ion separation before entering the MS and there is a possibility that DMS can substitute LC for fast preliminary analyte separation. [152]

The principle of DMS was first proposed by the Soviet Union in the early 1980s. [153] A lot of efforts have been put into the development of these sensors in the early days so that they can be used to detect land mines in the conflict in Afghanistan at that time. [154] Later two routes of development gradually appeared. The Gorshkov's team went after the cylindrical geometry DMS device, which was named as High Field Asymmetric Waveform Ion Mobility Spectrometry (FAIMS) a few years later. [154-156] One purpose of the cylindrical geometry is to utilize the ion-focusing effect of the inhomogeneous field from the curved electrodes. The other route is the planar geometry, which is referred more as Differential Mobility Spectrometry (DMS). [157] The planar geometry DMS is developed to let all ions transmit through the DMS device without discrimination when the separation fields are turned off, which cannot be achieved by cylindrical geometry. Nevertheless, the physical principles of FAIMS and DMS are the same. Nowadays the DMS interface for MS is commercially available, with SCIEX working on the planar DMS [158] and Thermo Scientific on the cylindrical FAIMS. [159]

1.4.1 Configuration of the DMS Interface

The DMS device used in this dissertation is the commercial planar DMS by SCIEX. [158] The configuration of the DMS interface is demonstrated in Figure 1.7(a). [160] Two sources of gas are provided in the DMS cell. One is the curtain gas inlet, which provides the curtain gas and the carrier gas. The other is the modifier gas, which can introduce modifier gas if needed. The ions generated from the nESI source are dried by the curtain gas, then undergo DMS separation in the DMS cell, and finally enter the mass spectrometer. Separation voltage (SV) and compensation voltage (CV) are applied to the DMS electrodes. The DMS cell is heated to temperatures higher than room temperature, ranging from 75°C to 225°C. [158]

1.4.2 Separation Mechanism

DMS separates ions by its mobility difference in the high and low field. [161] As shown in Figure 1.7(b), [152] separation voltage (SV) and compensation voltage (CV) are applied to the DMS electrodes. The SV is a square wave whose amplitude alternates between a positive high-field voltage V_{high} and a negative low-field voltage V_{low} . The square wave is set to make the net voltage-time integration equals to zero, viz., $V_{high}t_{high} + V_{low}t_{low} = 0$. [162] For a specific ion that enters the DMS cell, when only SV is applied to the DMS electrodes, due to the different mobility of the ion in the high and low field, it may follow the dashed ion path labeled in red and hit the electrode before exiting the DMS cell. The CV is applied to compensate for the ion's displacement caused by the SV. When the right CV is applied, the ion should exit the DMS cell by the solid ion path in purple and successfully enter the mass spectrometer.

Multiple factors can affect the mobility of the ion. Empirically, the relationship between the mobility of an ion at field E and the mobility of the same ion at zero field can be expressed by:

$$K\left(\frac{E}{N}\right) = K(0) \left[1 + \alpha\left(\frac{E}{N}\right) \right] \quad (1.12)$$

where K is the ion mobility coefficient at condition E/N , E is the electric field, N is the volume density of neutral particles, $K(0)$ is the ion mobility coefficient under low-field conditions, and $\alpha(E/N) \ll 1$ is a normalized function that describes how mobility changes with E/N . [162, 163] Three general shapes of alpha curves are shown in Figure 1.7(c). [152] For type A ions, ion mobility increases constantly with the separation field, which can be explained by ion-neutral clustering in the low field and ion-neutral declustering in the high field. For type C ions, ion mobility decreases constantly as the separation field increases, which may mean no clustering happens in the separation process. The ion mobility of type B ions is a combination of type A and type C ions, which corresponds to a type A cluster/decluster mechanism in the lower electric field

and a type C no-clustering mechanism in the higher electric field. Ion-neutral polarization mechanism [164] and dipole alignment theory [165] are also proposed to explain the mobility trend of type B ions.

From the discussion above we can see that the separation process is dominated by gas-phase chemical interactions, especially for type A and type B ions. Macroscopically, the separation can be affected by the mobility property of the ion itself, SV and CV setting, ionization source, carrier gas, temperature, pressure and shape of DMS device. [166]

1.4.3 Effect of Modifier in Analyte Separation

The introduction of modifier into the DMS cell changes the neutral composition and thus affects the separation. It not only inherently affects the mobility of the ion due to the change of collisional cross section of the neutral molecules, but also alters the ion-neutral cluster/decluster interactions. Though the actual effect of a specific modifier on a sample system have to go with a trial and error method due to the complexity of the DMS separation mechanism, some general trends have been summarized based on previous experiments. The introduction of polar vapor is found to promote type A mobility phenomenon. [167] A relatively high modifier concentration (e.g., >1%) was found beneficial to maximize the improvement of separation by modifier and to reduce the irreproducibility from uneven gas compositions. [168] Modifiers with high gas-phase proton affinity tend to cause proton transfer from the analyte ions and may affect the signal of the ion. [169] For now isopropyl alcohol has been found to be a good modifier to improve peak capacity and is recommended as the starting modifier in the SCIEX DMS user manual. [158]

1.5 Conclusions

Mass spectrometry is a powerful tool that is applied to chemical identification, quantification, and structural analysis. With soft ionization techniques such as ESI and MALDI, native ions with high molecular weight can be generated and analyzed, which is especially beneficial to the studies of large biomolecules. The development of mass analyzers enables ion analysis with higher resolution and higher mass range. Tandem mass spectrometry has been proved to be critical in probing ion structure and other applications such as gas-phase synthesis and chemical quantification. Ion/ion reactions have been used in various applications from spectrum simplification by proton transfer reactions to biomolecule structural analysis by gas-phase covalent modification reactions. Differential mobility spectrometry adds an orthogonal separation dimension to the mass spectrometry analysis, which makes it possible to analyze more complicated samples.

1.6 References

1. Bergquist, J.; Turner, C. Analytical Chemistry for a Sustainable Society – Trends and Implications. *Anal. Bioanal. Chem.* 410, 3235-3237 (2018).
2. Hare, D. J.; New, E. J. On the Outside Looking in: Redefining the Role of Analytical Chemistry in the Biosciences. *Chem. Commun.* 52, 8918-8934 (2016).
3. De Hoffmann, E.; Stroobant, Vincent. *Mass Spectrometry: Principles and Applications* (3rd ed.). John Wiley & Sons, Chichester, UK (2007).
4. Glish, G. L.; Vachet, R. W. The Basics of Mass Spectrometry in the Twenty-First Century. *Nat. Rev. Drug Discov.* 2, 140-150 (2003).
5. Thomson, J. J. XL. Cathode Rays. *Lond. Edinb. Dubl. Phil. Mag.* 44, 293-316 (1897).
6. Griffiths, J. A Brief History of Mass Spectrometry. *Anal. Chem.* 80, 5678-5683 (2008).
7. Yamashita, M.; Fenn, J. B. Electrospray Ion Source. Another Variation on the Free-Jet Theme. *J. Phys. Chem.* 88, 4451-4459 (1984).
8. Fenn, J. B.; Mann, M.; Meng, C. K.; Wong, S. F.; Whitehouse, C. M. Electrospray Ionization for Mass Spectrometry of Large Biomolecules. *Science* 246, 64-71 (1989).
9. Karas, M.; Hillenkamp, F. Laser Desorption Ionization of Proteins with Molecular Masses Exceeding 10,000 Daltons. *Anal. Chem.* 60, 2299-2301 (1988).
10. McLafferty, F. W. A Century of Progress in Molecular Mass Spectrometry. *Annu. Rev. Anal. Chem.* 4, 1-22 (2011).
11. Cunningham, R.; Ma, D.; Li, L. Mass Spectrometry-Based Proteomics and Peptidomics for Systems Biology and Biomarker Discovery. *Front. Biol.* 7, 313-335 (2012).
12. Mutenda, K. E.; Matthiesen, R. Analysis of Carbohydrates by Mass Spectrometry. In: Matthiesen, R. (ed.) *Mass Spectrometry Data Analysis in Proteomics*, pp. 289-302. Humana Press, Totowa, NJ (2007).
13. Kailemia, M. J.; Ruhaak, L. R.; Lebrilla, C. B.; Amster, I. J. Oligosaccharide Analysis by Mass Spectrometry: A Review of Recent Developments. *Anal. Chem.* 86, 196-212 (2014).
14. Siuzdak, G.; Bothner, B.; Yeager, M.; Brugidou, C.; Fauquet, C. M.; Hoey, K.; Change, C. Mass Spectrometry and Viral Analysis. *Chem. Biol.* 3, 45-48 (1996).
15. Downard, K. M.; Morrissey, B.; Schwahn, A. B. Mass Spectrometry Analysis of the Influenza Virus. *Mass Spectrom. Rev.* 28, 35-49 (2009).

16. Dominguez-Medina, S.; Fostner, S.; Defoort, M.; Sansa, M.; Stark, A.; Halim, M. A.; Vernhes, E.; Gely, M.; Jourdan, G.; Alava, T.; Boulanger, P.; Masselon, C.; Hentz, S. Neutral Mass Spectrometry of Virus Capsids above 100 Megadaltons with Nanomechanical Resonators. *Science* 362, 918-922 (2018).
17. Bedair, M.; Sumner, L. W. Current and Emerging Mass-Spectrometry Technologies for Metabolomics. *Trends Anal. Chem.* 27, 238-250 (2008).
18. Grayson, M. A. A History of Gas Chromatography Mass Spectrometry (GC/MS). In: Gross, M. L.; Caprioli, R. M. (eds.) *The Encyclopedia of Mass Spectrometry*, Vol. 9, pp. 152-158. Elsevier, Oxford, UK (2016).
19. Niessen, W. *Liquid Chromatography – Mass Spectrometry* (3rd ed.). CRC Press, Boca Raton, FL (2006).
20. Liu, W.; Hill, H. Jr. Chapter 5 – High-Performance Ion Mobility Spectrometry. In: Picó, A. (ed.) *Comprehensive Analytical Chemistry*, Vol. 68, pp. 275-305. Elsevier, Oxford, UK (2015).
21. Young, L. M.; Saunders, J. C.; Mahood, R. A.; Revill, C. H.; Foster, R. J.; Ashcroft, A. E.; Radford, S. E. ESI-IMS-MS: A Method for Rapid Analysis of Protein Aggregation and Its Inhibition by Small Molecules. *Methods* 95, 62-69 (2016).
22. Ben-Nissan, G.; Sharon, M. The Application of Ion-Mobility Mass Spectrometry for Structure/Function Investigation of Protein Complexes. *Curr. Opin. Chem. Bio.* 42, 25-33 (2018).
23. Fay, L. B.; Kussmann, M. Mass Spectrometry Technologies. In: Fay, L.B.; Kussmann, M. (eds.) *Mass Spectrometry and Nutrition Research*, pp. 3-50. The Royal Society of Chemistry, Cambridge, UK (2010).
24. Westman-Brinkmalm, A.; Brinkmalm, G. A Mass Spectrometer's Building Blocks. In: Ekman, R.; Silberring, J.; Westman-Brinkmalm, A.; Kraj, A. (eds.) *Mass Spectrometry: Instrumentation, Interpretation and Applications*, pp. 15-88. John Wiley & Sons, Hoboken, NJ (2009).
25. Siuzdak, G. An Introduction to Mass Spectrometry Ionization: An Excerpt from The Expanding Role of Mass Spectrometry in Biotechnology, 2nd ed.; MCC Press: San Diego, 2005. *JALA – J. Assoc. Lab. Autom.* 9, 50-63 (2004).
26. Siuzdak, G. *The Expanding Role of Mass Spectrometry in Biotechnology* (2nd ed.). MCC Press, San Diego, CA (2006).
27. Yost, R. A.; Fetterolf, D. D. Tandem Mass Spectrometry (MS/MS) Instrumentation. *Mass Spectrom. Rev.* 2, 1-45 (1983).
28. Reid, G. E.; McLuckey, S. A. 'Top Down' Protein Characterization via Tandem Mass Spectrometry. *J. Mass Spectrom.* 37, 663-675 (2002).

29. Koppelaar, D. W.; Barinaga, C. J.; Denton, M. B.; Sperline, R. P.; Hieftje, G. M.; Schilling, G. D.; Andrade, F. J.; Barnes, J. H.; IV, IV. MS Detectors. *Anal. Chem.* 77, 418A-427A (2005).
30. Dole, M.; Hines, R. L.; Mack, L. L.; Mobley, R. C.; Ferguson, L. D.; Alice, M. B. Gas Phase Macroions. *Macromolecules* 1, 96-97 (1968).
31. Loo, J. A.; Udseth, H. R.; Smith, R. D.; Futrell, J. H. Collisional Effects on the Charge Distribution of Ions from Large Molecules, Formed by Electrospray-Ionization Mass Spectrometry. *Rapid Commun. Mass Spectrom.* 2, 207-210 (1988).
32. Hilton, G. R.; Benesch, J. L. Two Decades of Studying Non-Covalent Biomolecular Assemblies by Means of Electrospray Ionization Mass Spectrometry. *J. R. Soc. Interface* 9, 801-816 (2012).
33. Mann, M. Electrospray: Its Potential and Limitations as an Ionization Method for Biomolecules. *Org. Mass Spectrom.* 25, 575-587 (1990).
34. Yamashita, M.; Fenn, J. B. Negative Ion Production with the Electrospray Ion Source. *J. Phys. Chem.* 88, 4671-4675 (1984).
35. Whitehouse, C. M.; Dreyer, R. N.; Yamashita, M.; Fenn, J. B. Electrospray Interface for Liquid Chromatographs and Mass Spectrometers. *Anal. Chem.* 57, 675-679 (1985).
36. Wong, S. F.; Meng, C. K.; Fenn, J. B. Multiple Charging in Electrospray Ionization of Poly(Ethylene Glycols). *J. Phys. Chem.* 92, 546-550 (1988).
37. Jardine, I. Electrospray Ionization Mass Spectrometry of Biomolecules. *Nature* 345, 747-748 (1990).
38. Olivares, J. A.; Nguyen, N. T.; Yonker, C. R.; Smith, R. D. On-Line Mass Spectrometric Detection for Capillary Zone Electrophoresis. *Anal. Chem.* 59, 1230-1232 (1987).
39. Mirza, U. A.; Chait, B. T.; Lander, H. M. Monitoring Reactions of Nitric Oxide with Peptides and Proteins by Electrospray Ionization-Mass Spectrometry. *J. Biol. Chem.* 270, 17185-17188 (1995).
40. Loos, G.; Schepdael, A. V.; Cabooter, D. Quantitative Mass Spectrometry Methods for Pharmaceutical Analysis. *Phil. Trans. R. Soc. A* 374, 20150366 (2016).
41. Ho, C. S.; Lam, C. W.; Chan, M. H.; Cheung, R. C.; Law, L. K.; Lit, L. C.; Ng, K. F.; Suen, M. W.; Tai, H. L. Electrospray Ionisation Mass Spectrometry: Principles and Clinical Applications. *Clin. Biochem. Rev.* 24, 3-12 (2003).
42. Banks, J. F., Jr.; Whitehouse, C. M. [21] Electrospray Ionization Mass Spectrometry. In: Karger, B. L.; Hancock, W. S. (eds.) *Methods in Enzymology*, Vol. 270, pp. 486-519. Academic Press, San Diego, CA (1996).

43. Schwartz, B. L.; Light-Wahl, K. J.; Smith, R. D. Observation of Noncovalent Complexes to the Avidin Tetramer by Electrospray Ionization Mass Spectrometry. *J. Am. Soc. Mass Spectrom.* 5, 201-204 (1994).
44. Ikonornou, M. G.; Kebarle, P. A Heated Electrospray Source for Mass Spectrometry of Analytes from Aqueous Solutions. *J. Am. Soc. Mass Spectrom.* 5, 791-799 (1994).
45. Covey, T. Analytical Characteristics of the Electrospray Ionization Process. In: Snyder, A. P. (ed.) *Biochemical and Biotechnological Applications of Electrospray Ionization Mass Spectrometry*, Vol. 619, pp. 21-59. American Chemical Society, Washington, DC (1996).
46. Wilm, M. S.; Mann, M. Electrospray and Taylor-Cone Theory, Dole's Beam of Macromolecules at Last? *Int. J. Mass Spectrom. Ion Process.* 136, 167-180 (1994).
47. Van Berkel, G. J.; Kertesz, V. Using the Electrochemistry of the Electrospray Ion Source. *Anal. Chem.* 79, 5510-5520 (2007).
48. Karas, M.; Bahr, U.; Dülcks, T. Nano-Electrospray Ionization Mass Spectrometry: Addressing Analytical Problems beyond Routine. *Fresenius J. Anal. Chem.* 366, 669-676 (2000).
49. Huang, G.; Li, G.; Cooks, R. G. Induced Nanoelectrospray Ionization for Matrix-Tolerant and High-Throughput Mass Spectrometry. *Angew. Chem. Int. Ed.* 50, 9907-9910 (2011).
50. Peng, Y.; Zhang, S.; Gong, X.; Ma, X.; Yang, C.; Zhang, X. Controlling Charge States of Peptides through Inductive Electrospray Ionization Mass Spectrometry. *Anal. Chem.* 83, 8863-8866 (2011).
51. Bruins, A. P. Mechanistic Aspects of Electrospray Ionization. *J. Chromatogr. A* 794, 345-357 (1998).
52. Fenn, J. B. Electrospray Wings for Molecular Elephants (Nobel Lecture). *Angew. Chem. Int. Ed.* 42, 3871-3894 (2003).
53. Kebarle, P.; Tang, L. From Ions in Solution to Ions in the Gas Phase: The Mechanism of Electrospray Mass Spectrometry. *Anal. Chem.* 65, 972-986 (1993).
54. Rayleigh, L. XX. On the Equilibrium of Liquid Conducting Masses Charged with Electricity. *Lond. Edinb. Dubl. Phil. Mag.* 14, 184-186 (1882).
55. Taflin, D. C.; Ward, T. L.; Davis, E. J. Electrified Droplet Fission and the Rayleigh Limit. *Langmuir*, 5, 376-384 (1989).
56. Konermann, L.; Ahadi, E.; Rodriguez, A. D.; Vahidi, S. Unraveling the Mechanism of Electrospray Ionization. *Anal. Chem.* 85, 2-9 (2013).
57. Iribarne, J. V.; Thomson, B. A. On the Evaporation of Small Ions from Charged Droplets. *J. Chem. Phys.* 64, 2287-2294 (1976).

58. Iavarone, A. T.; Williams, E. R. Mechanism of Charging and Supercharging Molecules in Electrospray Ionization. *J. Am. Chem. Soc.* 125, 2319-2327 (2003).
59. Ahadi, E.; Konermann, L. Modeling the Behavior of Coarse-Grained Polymer Chains in Charged Water Droplets: Implications for the Mechanism of Electrospray Ionization. *J. Phys. Chem. B* 116, 104-112 (2012).
60. Konermann, L.; Rodriguez, A. D.; Liu, J. On the Formation of Highly Charged Gaseous Ions from Unfolded Proteins by Electrospray Ionization. *Anal. Chem.* 84, 6798-6804 (2012).
61. Thomson, B. A.; Iribarne, J. V. Field Induced Ion Evaporation from Liquid Surfaces at Atmospheric Pressure. *J. Chem. Phys.* 71, 4451-4463 (1979).
62. Loscertales, I. G.; De la Mora, J. F. Experiments on the Kinetics of Field Evaporation of Small Ions from Droplets. *J. Chem. Phys.* 103, 5041-5060 (1995).
63. Wilm, M. Principles of Electrospray Ionization. *Mol. Cell. Proteomics* 10, M111.009407 (2011).
64. De la Mora, J. F. Electrospray Ionization of Larger Multiply Charge Species Proceeds via Dole's Charged Residue Mechanism. *Anal. Chim. Acta* 406, 93-104 (2000).
65. Verkerk, U. H.; Kebarle, P. Ion-Ion and Ion-Molecule Reactions at the Surface of Proteins Produced by Nanospray. Information on the Number of Acidic Residues and Control of the Number of Ionized Acidic and Basic Residues. *J. Am. Soc. Mass Spectrom.* 16, 1325-1341 (2005).
66. Yen, T.; Judith, M. J.; Voyksner, R. D. Processes that Affect Electrospray Ionization-Mass Spectrometry of Nucleobases and Nucleosides. *J. Am. Soc. Mass Spectrom.* 7, 1106-1108 (1996).
67. Felitsyn, N.; Peschke, M.; Kebarle, P. Origin and Number of Charges Observed on Multiply-Protonated Native Proteins Produced by ESI. *Int. J. Mass Spectrom.* 219, 39-62 (2002).
68. Mellon, F. A. Mass Spectrometry | Principles and Instrumentation. In: Caballero, B. (ed.) *Encyclopedia of Food Sciences and Nutrition* (2nd ed.), pp. 3739-3749. Academic Press, Cambridge, UK (2003).
69. Niessen, W. M. MS-MS and MSⁿ. In: Lindon, J. C.; Tranter, G. E.; Koppelaar, D. W. (eds.) *Encyclopedia of Spectroscopy and Spectrometry* (3rd ed.), pp. 936-941. Academic Press, San Diego, CA (2017).
70. Sudakov, M. Y.; Apatskaya, M. V. Concept of the Effective Potential in Describing the Motion of Ions in a Quadrupole Mass Filter. *J. Exp. Theor. Phys.* 115, 194-200 (2012).
71. Schwartz, J. C.; Senko, M. W.; Syka, J. E. A Two-Dimensional Quadrupole Ion Trap Mass Spectrometer. *J. Am. Soc. Mass Spectrom.* 13, 659-669 (2002).

72. March, R. E. An Introduction to Quadrupole Ion Trap Mass Spectrometry. *J. Mass Spectrom.* 32, 351-369 (1997).
73. Douglas, D. J.; Frank, A. J.; Mao, D. Linear Ion Traps in Mass Spectrometry. *Mass Spectrom. Rev.* 24, 1-29 (2005).
74. Londry, F. A.; Hager, J. W. Mass Selective Axial Ion Ejection from a Linear Quadrupole Ion Trap. *J. Am. Soc. Mass Spectrom.* 14, 1130-1147 (2003).
75. Soni, M. H.; Cooks, R. G. Selective Injection and Isolation of Ions in Quadrupole Ion Trap Mass Spectrometry Using Notched Waveforms Created Using the Inverse Fourier Transform. *Anal. Chem.* 66, 2488-2496 (1994).
76. Hilger, R. T.; Santini, R. E.; Luongo, C. A.; Prentice, B. M.; McLuckey, S. A. A Method for Isolating Ions in Quadrupole Ion Traps Using an Excitation Waveform Generated by Frequency Modulation and Mixing. *Int. J. Mass Spectrom.* 377, 329-337 (2015).
77. McLuckey, S. A.; Wells, J. M. Mass Analysis at the Advent of the 21st Century. *Chem. Rev.* 101, 571-606 (2001).
78. Wolff, M. M.; Stephens, W. E. A Pulsed Mass Spectrometer with Time Dispersion. *Rev. Sci. Instrum.* 24, 616-617 (1953).
79. Boesl, U. Time-of-Flight Mass Spectrometry: Introduction to the Basics. *Mass Spectrom. Rev.* 36, 86-109 (2017).
80. Chernushevich, I. V.; Merenbloom, S. I.; Liu, S.; Bloomfield, N. A W-Geometry Ortho-TOF MS with High Resolution and Up to 100% Duty Cycle for MS/MS. *J. Am. Soc. Mass Spectrom.* 28, 2143-2150 (2017).
81. Toyoda, M. Development of Multi-Turn Time-of-Flight Mass Spectrometers and their Applications. *Eur. J. Mass Spectrom.* 16, 397-406 (2010).
82. Murphy, D. M. The sTOF, a Favorable Geometry for a Time-of-Flight Analyzer. *J. Am. Soc. Mass Spectrom.* 28, 242-246 (2017).
83. Leney, A. C.; Heck, A. J. Native Mass Spectrometry: What is in the Name? *J. Am. Soc. Mass Spectrom.* 28, 5-13 (2017).
84. De Hoffmann, E. Tandem Mass Spectrometry: A Primer. *J. Mass Spectrom.* 31, 129-137 (1996).
85. McLuckey, S. A.; Mentinova, Marija. Ion/Neutral, Ion/Electron, Ion/Photon, and Ion/Ion Interactions in Tandem Mass Spectrometry: Do We Need Them All? Are They Enough? *J. Am. Soc. Mass Spectrom.* 22, 3-12 (2011).
86. Leitner, A. A Review of the Role of Chemical Modification Methods in Contemporary Mass Spectrometry-Based Proteomics Research. *Anal. Chim. Acta* 1000, 2-19 (2018).

87. Foreman, D. J.; Betancourt, S. K.; Pilo, A. L.; McLuckey, S. A. Novel Peptide Ion Chemistry Associated with gold (I) Cationization: Preferential Cleavage at Lysine Residues. *Int. J. Mass Spectrom.* 427, 114-122 (2018).
88. Foreman, D. J.; Dziekonski, E. T.; McLuckey, S. A. Maximizing Selective Cleavages at Aspartic Acid and Proline Residues for the Identification of Intact Proteins. *J. Am. Soc. Mass Spectrom.* 30, 34-44 (2019).
89. Cleland, T. P.; DeHart, C. J.; Fellers, R. T.; VanNispen, A. J.; Greer, J. B.; LeDuc, R. D.; Parker, W. R.; Thomas, P. M.; Kelleher, N. L.; Brodbelt, J. S. High-Throughput Analysis of Intact Human Proteins Using UVPD and HCD on an Orbitrap Mass Spectrometer. *J. Proteome Res.* 16, 2072-2079 (2017).
90. Wells, J. M.; McLuckey, S. A. Collision-Induced Dissociation (CID) of Peptides and Proteins. *Methods Enzymol.* 402, 148-185 (2005).
91. McLuckey, S. A. Principles of Collisional Activation in Analytical Mass Spectrometry. *J. Am. Soc. Mass Spectrom.* 3, 599-614 (1992).
92. Charles, M. J.; McLuckey, S. A.; Glish, G. L. Competition between Resonance Ejection and Ion Dissociation during Resonant Excitation in a Quadrupole Ion Trap. *J. Am. Soc. Mass Spectrom.* 5, 1031-1041 (1994).
93. Tolmachev, A. V.; Vilkov, A. N.; Bogdanov, B.; Păsa-Tolić, L.; Masselon, C. D.; Smith, R. D. Collisional Activation of Ions in RF Ion Traps and Ion Guides: The Effective Ion Temperature Treatment. *J. Am. Soc. Mass Spectrom.* 15, 1616-1628 (2004).
94. Goeringer, D. E.; Wiehland, L. A.; Danailov, D. M. Prediction of Collective Characteristics for Ion Ensembles in Quadrupole Ion Traps without Trajectory Simulations. *J. Am. Soc. Mass Spectrom.* 17, 889-902 (2006).
95. McLuckey, S. A.; Goeringer, D. E. Slow Heating Methods in Tandem Mass Spectrometry. *J. Mass Spectrom.* 32, 461-474 (1997).
96. March, R. E.; Hughes, R. J. *Quadrupole Storage Mass Spectrometry*. John Wiley & Sons, New York, NY (1989).
97. McLuckey, S. A.; Goeringer, D. E.; Glish, G. L. Selective Ion Isolation / Rejection over a Broad Mass Range in the Quadrupole Ion Trap. *J. Am. Soc. Mass Spectrom.* 2, 11-21 (1991).
98. Plomley, J. B.; March, R. E. Tandem Mass Spectrometry of Polychlorodibenzo-p-Dioxin and Polychlorodibenzofuran in a Quadrupole Ion Trap. 1. Comparison of Single-Frequency, Secular Frequency Modulation, and Multifrequency Resonant Excitation Modes. *Anal. Chem.* 68, 2345-2352 (1996).
99. Prentice, B. M.; Santini, R. E.; McLuckey, S. A. Adaptation of a 3-D Quadrupole Ion Trap for Dipolar DC Collisional Activation. *J. Am. Soc. Mass Spectrom.* 22, 1486-1492 (2011).

100. Webb, I. K.; Londry, F. A.; McLuckey, S. A. Implementation of Dipolar Direct Current (DDC) Collision-Induced Dissociation in Storage and Transmission Modes on a Quadrupole/Time-of-Flight Tandem Mass Spectrometer. *Rapid Commun. Mass Spectrom.* 25, 2500-2510 (2011).
101. Prentice, B. M.; McLuckey, S. A. Dipolar DC Collisional Activation in a “Stretched” 3-D Ion Trap: The Effect of Higher Order Fields on RF-Heating. *J. Am. Soc. Mass Spectrom.* 23, 736-744 (2012).
102. Webb, I. K.; Gao, Y.; Londry, F. A.; McLuckey, S. A. Trapping Mode Dipolar DC Collisional Activation in the RF-Only Ion Guide of a Linear Ion Trap/Time-of-Flight Instrument for Gaseous Bio-Ion Declustering. *J. Mass Spectrom.* 48, 1059-1065 (2013).
103. Dodonov, A.; Kozlovsky, V.; Loboda, A.; Raznikov, V.; Sulimenkov, I.; Tolmachev, A.; Kraft, A.; Wollnik, H. A New Technique for Decomposition of Selected Ions in Molecule Ion Reactor Coupled with Ortho-Time-of-Flight Mass Spectrometry. *Rapid Commun. Mass Spectrom.* 11, 1649-1656 (1997).
104. Lin, M.; Campbell, J. M.; Mueller, D. R.; Wirth, U. Intact Protein Analysis by Matrix-Assisted Laser Desorption/Ionization Tandem Time-of-Flight Mass Spectrometry. *Rapid Commun. Mass Spectrom.* 17, 1809-1814 (2003).
105. Xia, Y.; Liang, X.; McLuckey, S. A. Ion Trap versus Low-Energy Beam-Type Collision-Induced Dissociation of Protonated Ubiquitin Ions. *Anal. Chem.* 78, 1218-1227 (2006).
106. Brodbelt, J. S. Shedding Light on the Frontier of Photodissociation. *J. Am. Soc. Mass Spectrom.* 22, 197-206 (2011).
107. Reilly, J. P. Ultraviolet Photofragmentation of Biomolecular Ions. *Mass Spectrom. Rev.* 28, 425-447 (2009).
108. Julian, R. R. The Mechanism behind Top-Down UVPD Experiments: Making Sense of Apparent Contradictions. *J. Am. Soc. Mass Spectrom.* 28, 1823-1826 (2017).
109. Ly, T.; Julian, R. R. Ultraviolet Photodissociation: Developments towards Applications for Mass-Spectrometry-Based Proteomics. *Angew. Chem. Int. Ed.* 48, 7130-7137 (2009).
110. Ko, B. J.; Brodbelt, J. S. Comparison of Glycopeptide Fragmentation by Collision Induced Dissociation and Ultraviolet Photodissociation. *Int. J. Mass Spectrom.* 377, 385-392 (2015).
111. Biemann, K.; Martin, S. A. Mass Spectrometric Determination of the Amino Acid Sequence of Peptides and Proteins. *Mass Spectrom. Rev.* 6, 1-76 (1987).
112. Chait, B. T. Mass Spectrometry: Bottom-Up or Top-Down? *Science* 314, 65-66 (2006).
113. Pandeswari, P. B.; Sabareesh, V. Middle-Down Approach: A Choice to Sequence and Characterize Proteins/Proteomes by Mass Spectrometry. *RSC Adv.* 9, 313 (2019).

114. Paizs, B.; Suhai, S. Fragmentation Pathways of Protonated Peptides. *Mass Spectrom. Rev.* 24, 508-548 (2005).
115. Brodbelt, J. S. Ion Activation Methods for Peptides and Proteins. *Anal. Chem.* 88, 30-51 (2016).
116. Yalcin, T.; Khouw, C.; Csizmadia, I. G.; Peterson, M. R.; Harrison, A. G. Why are B Ions Stable Species in Peptide Spectra? *J. Am. Soc. Mass Spectrom.* 6, 1164-1174 (1995).
117. Riba-Garcia, I.; Giles, K.; Bateman, R. H.; Gaskell, S. J. Evidence for Structural Variants of a- and b-Type Peptide Fragment Ions Using Combined Ion Mobility/Mass Spectrometry. *J. Am. Soc. Mass Spectrom.* 19, 609-613 (2008).
118. Chawner, R.; Holman, S. W.; Gaskell, S. J.; Eyers, C. Peptide Scrambling during Collision-Induced Dissociation is Influenced by N-terminal Residue Basicity. *J. Am. Soc. Mass Spectrom.* 25, 1927-1938 (2014).
119. Rappsilber, J. The Beginning of a Beautiful Relationship: Cross-Linking/Mass Spectrometry and Modelling of Proteins and Multi-Protein Complexes. *J. Struct. Biol.* 173, 530-540 (2011).
120. Sackau, D.; Mak, M.; Przybylski, M. Protein Surface Topology-Probing by Selective Chemical Modification and Mass Spectrometric Peptide Mapping. *Proc. Natl. Acad. Sci. U.S.A.* 89, 5630-5634 (1992).
121. Lee, M.; Kang, M.; Moon, B.; Oh, H. B. Gas-Phase Peptide Sequencing by TEMPO-Mediated Radical Generation. *Analyst*, 134, 1706-1712 (2009).
122. Chabinyk, M. L.; Craig, S. L.; Regan, C. K.; Brauman, J. I. *Science*, 279, 1882-1886 (1998).
123. McLuckey, S. A. The Emerging Role of Ion/Ion Reactions in Biological Mass Spectrometry: Considerations for Reagent Ion Selection. *Eur. J. Mass Spectrom.* 16, 429-436 (2010).
124. McIver, R. T., Jr. Chemical Reactions without Solvation. *Sci. Am.* 243, 186-197 (1980).
125. McLuckey, S. A.; Stephenson, J. L., Jr. Ion/Ion Chemistry of High-Mass Multiply Charged Ions. *Mass Spectrom. Rev.* 17, 369-407 (1998).
126. Wells, J. M.; Chrisman, P. A.; McLuckey, S. A. "Dueling" ESI: Instrumentation to Study Ion/Ion Reactions of Electrospray-Generated Cations and Anions. *J. Am. Soc. Mass Spectrom.* 13, 614-622 (2002).
127. Ouyang, Z.; Gao, L.; Fico, M.; Chappel, W. J.; Noll, R. J.; Cooks, R. G. Quadrupole Ion Traps and Trap Arrays: Geometry, Material, Scale, Performance. *Eur. J. Mass Spectrom.* 13, 13-18 (2007).
128. Hager, J. W. A New Linear Ion Trap Mass Spectrometer. *Rapid Commun. Mass Spectrom.* 16, 512-526 (2002).

129. Xia, Y.; Wu, J.; McLuckey, S. A.; Londry, F. A.; Hager, J. W. Mutual Storage Mode Ion/Ion Reactions in a Hybrid Linear Ion Trap. *J. Am. Soc. Mass Spectrom.* 16, 71-81 (2005).
130. Syka, J. E.; Coon, J. J.; Schroeder, M. J.; Shabanowitz, J.; Hunt, D. F. Peptide and Protein Sequence Analysis by Electron Transfer Dissociation Mass Spectrometry. *Proc. Natl. Acad. Sci. U.S.A.* 101, 9528-9533 (2004).
131. Wu, J.; Hager, J. W.; Xia, Y.; Londry, F. A.; McLuckey, S. A. Positive Ion Transmission Mode Ion/Ion Reactions in a Hybrid Linear Ion Trap. *Anal. Chem.* 76, 5006-5015 (2004).
132. Liang, X.; McLuckey, S. A. Transmission Mode Ion/Ion Proton Transfer Reactions in a Linear Ion Trap. *J. Am. Soc. Mass Spectrom.* 18, 882-890 (2007).
133. Liang, X.; Hager, J. W.; McLuckey, S. A. Transmission Mode Ion/Ion Electron-Transfer Dissociation in a Linear Ion Trap. *Anal. Chem.* 79, 3363-3370 (2007).
134. Rojas-Betancourt, S.; Stutzman, J. R.; Londry, F. A.; Blanksby, S. J.; McLuckey, S. A. Gas-Phase Chemical Separation of Phosphatidylcholine and Phosphatidylethanolamine Cations via Charge Inversion Ion/Ion Chemistry. *Anal. Chem.* 87, 11255-11262 (2015).
135. Stephenson, J. L.; McLuckey, S. A. Ion/Ion Reactions in the Gas Phase: Proton Transfer Reactions Involving Multiply-Charged Proteins. *J. Am. Chem. Soc.* 118, 7390-7397 (1996).
136. Prentice, B. M.; McLuckey, S. A. Gas-Phase Ion/Ion Reactions of Peptides and Proteins: Acid/Base, Redox, and Covalent Chemistries. *Chem. Commun.* 49, 947-965 (2013).
137. McLuckey, S. A.; Stephenson, J. L.; Asano, K. G. Ion/Ion Proton-Transfer Kinetics: Implications for Analysis of Ions Derived from Electrospray of Protein Mixtures. *Anal. Chem.* 70, 1198-1202 (1998).
138. Wells, J. M.; Chrisman, P. A.; McLuckey, S. A. Formation and Characterization of Protein-Protein Complexes in Vacuo. *J. Am. Chem. Soc.* 125, 7238-7249 (2003).
139. Stephenson, J. L.; McLuckey, S. A. Ion/Ion Proton Transfer Reactions for Protein Mixture Analysis. *Anal. Chem.* 68, 4026-4032 (1996).
140. McLuckey, S. A.; Reid, G. E.; Wells, J. M. Ion Parking during Ion/Ion Reactions in Electrodynamic Ion Traps. *Anal. Chem.* 74, 336-346 (2002).
141. Huang, T.; McLuckey, S. A. Top-Down Protein Characterization Facilitated by Ion/Ion Reactions on a Quadrupole/Time of Flight Platform. *Proteomics* 10, 3577-3588 (2010).
142. Pitteri, S. J.; Chrisman, P. A.; Hogan, J. M.; McLuckey, S. A. Electron Transfer Ion/Ion Reactions in a Three-Dimensional Quadrupole Ion Trap: Reactions of Doubly and Triply Protonated Peptides with $\text{SO}_2^{\cdot-}$. *Anal. Chem.* 77, 1831-1839 (2005).
143. Newton, K. A.; McLuckey, S. A. Generation and Manipulation of Sodium Cationized Peptides in the Gas Phase. *J. Am. Soc. Mass Spectrom.* 15, 607-615 (2004).

144. Mentinova, M.; McLuckey, S. A. Covalent Modification of Gaseous Peptide Ions with N-Hydroxysuccinimide Ester Reagent Ions. *J. Am. Chem. Soc.* 132, 18248-18257 (2010).
145. McGee, W. M.; Mentinova, M.; McLuckey, S. A. Gas-Phase Conjugation to Arginine Residues in Polypeptide Ions via N-Hydroxysuccinimide Ester-Based Reagent Ions. *J. Am. Chem. Soc.* 134, 11412-11414 (2012).
146. Peng, Z.; McGee, W. M.; Bu, J.; Barefoot, N. Z.; McLuckey, S. A. Gas Phase Reactivity of Carboxylates with N-Hydroxysuccinimide Esters. *J. Am. Soc. Mass Spectrom.* 26, 174-180 (2015).
147. Han H.; McLuckey, S. A. Selective Covalent Bond Formation in Polypeptide Ions via Gas-Phase Ion/Ion Reaction Chemistry. *J. Am. Chem. Soc.* 131, 12884-12885 (2009).
148. Prentice, B. M.; Gilbert, J. D.; Stutzman, J. R.; Forrest, W. P.; McLuckey, S. A. Gas-Phase Reactivity of Carboxylic Acid Functional Groups with Carbodiimides. *J. Am. Soc. Mass Spectrom.* 24, 30-37 (2013).
149. Pilo, A. L.; Bu, J.; McLuckey, S. A. Gas-Phase Oxidation of Neutral Basic Residues in Polypeptide Cations by Periodate. *J. Am. Soc. Mass Spectrom.* 27, 1979-1988 (2016).
150. Pilo, A. L.; Bu, J.; McLuckey, S. A. Transformation of $[M+2H]^{2+}$ Peptide Cations to $[M-H]^+$, $[M+H+O]^+$, and M^{+} Cations via Ion/Ion Reactions: Reagent Anions Derived from Persulfate. *J. Am. Soc. Mass Spectrom.* 26, 1103-1114 (2015).
151. Cumeras, R.; Figueras, E.; Davis, C. E.; Baumbach, J. I.; Gràcia, I. Review on Ion Mobility Spectrometry. Part 1: Current Instrumentation. *Analyst* 140, 1376-1390 (2015).
152. Kolakowski, B. M.; Mester, Z. Review of Applications of High-Field Asymmetric Waveform Ion Mobility Spectrometry (FAIMS) and Differential Mobility Spectrometry (DMS). *Analyst*, 132, 842-864 (2007).
153. Gorshkov, M. P. Inventor's Certificate of USSR No. 966583, G01N27/62 (1982).
154. Schneider, B. B.; Nazarov, E. G.; Londry, F.; Vouros, P.; Covey, T. R. Differential Mobility Spectrometry/Mass Spectrometry History, Theory, Design Optimization, Simulations, and Applications. *Mass Spectrom. Rev.* 35, 687-737 (2016).
155. Carnahan, B. L.; Day, S.; Kouznetsov, V.; Tarassov, A. Field Ion Spectrometry: A New Technology for Cocaine and Heroin Detection. In: Pilon, P.; Burmeister, S. (eds.) *Chemistry- and Biology-Based Technologies for Contraband Detection*, Vol. 2397, pp. 106-120. International Society for Optics and Photonics, Boston, MA (1997).
156. Purves, R. W.; Guevremont, R. Electrospray Ionization High-Field Asymmetric Waveform Ion Mobility Spectrometry-Mass Spectrometry. *Anal. Chem.* 71, 2346-2357 (1999).
157. Nazarov, E. G. A Journey into DMS/FAIMS Technology. *Int. J. Ion Mobil. Spec.* 15, 83-84 (2012).

158. SCIEX. *Analyst® 1.6.3 Software. SelexION® Technology for 5500 and 5600 Series Systems and SelexION®+ Technology for 6500+ Series Systems User Guide* [PDF file] (2015). Retrieved from <https://sciex.com/Documents/manuals/selexion-selexion-plus-5500-6500-6500plus-user-guide-en.pdf>
159. Thermo Scientific. *Specification Sheet: FAIMS Pro Interface* [PDF file] (2018). Retrieved from <https://assets.thermofisher.com/TFS-Assets/CMD/Specification-Sheets/ps-65185-ms-faims-pro-interface-ps65185-en.pdf>
160. Campbell, J. L.; Le Blanc, J. C.; Schneider, B. B. Probing Electrosprya Ionization Dynamics Using Differential Mobility Spectrometry: The Curious Case of 4-Aminobenzoic Acid. *Anal. Chem.* 84, 7857-7864 (2012).
161. Campbell, J. L.; Le Blanc, J. C.; Kibbey, R. G. Differential Mobility Spectrometry: A Valuable Technology for Analyzing Challenging Biological Samples. *Bioanalysis* 7, 853-856 (2015).
162. Purves, R. W.; Guevremont, R. Mass Spectrometric Characterization of a High-Field Asymmetric Waveform Ion Mobility Spectrometer. *Rev. Sci. Instrum.* 69, 4094-4105 (1998).
163. Buryakov, I. A.; Krylov, E. V.; Makas, A. L.; Nazarov, E. G.; Pervukhin, V. V.; Rasulev, U. K. Separation of Ions According to Mobility in a Strong AC Electric Field. *Sov. Tech. Phys. Lett.* 17: 446-447 (1991).
164. Buryakov, I. A.; Krylov, E. V.; Makas, A. L.; Nazarov, E. G.; Pervukhin V. V.; Rasulev, U.K. Drift Spectrometer for the Control of Amine Traces in the Atmosphere. *J. Anal. Chem.* 48, 156-165 (1993).
165. Shvartsburg, A. A.; Bryskiewicz, T.; Purves, R. W.; Tang, K.; Guevremont, R.; Smith, R. D. Field Asymmetric Waveform Ion Mobility Spectrometry Studies of Proteins: Dipole Alignment in Ion Mobility Spectrometry? *J. Phys. Chem. B* 110, 21966-21980 (2006).
166. Schneider, B. B.; Covey, T. R.; Coy, S. L.; Krylov, E. V.; Nazarov, E. G. Control of Chemical Effects in the Separation Process of a Differential Mobility Mass Spectrometer System. *Eur. J. Mass Spectrom.* 16, 57-71 (2010).
167. Schneider, B. B.; Nazarov, E. G.; Covey, T. R. Peak Capacity in Differential Mobility Spectrometry: Effects of Transport Gas and Gas Modifiers. *Int. J. Ion Mobil. Spec.* 15,141-150 (2012).
168. Rorrer, L. C., III; Yost, R. A. Solvent Vapor Effects on Planar High-Field Asymmetric Waveform Ion Mobility Spectrometry. *Int. J. Mass Spectrom.* 300, 173-181 (2011).
169. Blagojevic, V.; Koyanagi, G. K.; Bohme, D. K. Multi-Component Ion Modifiers and Arcing Suppressants to Enhance Differential Mobility Spectrometry for Separation of Peptides and Drug Molecules. *J. Am. Soc. Mass Spectrom.* 25, 490-497 (2014).

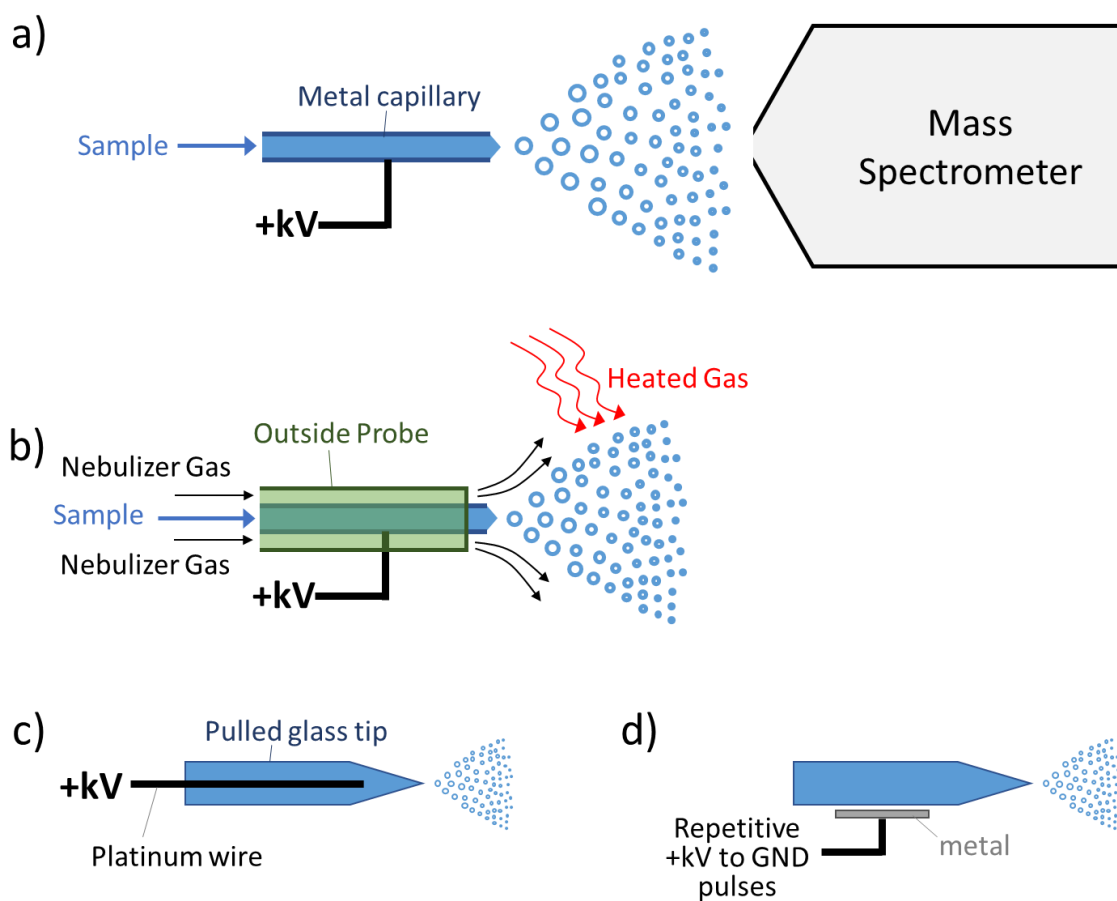


Figure 1.1 Cartoon schematics for different ESI setups. (a) conventional ESI, (b) ESI with auxiliary gas and heat, (c) nano-electrospray ionization (nESI), (d) inductive nESI. The abbreviation “+kV” is short for “positive kilovolts”. “GND” is abbreviated for “Ground”.

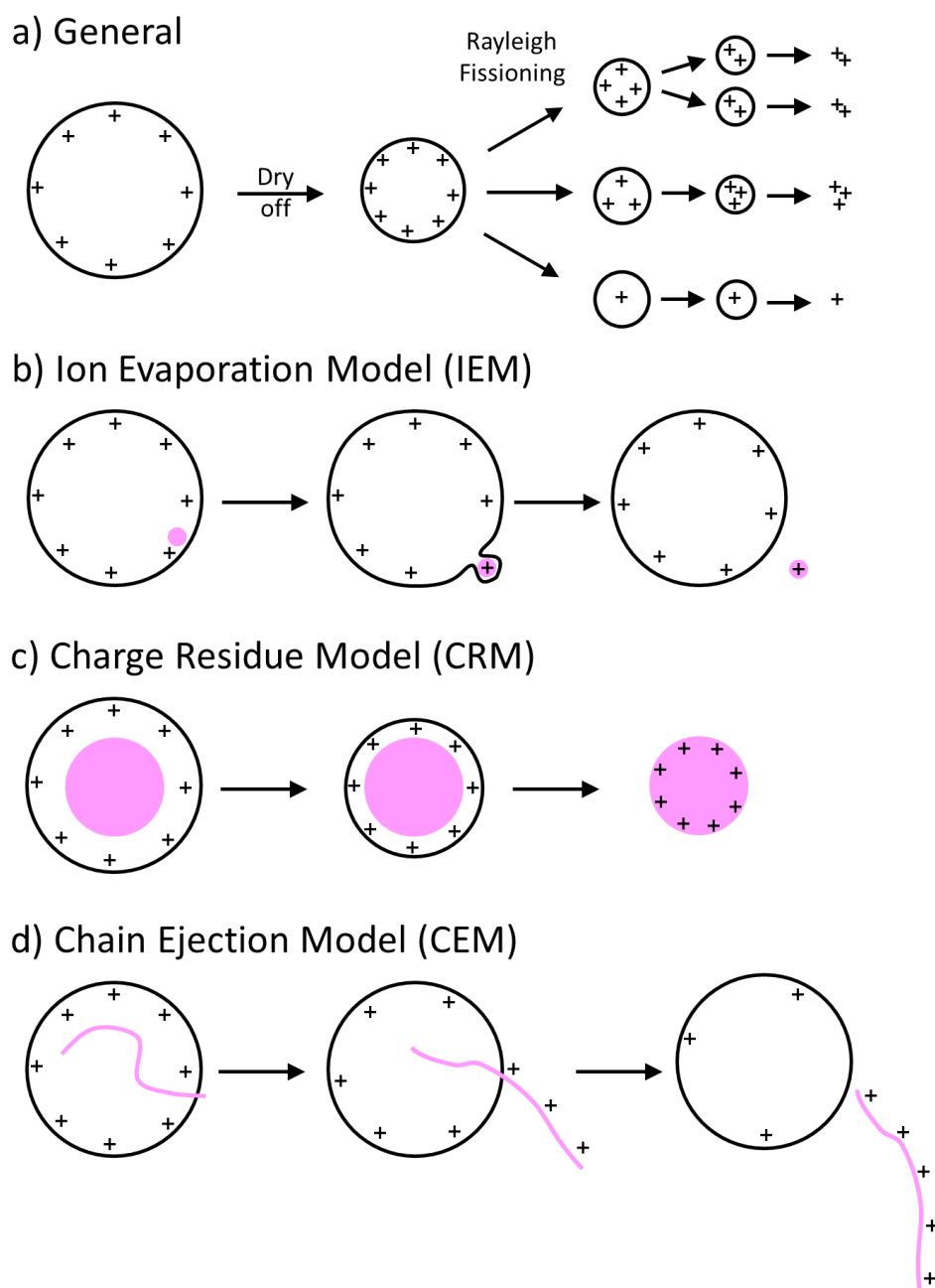
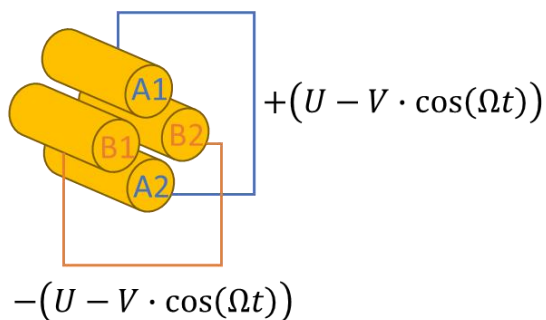
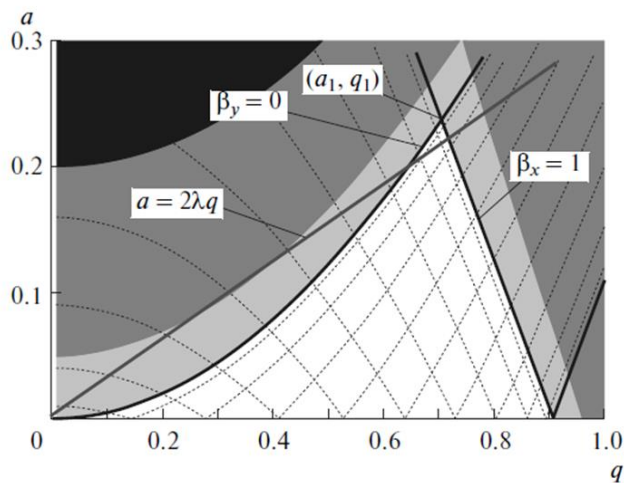


Figure 1.2 Schematic drawings for the general process and the three main models for ionization mechanism in ESI. (a) General fissioning process of ESI charged droplet; (b) Ion Evaporation Model (IEM); (c) Charge Residue Model (CRM); (d) Chain Ejection Model (CEM). The circle is the droplet; the pink filled circle or chain is the analyte; the plus signs are the positive charges.

a) Quadrupole



b) Mathieu Stability Diagram



c) Quadrupole Ion Trap (QIT)



Figure 1.3 Schematics for quadrupole and quadrupole ion trap. (a) Cartoon of quadrupole. (b) Mathieu stability diagram, with the darker shade meaning more unstable region of the ions. (c) Cartoon of the 2D quadrupole ion trap. Figure (b) is reprinted with permission from *J. Exp. Theor. Phys.* 115, 194-200 (2012) © 2012 Pleiades Publishing, Inc.

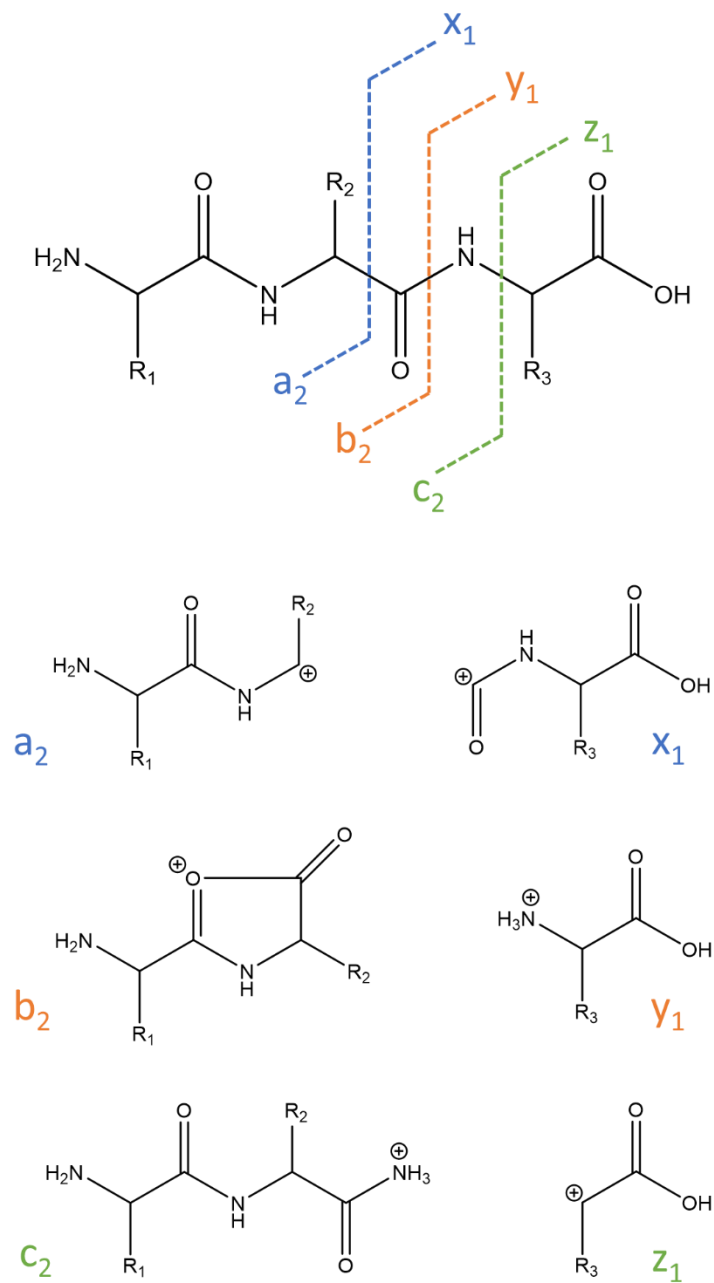


Figure 1.4 Nomenclature of common peptide backbone cleavages and structures of their corresponding fragment ions.

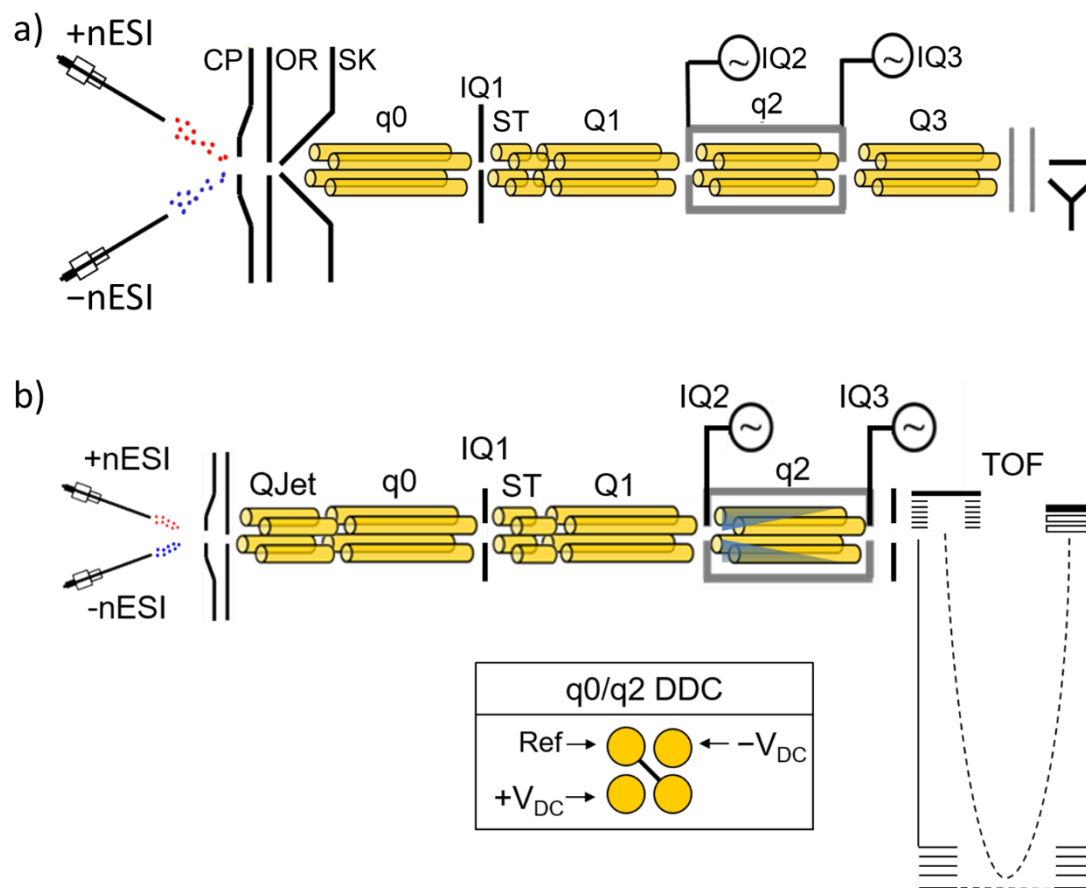
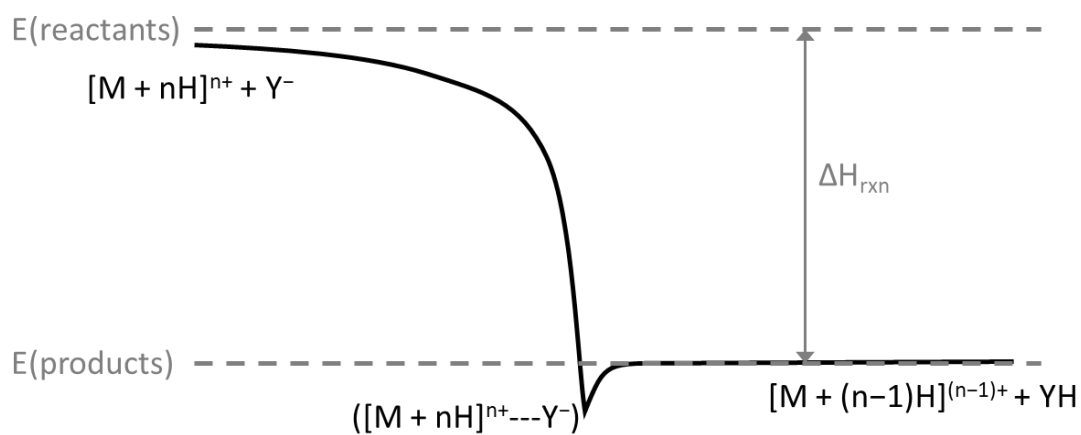


Figure 1.5 Instrument schematics for the ion/ion reactions in the dissertation. (a) QTRAP 4000 (SCIEX, Concord, Canada), modified for ion/ion reactions. (b) TripleTOF 5600 (SCIEX, Concord, Canada), modified for ion/ion reactions.

a) ion/ion reaction



b) ion/molecule reaction

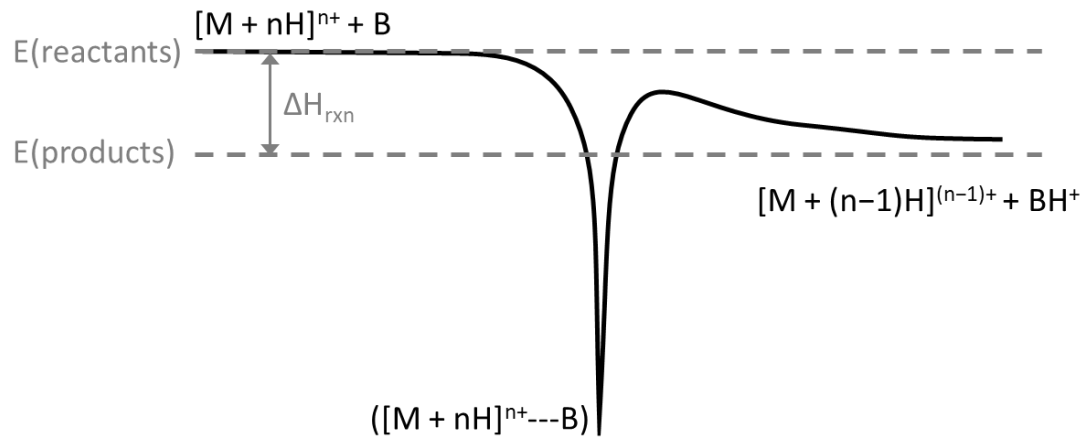


Figure 1.6 Generic energy diagram for (a) ion/ion proton transfer reaction and (b) ion/molecule proton transfer reaction

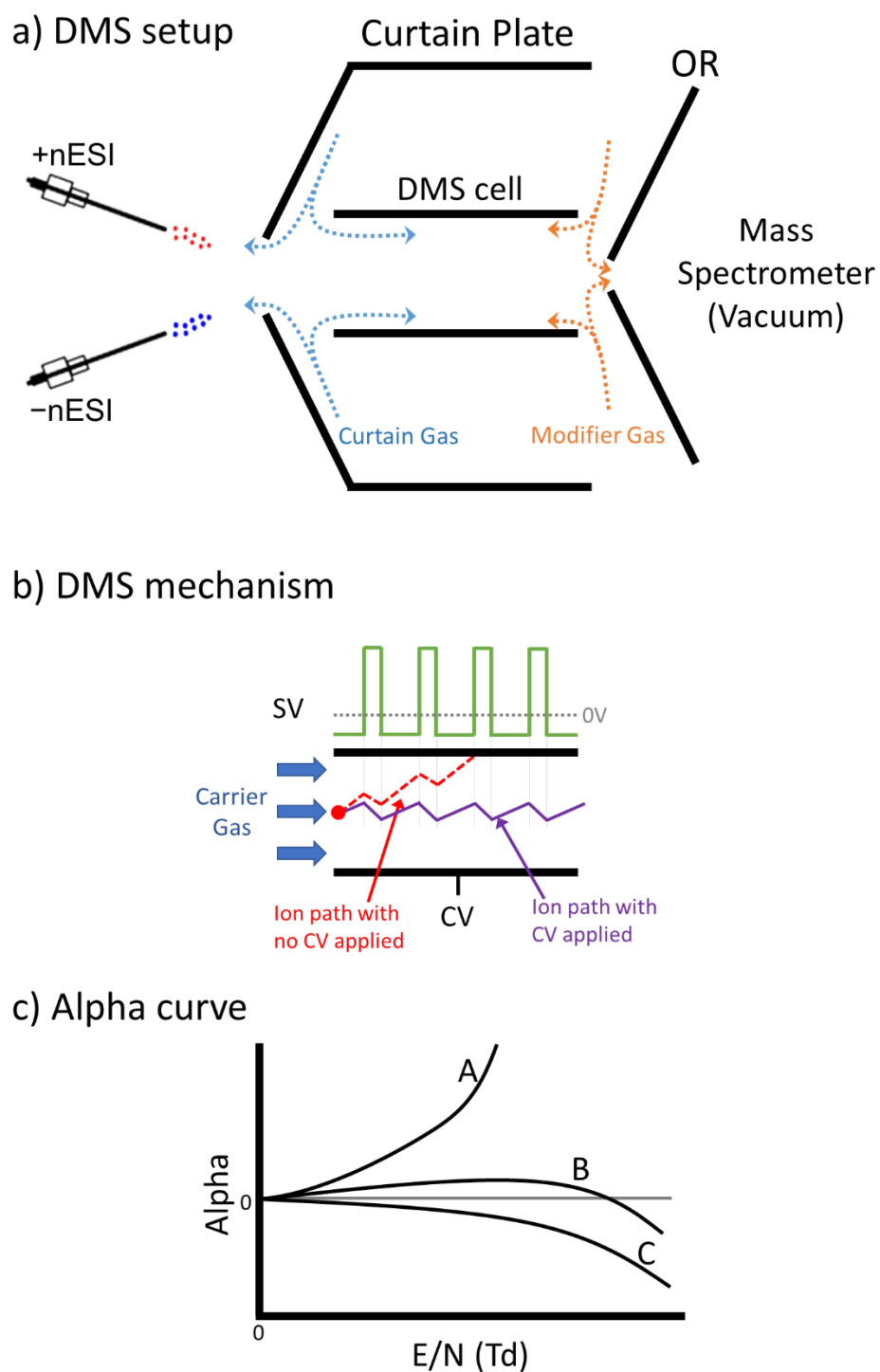


Figure 1.7 Schematic for (a) DMS setup with detailed gas flow, (b) DMS mechanism explanation, and (c) three general shapes of alpha curves. OR is short for orifice. SV is abbreviated for Separation Voltage. CV is abbreviated for Compensation Voltage.

CHAPTER 2. GAS-PHASE REARRANGEMENT REACTION OF SCHIFF-BASE-MODIFIED PEPTIDE IONS

A version of this chapter has been published by Rapid Communications in Mass Spectrometry © 2018 John Wiley and Sons, Ltd.

2.1 Introduction

Tandem mass spectrometry is widely used to probe ion structures by generating informative product ions via fragmentation. [1-3] Fragmentation patterns can be highly sensitive to ion type (e.g., protonated molecule versus radical cation) such that complementary information can be obtained by interrogating different analyte ion types. [4, 5] As an approach to the transformation of an analyte from one ion type to another within the mass spectrometer, gas-phase ion/ion reactions have been developed. [6, 7] Small particle transfer ion/ion reactions, e.g., proton and electron transfer reactions, change the analyte charge state, which can open up different fragmentation pathways. [8, 9] Gas-phase covalent modification ion/ion reactions are functional group specific reactions that selectively target particular functional groups and thereby alter fragmentation pathways. [6, 7] Moreover, unique chemistries have been observed via gas-phase ion/ion reactions compared to the solution phase. [7, 10] Examples of gas-phase covalent modification reactions include the reactions between N-hydroxysuccinimide (NHS) esters and nucleophiles like primary amines, [11] guanidine groups [12] and carboxylates; [13] gas-phase oxidation of peptides with periodate [14] or persulfate derivatives; [15] carboxylic acid group labelling with carbodiimide reagents; [16] and the Schiff base formation between formyl-benzenesulfonic acids and primary amines. [17]

The gas-phase modification of bio-ions via Schiff base formation was first described in 2009. [17] Formation of Schiff base is achieved by the reaction between a primary amine (i.e., the N-terminus or ϵ -amine group of a lysine residue) in a peptide analyte ion and the formyl group in the 4-formyl-1,3-benzenedisulfonic acid (FBDSA) reagent. Gas-phase collisional activation of the Schiff-base-modified analyte ions has been noted to result in a higher sequence coverage compared to the unmodified peptides in several scenarios. [17-20] Cotham et al. took advantage of the benzene chromophore in FBDSA and modified the analyte peptide in solution with this reagent to enhance the ultra-violet photodissociation (UVPD) efficiency. [21] They also found that the Schiff base modification of phosphopeptides with FBDSA helps retain the phosphate group during the fragmentation process. Fragmentation of the unmodified phosphopeptide often results in loss of the phosphate functionality and thereby precludes identification of the phosphate position. In the case of Schiff-base-modified peptides, on the other hand, the sulfonate group on the reagent disrupts the phosphate neutral loss process and stabilizes the phosphate group when collision-induced dissociation (CID) is applied. [22]

Studies of Schiff-base-modified polypeptide ions via tandem mass spectrometry using CID have resulted predominantly in b/y-type fragment ions, [17-22] in analogy with unmodified ions. [23] However, in this study, we focus on fragmentation products generated via CID that are unique to the Schiff-base-modified peptide. This work has revealed the existence of a fragmentation pathway that is specific to the Schiff base modification, which should be recognized when using this modification for structural characterization purposes. Possible mechanisms are proposed.

2.2 Experimental

2.2.1 Materials.

HPLC-grade water and methanol were purchased from Fisher Scientific (Waltham, MA, USA). 4-formyl-1,3-benzenedisulfonic acid (FBDSA) and 2-formyl-benzene(mono)sulfonic acid (FBMSA) were purchased from Sigma-Aldrich (St. Louis, MO, USA). Model peptides KGAGGKGAGGKL, RARARAA, AHAAHA and HAHAAHA were synthesized by NeoBioLab (Cambridge, MA, USA); KAKAKAA was synthesized by Pepnome Ltd (Shenzhen, China). All peptide solutions for electrospray were prepared in 50/50 (v/v) methanol/water (~ 0.2 mM). The FBDSA and FBMSA reagent solutions for electrospray were prepared in water (~ 3 mM).

2.2.2 Mass Spectrometry.

All experiments were performed on a QTRAP[®] 4000 hybrid triple quadrupole/linear ion trap mass spectrometer (SCIEX, Concord, ON, Canada) previously modified for ion/ion reactions, [24] unless specifically noted. Alternately pulsed nano-electrospray (nESI) [25] allowed for sequential injections of reagent and analyte ions, which were sequentially isolated in the Q1-mass filter prior to their injection into the q2 reaction cell. After a defined mutual storage reaction time, the product ions were then transferred to Q3. The ions then underwent further probing via MSⁿ using ion trap collisional activation and mass analysis via mass-selective axial ejection (MSAE). [26] The exact mass measurement experiments were performed on a TripleTOF[®] 5600 mass spectrometer (SCIEX, Concord, ON, Canada) previously modified for ion/ion reactions. [24]

2.3 Results and Discussion

2.3.1 Novel Fragmentation Pathway from Schiff-Base-Modified Lysine-Containing Peptides.

Gas-phase Schiff base formation has been demonstrated as an approach to provide structural information complementary to that derived from unmodified species in the tandem mass spectrometry of polypeptide ions. [17-22] It involves the reactivity between a peptide primary amine group, either on the N-terminus or the lysine side chain, and the formyl group on the reagent ion. The reagents used in this study are 4-formyl-1,3-benzenedisulfonic acid (FBDSA) and 2-formyl-benzene(mono)sulfonic acid (FBMSA) (structures shown in Scheme 2.1(c)). Each reagent contains a benzaldehyde reactive group and one or two sulfonate group(s).

The Schiff base modification and ion trap CID of the Schiff-base-modified peptide ion are illustrated by the spectra provided in Figure 2.1. Using a model peptide of sequence KAKAKAA, the doubly protonated peptide, $[M + 2H]^{2+}$, was formed via positive nESI and reacted with singly deprotonated FBDSA, $[FBDSA - H]^-$, resulting in an electrostatically bound complex, $[M + FBDSA + H]^+$, and a proton transfer product, $[M + H]^+$, as seen in Figure 2.1(a). Upon CID of the complex (see Figure 2.1(b)), a signature water loss from the complex reflects the formation of a Schiff-base-modified peptide cation, $[M + H + \blacklozenge]^+$, where the black diamond (\blacklozenge) depicts the mass shift caused by the modification (+248 Da). Further CID of the Schiff-base-modified species (see Figure 2.1(c)) gives rise to b/y fragment ions, both modified (e.g., b_6^{\blacklozenge} and y_6^{\blacklozenge}) and unmodified (e.g., b_3 and y_4), which implies different Schiff base modification sites, either the N-terminus or any one of the lysine side chains. Besides the b/y fragment ions, a highly abundant peak, labelled as $[M + H + \blacklozenge]^+$, was observed 267 Da lower in mass than the peak from the Schiff-base-modified peptide $[M + H + \blacklozenge]^+$, which is inconsistent with commonly observed neutral losses from peptide ions. The hollow diamond (\blacklozenge) in Figure 2.1(c) refers to the mass shift of the novel product, -267 Da from the precursor $[M + H + \blacklozenge]^+$, or an apparent -19 Da from the mass of the protonated peptide,

$[M + H]^+$. Similarly, there are peaks that are observed -267 Da lower in mass than the modified b ions (b_6^\blacklozenge , b_5^\blacklozenge , b_4^\blacklozenge , and b_3^\blacklozenge), which are also labeled with the hollow diamond (as in b_6^\diamond , b_5^\diamond , b_4^\diamond , and b_3^\diamond).

Evidence for an analogous reaction is noted in the negative mode (Figure 2.1(d)-(f)). The singly protonated peptide was charge inverted by the doubly deprotonated FBDSA to form a negatively charged complex, $[M + FBDSA - H]^-$ (Figure 2.1(d)). CID of the electrostatically bound complex generates a Schiff-base-modified peptide anion $[M - H + \blacklozenge]^-$ (Figure 2.1(e)). As above, the solid diamond (\blacklozenge) indicates the mass shift of the Schiff base modification (+248 Da). CID of the Schiff-base-modified peptide anion $[M - H + \blacklozenge]^-$ mainly leads to backbone fragment ions, including modified b/y and c fragment ions (e.g., b_5^\blacklozenge , y_5^\blacklozenge and c_2^\blacklozenge) and unmodified backbone fragment ions (e.g., a_5) (Figure 2.1(f)). In previous negative mode Schiff base modification studies [18-20], another common CID fragmentation product from $[M - H + \blacklozenge]^-$ is deprotonated FBDSA $[FBDSA - H]^-$ (m/z 265 Da). The precursor $[M - H + \blacklozenge]^-$ population can consist of both Schiff-base-modified peptides and the unreacted electrostatic complex of FBDSA and peptide with one water loss from somewhere else in the peptide. The latter type of $[M - H + \blacklozenge]^-$ ion can give rise to the $[FBDSA - H]^-$ CID product. In Figure 2.1(f), however, no $[FBDSA - H]^-$ peak (m/z 265) was observed. Rather, there are two dominant singly negatively charged peaks of m/z 266 (i.e., the peak labeled with $[NL - H]^-$ in red) and m/z 249 (the peak labeled with * in red) in the lower mass region. These two fragments are inconsistent with any common peptide fragment pathways. Considering that the neutral loss (NL), i.e., the mass difference between the unidentified peak and the Schiff-base-modified peptide, is 267 Da, the m/z 266 product ion was assigned as $[NL - H]^-$, and the m/z 249 product was assigned as $[NL - H - NH_3]^-$ due to the 17 Da difference. Activation of the m/z 266 Da ion ($[NL - H]^-$) formed in the CID spectrum of the Schiff-base-modified

KAKAKAA anion with FBDSA leads exclusively to ammonia loss, as shown in the Figure 2.3(c), which implies that the neutral loss structure contains an amine group.

Analogous results were obtained using singly deprotonated FBMSA in reaction with doubly protonated KAKAKAA. The Schiff-base-modified peptide product, $[M + H + \blacklozenge]^+$ ($\blacklozenge = +168$ Da), was directly formed upon ion/ion reaction along with the proton transfer product, $[M + H]^+$ (Figure 2.2(a)). Upon activation of the $[M + H + \blacklozenge]^+$ product, the resulting product ion spectrum (Figure 2.2(b)) contained a dominant $[M + H + \diamond]^+$ product that is -187 Da from the $[M + H + \blacklozenge]^+$ ion, and b/y ions with the same mass shift (b_3^\diamond , b_4^\diamond , b_5^\diamond , and b_6^\diamond), all of which are labeled with the hollow diamond ($\diamond = -19$ Da). Other backbone fragmentation products were observed in the spectrum in relatively low abundances. The 187 Da mass loss in the case of the FBMSA reagent is 80 Da less than that observed from the reactions with the FBDSA reagent, which is consistent with the difference in mass between FBMSA and FBDSA.

The $[M + H + \diamond]^+$ ions generated from Schiff-base-modified KAKAKAA cations with FBDSA and FBMSA were subjected to CID (Figure 2.3(a) and (b)). The essentially identical dissociation patterns for the two spectra indicate that the $[M + H + \diamond]^+$ ions generated from modified peptides with different reagents are of the same structure or mixture of structures. The fragment peaks with the same mass shift ($\diamond = -19$ Da) are mostly b ions (b_2^\diamond , b_3^\diamond , b_4^\diamond , b_5^\diamond , b_6^\diamond) and some y ions (y_5^\diamond , y_6^\diamond). Their fragmentation sites and abundance ratios are similar to the modified b/y fragment ions (b_2^\blacklozenge , b_3^\blacklozenge , b_4^\blacklozenge , b_5^\blacklozenge , b_6^\blacklozenge , y_5^\blacklozenge , y_6^\blacklozenge) in Figure 2.1(c), which indicates that the mass shift is related to the Schiff base modification. Unmodified b/y fragment ions were also observed.

Experiments analogous to those performed for the KAKAKAA peptide were also performed with the peptide KGAGGKGAGGKL and reagent FBDSA (see Figure 2.2(c), Figure 2.2(d), Figure 2.3(d), and Figure 2.3(e)) leading to similar results. For example, the same loss of

267 Da from activation of Schiff-base-modified peptide cation, $[M + H + \diamond]^+$ ($\diamond = +248$ Da), leading to a dominant $[M + H + \diamond]^+$ product ($\diamond = -19$) was noted (Figure 2.2(c)). Activation of Schiff-base-modified peptide anion $[M - H + \diamond]^-$ ($\diamond = +248$ Da) gave rise primarily to modified backbone fragment ions (e.g., b_{11}^\diamond , y_{11}^\diamond), as shown in Figure 2.2(d). However, the m/z 266 ion (labeled as $[NL - H]^-$ in red) was also observed, but in much lower relative abundance compared to those in the CID spectrum of Schiff-base-modified KAKAKAA anion (Figure 2.1(f)). The results for the KGAGGKGAGGKL peptide ions indicate that the unusual products noted here arise from a process with at least some generality.

2.3.2 Proposed Reaction and Mechanism.

The general experimental steps and observations in positive mode and negative mode with FBDSA as the reagent are summarized in Scheme 2.1(a) and Scheme 2.1(b), respectively. The formation of the unusual product ions and the neutral losses implies a previously unidentified reaction and fragmentation pathway when at least some Schiff-base-modified peptides are subjected to ion trap collisional activation. Considering that the neutral losses for Schiff-base-modified KAKAKAA with FBDSA and FBMSA are 267 Da and 187 Da, respectively, which has the same 80 Da mass difference as the two reagents, it is clear that the neutral loss has the partial structure of the reagents. As mentioned above, the existence of singly negatively charged ions at m/z 266 ($[NL - H]^-$) and m/z 249 ($[NL - H - NH_3]^-$) in the product ion spectra of the modified KAKAKAA and KGAGGKGAGGKL anions generated with FBDSA (Figure 2.1(f) and Figure 2.2(d)) indicates the presence of a relatively acidic site on the 267 Da species. The loss of 17 Da in the CID of $[NL - H]^-$ (Figure 2.3(c)) suggests the presence of an amino group. Considering these observations collectively, the neutral loss is proposed to be 4-(aminomethyl)benzene-1,3-disulfonic acid (AMBDSA, 267 Da) for FBDSA or 2-(aminomethyl)benzene(mono)sulfonic acid

(AMBMSA, 187 Da) for FBMSA (structures in Scheme 2.1(c)). An exact mass measurement of the m/z 266 ($[\text{NL} - \text{H}]^-$) and m/z 249 ($[\text{NL} - \text{H} - \text{NH}_3]^-$) ions using a quadrupole/time-of-flight (QTOF) instrument verified the elemental composition of the proposed product. We note that while the m/z 249 ion can be generated from ammonia loss from deprotonated AMBDSA, a mechanism for the direct formation of the product at m/z 249 (Scheme 2.2) might also contribute to at least some of the m/z 249 signal.

Based on the structures of the neutral loss species, proposed mechanisms for the rearrangement of lysine-containing Schiff-base-modified peptides are shown in Scheme 2.3. The amino groups on the N-terminus and on the ϵ -amino group of the lysine side chain are used here as an example. Either amino group could be modified with the imine bond. The lone electron pair on the nitrogen of the amine attacks the electrophilic carbon of imine to form an eight-membered ring. Further proton transfer and ring rearrangements generate a more stable six-membered ring. Finally, the leaving group is eliminated with a proton to form the neutral loss amine and thus the rearranged peptide product with a ring imine.

Based on the proposed mechanism for the rearrangement reaction, the imine (on the N-terminus or the lysine side chains) could react with amino groups (unmodified N-terminus or lysine side chain amino groups), which is consistent with the CID spectra of $[\text{M} + \text{H} + \diamond]^+$ and $[\text{M} - \text{H} + \diamond]^-$ ions derived from the peptides KAKAKAA and KGAGGKGAGGKL (Figure 2.3). Note that analogous experiments with the model peptide AKAAKA (Figure 2.4) showed the rearrangement reaction taking place at significantly lower levels than with the N-terminal lysine-containing model peptides, which suggests that a lysine at the N-terminal position is particularly reactive.

2.3.3 Reactivity of Histidine- or Arginine-Containing Schiff-Base-Modified Peptides.

Previous studies have indicated that initial Schiff base formation takes place primarily at neutral primary amines to generate the imine. However, the other common basic residues (i.e., nucleophiles), histidine and arginine, might also be able to engage in a rearrangement process involving the imine via mechanisms analogous to those provided in Scheme 2.3. To compare with KAKAKAA results, model peptides RARARAA and HAHAHAA were chosen to study the effect of amino acid residue type. The experimental data are summarized in Figure 2.5.

For positive mode Schiff base modification of RARARAA, doubly protonated RARARAA was subjected to ion/ion reaction with deprotonated FBDSA anions to generate an ion/ion complex of the form $[M + H + FBDSA]^+$. Activation of this complex resulted in the signature water loss to generate the covalently modified product $[M + H + \blacklozenge]^+$. Further activation of this product yielded dominant formation of the rearrangement product, viz., $[M + H + \blacklozenge]^+$, indicated in red in Figure 2.5(a), which is similar to the results from Schiff-base-modified peptide KAKAKAA (Figure 2.1(c)). Since methanediimine loss from the arginine side-chain (labeled with solid square) generates an ornithine residue, [27] which contains an amino group, the rearrangement products with ornithine-containing fragments could also arise from reactions with the ornithine side-chain. Other fragments derived from neutral losses (e.g., ammonia and water) as well as backbone cleavages (e.g., y_3 , y_4 , y_5 , y_6 , and b_6^\blacklozenge) were observed at lesser abundances. Furthermore, the presence of the modified b_6^\blacklozenge ion and lack of any modified y -ions indicate that the FBDSA is covalently attached to the N-terminal region of the peptide, which is consistent with Schiff-base reactivity at a primary amine. The neutral arginine side chain could react with the imine bond through a similar mechanism, as shown in Scheme 2.4(a). In the example of arginine in the N-terminus position, the lone pair on the nitrogen of the guanidine group attacks the imine carbon and forms a nine-membered ring. Rearrangement of the ring and further proton transfer leads to

the formation of the imine ring structure along with the loss of neutral AMBDSA or AMBMSA. When the arginine side chain is protonated, a similar process could occur, as shown in Scheme 2.4(b).

As for negative mode Schiff base modification, singly protonated RARARAA reacted with doubly deprotonated FBDSA anions to form an electrostatic complex $[M - H + FBDSA]^-$, which upon activation generated the signature water loss peak $[M - H + \diamond]^-$. Activation of $[M - H + \diamond]^-$ species formed mainly neutral loss fragments (e.g., ammonia and methanediimine losses) and deprotonated FBDSA $[FBDSA - H]^-$ (Figure 2.5(b)), which indicates that the water loss from the electrostatic complex is partly due to water loss from the peptide itself and not coming from the formation of the imine bond. [18-20] The m/z 249 Da peak was also seen (labeled with 249 in red). No abundant peptide rearrangement product ions were seen, which is consistent with the low signal for the m/z 249 ion. The attack from the imine to the guanidinium group in the positive mode may be more facile than that from the neutral guanidine group to the neutral imine group in the negative mode (Scheme 2.4) but further studies would be required to make such a generalization. We note, however, for the limited set of peptide ions examined in this work, peptide anions generally showed notably less contribution from ions generated by the rearrangement reactions described here than the corresponding positive ions.

The Schiff-base-modified histidine-containing peptides generated by reaction with FBDSA ions showed a different neutral loss associated with a rearrangement (330 Da) than the lysine and arginine containing peptides (267 Da) upon activation (Figure 2.5(c) and (d)). The doubly protonated peptide HAHAAHA reacted with singly deprotonated FBDSA in the positive mode to form an ion/ion complex $[M + H + FBDSA]^+$, which upon CID gave the signature water loss indicating formation of Schiff base modification product $[M + H + \diamond]^+$. Further activation of the

Schiff-base-modified peptide generated backbone cleavages (e.g., b_6^\diamond and y_5) as well as a peak labeled as $[M + H + \spadesuit]^+$ ($\spadesuit = -82$ Da) that is 330 Da lower in mass than the precursor ion $[M + H + \diamond]^+$ (Figure 2.5(c)). In the negative mode, mutual storage of the singly protonated peptide HAHAAHAA and the doubly deprotonated FBDSA led to the formation of a complex $[M - H + FBDSA]^-$ and upon CID of the complex the signature water loss peak $[M - H + \diamond]^-$ was generated. Activation of the ion generated by water loss (Figure 2.5(d)) gave rise predominantly to modified backbone fragment ions (e.g., b_6^\diamond) and neutral losses (e.g., CO_2 losses). $[FBDSA - H]^-$ ions were also observed, along with the m/z 249 Da ion (labeled as 249 in red) and an m/z 329 ion (labeled as $[NL(\spadesuit) - H]^-$), which presumably is the deprotonated species derived from the 330 Da molecule that was observed to be lost in the positive mode experiment described above. The m/z 249 ion can also be generated from the m/z 329 ion through a mechanism shown in the Scheme 2.2.

The rearrangement reaction between the histidine side chain and the imine bond differs from those of the primary amine and guanidine groups because of the ring structure of the imidazole group. The AMBDSA neutral loss observed with lysine and arginine could not form through a similar process for histidine. Instead, the 330 Da neutral loss could be explained by the reaction between the imine bond and the histidine side chain, as shown in Scheme 2.5. With the rearrangement, the histidine side chain moiety transfers to the original imine carbon, and the imine bond shifts to the other carbon connected to the imine nitrogen. Further activation of the rearranged structure could lead to the 330 Da neutral loss. This mechanism is especially favored if the histidine residue is located on the N-terminus of the peptide, since that location enables the rearrangement to occur with a 6-membered ring transition state structure. When histidine is not present at the N-terminus, the mechanism just mentioned is apparently not particularly competitive, as indicated with the analogous experiment performed with doubly protonated AHAAAHA. Activation of the

Schiff-base-modified peptide AHAAAHA in the positive mode (Figure 2.6) yielded abundant backbone cleavages (e.g., b_6^+ and y_4) but no discernable 330 Da neutral loss, in contrast with the modified HAHAAHA ion (Figure 2.5(c)). Interestingly, the AMBDSA neutral loss rearrangement product was seen in low abundance in the spectrum of Figure 2.6, which could implicate the rearrangement reaction involving the imine and amide nitrogen (Scheme 2.6), albeit with lower probability due to the lesser nucleophilicity of an amide nitrogen relative to a primary amine.

2.4 Conclusions

Rearrangement of gas-phase Schiff-base-modified peptides has been observed and characterized using tandem mass spectrometry. Evidence for the reaction is provided by the appearance of a product ion that is nominally 19 Da lower in mass than that of the protonated or deprotonated peptide upon collisional activation of the Schiff-base-modified peptide. Sequence ions with the same -19 Da mass difference may also be observed at relatively low abundance. Upon casual inspection, these products could be mistaken as arising from a water loss but the mass is off by 1 Da. The results are consistent with a nucleophilic attack on the imine site generated via Schiff base formation. The side chains of lysine, arginine, and histidine all show evidence for participation in the rearrangement reaction. Based on the experimental results, Schiff-base-modified peptides of positive polarity more readily undergo the rearrangement reaction compared to the corresponding negatively charged ions. Plausible mechanisms were proposed for the rearrangement reactions between the imine bond and the amine, guanidine and histidine side chain groups. The possible contribution from this rearrangement reaction, at least under ion trap collisional activation conditions, should be taken into account in any work flow involving the Schiff base modification of polypeptide ions.

2.5 References

1. McLafferty FW. Tandem mass spectrometry. *Science* 1981;214(4518), 280-287. doi:10.1126/science.7280693.
2. Santos LS, Pavam CH, Almeida WP, Coelho F, Eberlin MN. Probing the mechanism of the Baylis-Hillman reaction by electrospray ionization mass and tandem mass spectrometry. *Angew Chem Int Ed* 2004;43(33):4330-4333. doi:10.1002/anie.200460059.
3. Aebersold R, Mann M. Mass-spectrometric exploration of proteome structure and function. *Nature* 2016;537(7620):347-355. doi:10.1038/nature19949.
4. Reid GE, Roberts KD, Simpson RJ, O'Hair RA. Selective identification and quantitative analysis of methionine containing peptides by charge derivatization and tandem mass spectrometry. *J Am Soc Mass Spectrom* 2005;16(7):1131-1150. doi:10.1016/j.jasms.2005.03.015.
5. Kinter M, Sherman NE. *Protein Sequencing and Identification Using Tandem Mass Spectrometry*. New York, NY: John Wiley & Sons; 2005.
6. McLuckey SA, Mentinova M. Ion/neutral, ion/electron, ion/photon, and ion/ion interactions in tandem mass spectrometry: do we need them all? Are they enough? *J Am Soc Mass Spectrom* 2011;22(1):3-12. doi:10.1007/s13361-010-0004-9.
7. Prentice BM, McLuckey SA. Gas-phase ion/ion reactions of peptides and proteins: acid/base, redox, and covalent chemistries. *Chem Commun* 2013;49(10):947-965. doi:10.1039/c2cc36577d.
8. Stephenson JL Jr, McLuckey SA. Ion/ion proton transfer reactions for protein mixture analysis. *Anal Chem* 1996;68(22):4026-4032. doi:10.1021/ac9605657.
9. Syka JE, Coon JJ, Schroeder MJ, Shabanowitz J, Hunt DF. Peptide and protein sequence analysis by electron transfer dissociation mass spectrometry. *Proc Natl Acad Sci U S A* 2004;101(26):9528-9533. doi:10.1073/pnas.0402700101.
10. Pilo AL, McLuckey SA. Selective gas-phase ion/ion reactions: enabling disulfide mapping via oxidation and cleavage of disulfide bonds in intermolecularly-linked polypeptide ions. *Anal Chem* 2016;88(18):8972-8979. doi:10.1021/acs.analchem.6b01043.
11. Mentinova M, McLuckey SA. Covalent modification of gaseous peptide ions with N-hydroxysuccinimide ester reagent ions. *J Am Chem Soc* 2010;132(51):18248-18257. doi:10.1021/ja107286p.
12. McGee WM, Mentinova M, McLuckey SA. Gas-phase conjugation to arginine residues in polypeptide ions via N-hydroxysuccinimide ester-based reagent ions. *J Am Chem Soc* 2012;134(28):11412-11414. doi:10.1021/ja304778j.

13. Peng Z, McGee WM, Bu J, Barefoot NZ, McLuckey SA. Gas phase reactivity of carboxylates with N-hydroxysuccinimide esters. *J Am Soc Mass Spectrom* 2015;26(1):174-180. doi:10.1007/s13361-014-1002-0.
14. Pilo AL, Bu J, McLuckey SA. Gas-phase oxidation of neutral basic residues in polypeptide cations by periodate. *J Am Soc Mass Spectrom* 2016;27(12):1979-1988. doi:10.1007/s13361-016-1491-0.
15. Pilo AL, Bu J, McLuckey SA. Transformation of $[M+2H]^{2+}$ peptide cations to $[M-H]^+$, $[M+H+O]^+$, and M^{++} cations via ion/ion reactions: reagent anions derived from persulfate. *J Am Soc Mass Spectrom* 2015;26(7):1103-1114. doi:10.1007/s13361-015-1125-y.
16. Prentice BM, Gilbert JD, Stutzman JR, Forrest WP, McLuckey SA. Gas-phase reactivity of carboxylic acid functional groups with carbodiimides. *J Am Soc Mass Spectrom* 2013;24(1):30-37. doi:10.1007/s13361-012-0506-8.
17. Han H, McLuckey SA. Selective covalent bond formation in polypeptide ions via gas-phase ion/ion reaction chemistry. *J Am Chem Soc* 2009;131(36):12884-12885. doi:10.1021/ja904812d.
18. Hassell KM, Stutzman JR, McLuckey SA. Gas-phase bioconjugation of peptides via ion/ion charge inversion: Schiff base formation on the conversion of cations to anions. *Anal Chem* 2010;82(5):1594-1597. doi:10.1021/ac902732v.
19. Stutzman JR, Luongo CA, McLuckey SA. Covalent and non-covalent binding in the ion/ion charge inversion of peptide cations with benzene-disulfonic acid anions. *J Mass Spectrom* 2012;47(6):669-675. doi:10.1002/jms.2968.
20. Stutzman JR, Hassell KM, McLuckey SA. Dissociation behavior of tryptic and intramolecular disulfide-linked peptide ions modified in the gas phase via ion/ion reactions. *Int J Mass Spectrom* 2012;312:195-200. doi:10.1016/j.ijms.2011.07.002.
21. Cotham VC, Shaw JB, Brodbelt JS. High-throughput bioconjugation for enhanced 193 nm photodissociation via droplet phase initiated ion/ion chemistry using a front-end dual spray reactor. *Anal Chem* 2015;87(18):9396-9402. doi:10.1021/acs.analchem.5b02242.
22. Cotham VC, McGee WM, Brodbelt JS. Modulation of phosphopeptide fragmentation via dual spray ion/ion reactions using a sulfonate-incorporating reagent. *Anal Chem* 2016;88(16):8158-8165. doi:10.1021/acs.analchem.6b01901.
23. Brodbelt JS. Ion activation methods for peptides and proteins. *Anal Chem* 2016;88(1):30-51. doi:10.1021/acs.analchem.5b04563.
24. Xia Y, Wu J, McLuckey SA, Londry FA, Hager JW. Mutual storage mode ion/ion reactions in a hybrid linear ion trap. *J Am Soc Mass Spectrom* 2005;16(1):71-81. doi:10.1016/j.jasms.2004.09.017.

25. Liang X, Xia Y, McLuckey SA. Alternately pulsed nanoelectrospray ionization/atmospheric pressure chemical ionization for ion/ion reactions in an electrodynamic ion trap. *Anal Chem* 2006;78(9):3208-3212. doi:10.1021/ac052288m.
26. Londry FA, Hager JW. Mass selective axial ion ejection from a linear quadrupole ion trap. *J Am Soc Mass Spectrom* 2003;14(10):1130-1147. doi:10.1016/S1044-0305(03)00446-X.
27. McGee WM, McLuckey SA. Gas phase dissociation behavior of acyl-arginine peptides. *Int J Mass Spectrom* 2013;354-355:181-187. doi:10.1016/j.ijms.2013.05.022.

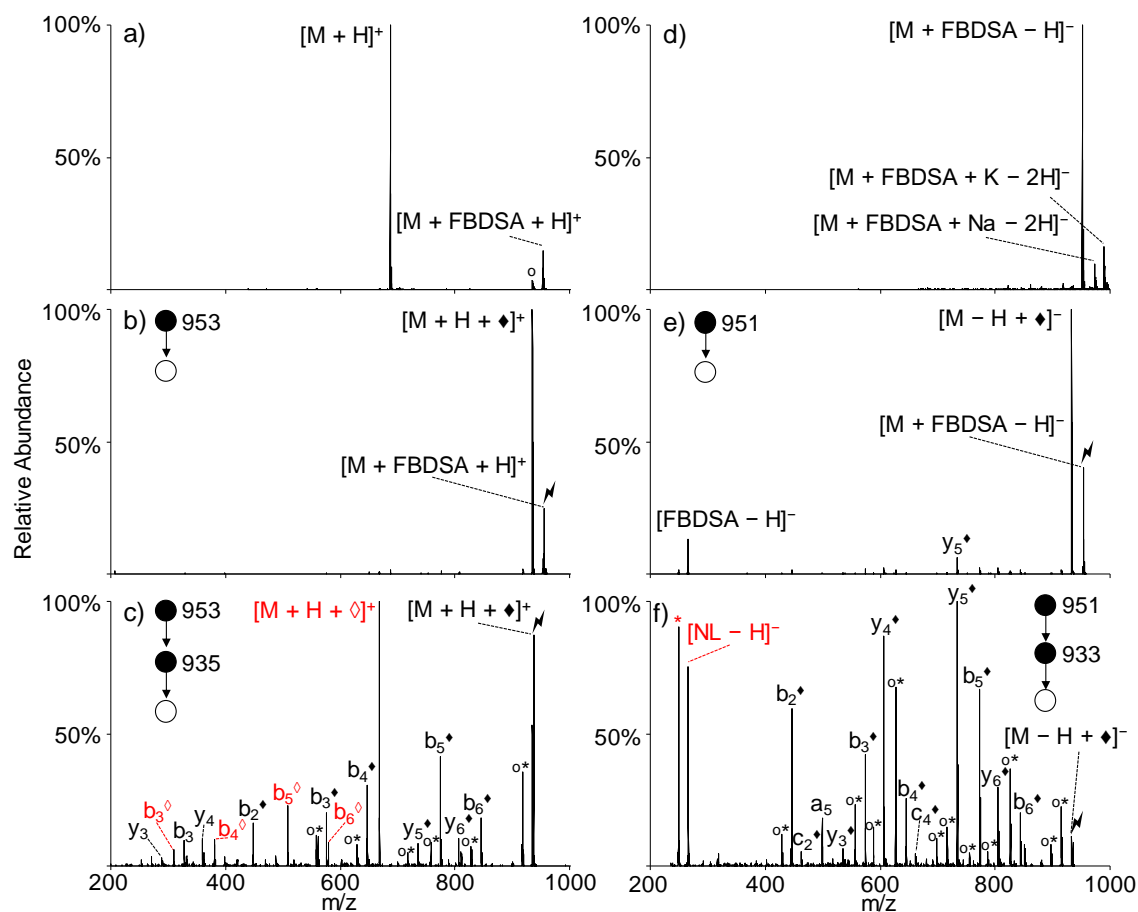


Figure 2.1 Spectra illustrating the gas-phase Schiff base modification of KAKAKAA with FBDSA and its special fragmentation pathway. Positive mode (a) ion/ion reaction between doubly protonated peptide cation $[M+2H]^{2+}$ and singly deprotonated FBDSA $[FBDSA-H]^-$, (b) CID of the ion/ion complex $[M+FBDSA+H]^+$ forming a Schiff-base-modified peptide $[M+H+◆]^+$, (c) Ion-trap CID of $[M+H+◆]^+$. Negative mode (d) ion/ion reaction between singly protonated peptide cation $[M+H]^+$ and doubly deprotonated FBDSA $[FBDSA-2H]^{2-}$, (e) CID of the ion/ion complex $[M+FBDSA-H]^-$ forming a Schiff-base-modified peptide $[M-H+◆]^-$, (f) ion-trap CID of $[M-H+◆]^-$. Degree symbols (°) denote water losses (-18 Da). Asterisks (*) denote ammonia losses (-17 Da). Solid diamonds (◆) denote ion mass shift with Schiff base modification (+248 Da). Hollow diamonds (◇) denote the special fragmentation products (-19 Da) and all products in the special fragmentation pathway are labeled in red.

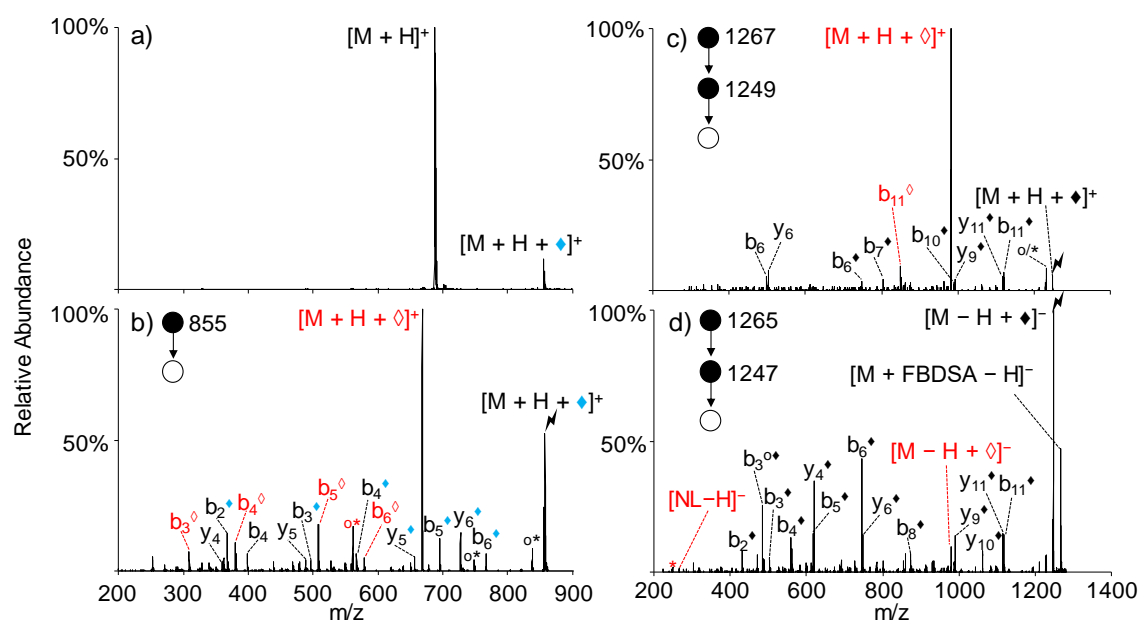


Figure 2.2 Spectra illustrating the gas-phase Schiff base modification and rearrangement reaction of KAKAKAA with FBMSA ((a) and (b)) and KGAGGKGAGGKL with FBDSA ((c) and (d)). KAKAKAA and FBMSA in positive mode: (a) ion/ion reaction between doubly protonated KAKAKAA, $[M+2H]^{2+}$, and singly deprotonated FBMSA $[FBMSA-H]^-$, (b) Ion trap CID of the Schiff-base-modified peptide $[M+H+\diamond]^+$. KGAGGKGAGGKL and FBDSA in both modes: ion trap CID of (c) the Schiff-base-modified peptide $[M+H+\diamond]^+$ in positive mode and (d) the Schiff-base-modified peptide $[M-H+\diamond]^-$ in negative mode. Degree symbols ($^\circ$) denote water losses (-18 Da). Asterisks ($*$) denote ammonia losses (-17 Da). Solid diamonds (\blacklozenge) denote ion mass shift with Schiff base ($\blacklozenge=+168$ Da for FBMSA, $\blacklozenge=+248$ Da for FBDSA). Hollow diamonds (\diamond) denote peptide rearrangement products (-19 Da) and all products in rearrangement pathway are labeled in red.

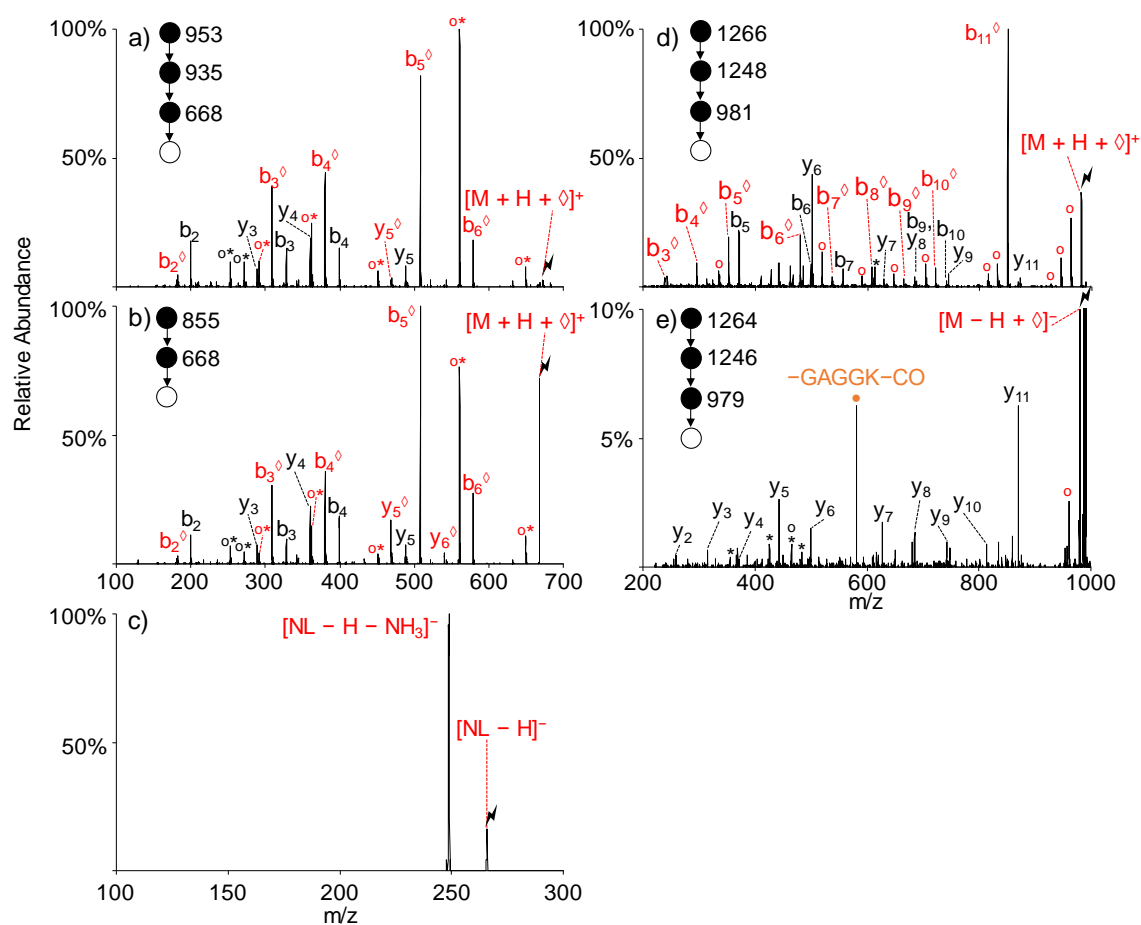


Figure 2.3 Ion trap activation of the ions generated via rearrangement for Schiff-base-modified KAKAKAA and KGAGGKGAGGKL, including (a) $[M + H + \Delta]^+$ generated from CID of Schiff-base-modified KAKAKAA cation $[M + \text{FBDSA} + \text{H} - \text{H}_2\text{O}]^+$, (b) $[M + H + \Delta]^+$ generated from CID of Schiff-base-modified KAKAKAA cation $[M + \text{FBMSA} + \text{H} - \text{H}_2\text{O}]^+$, (c) $[\text{NL} - \text{H}]^-$ generated from CID of Schiff-base-modified KAKAKAA anion $[M + \text{FBDSA} - \text{H} - \text{H}_2\text{O}]^-$, (d) $[M + H + \Delta]^+$ generated from CID of Schiff-base-modified KGAGGKGAGGKL cation $[M + \text{FBDSA} + \text{H} - \text{H}_2\text{O}]^+$, and (e) $[M - H + \Delta]^-$ generated from CID of Schiff-base-modified KGAGGKGAGGKL anion $[M + \text{FBDSA} - \text{H} - \text{H}_2\text{O}]^-$ (spectrum y-axis zoomed in 10 times to reduce the noise peak). Degree symbols ($^\circ$) denote water losses (-18 Da). Asterisks (*) denote ammonia losses (-17 Da). Hollow diamonds (\diamond) denote peptide rearrangement products (-19 Da) and all products in rearrangement pathway are labeled in red. The peak labeled with an orange solid circle (581 Da) is proposed to be a ring cleavage fragment (proposed structure in Scheme 2.7).

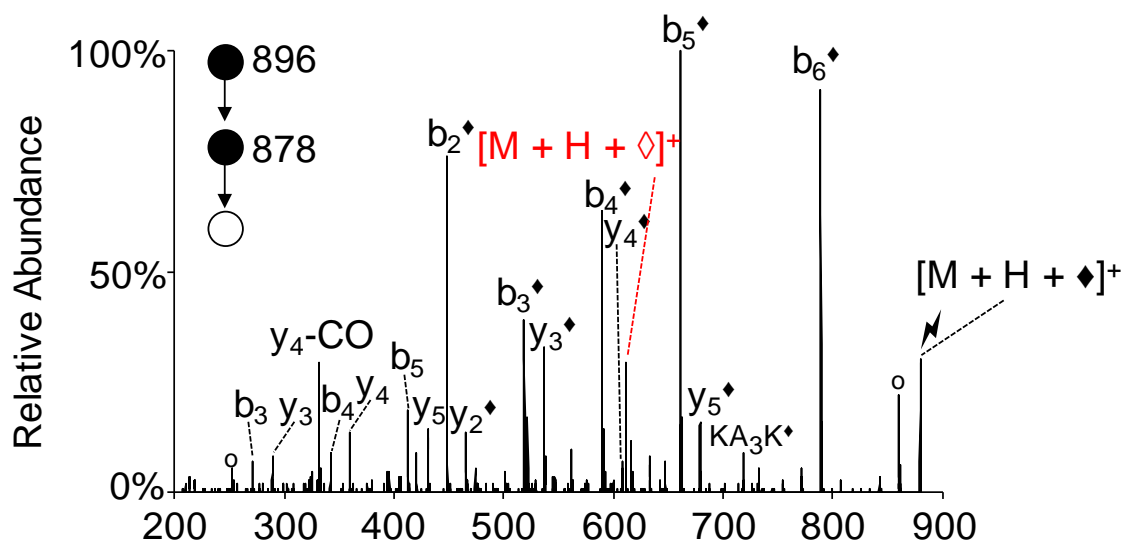


Figure 2.4 Ion trap CID of the gas-phase Schiff-base-modified peptide ions formed using deprotonated FBDSA and doubly protonated AKAAAKA. Degree symbols (°) denote water losses (−18 Da). Black solid diamonds (◆) denote ions with Schiff base modification (+248 Da). Hollow diamonds (◊) denote peptide rearrangement products (−19 Da) and all rearrangement products are labeled in red.

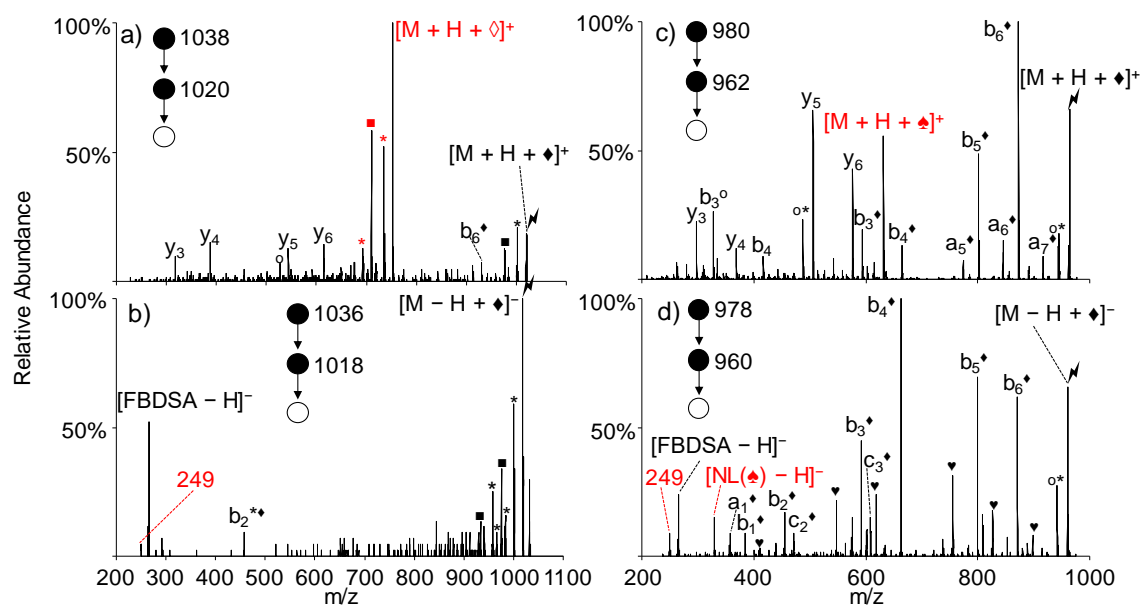


Figure 2.5 Ion trap CID of the gas-phase Schiff-base-modified peptides formed using (a) singly deprotonated FBDSA and doubly protonated RARARAA, (b) doubly deprotonated FBDSA and singly protonated RARARAA, (c) singly deprotonated FBDSA and doubly protonated HAHAHAA, and (d) doubly deprotonated FBDSA and singly protonated HAHAHAA. Degree symbols ($^{\circ}$) denote water losses (-18 Da). Asterisks (*) denote ammonia losses (-17 Da). Black solid diamonds (\blacklozenge) denote ions with Schiff base modification ($+248$ Da). Solid squares (\blacksquare) denote the arginine side chain methanediimine ($\text{H}_2\text{N}=\text{C}=\text{NH}_2$) losses to form ornithine (-42 Da). Solid hearts (\heartsuit) denote carbon dioxide losses (-44 Da). Hollow diamonds (\diamond) denote peptide rearrangement products (-19 Da) with the formation of the AMBDSA neutral loss. Solid spades (\spadesuit) denote histidine-specific rearrangement products (-82 Da) with the formation of the 330 Da neutral loss. All rearrangement related products are labeled in red.

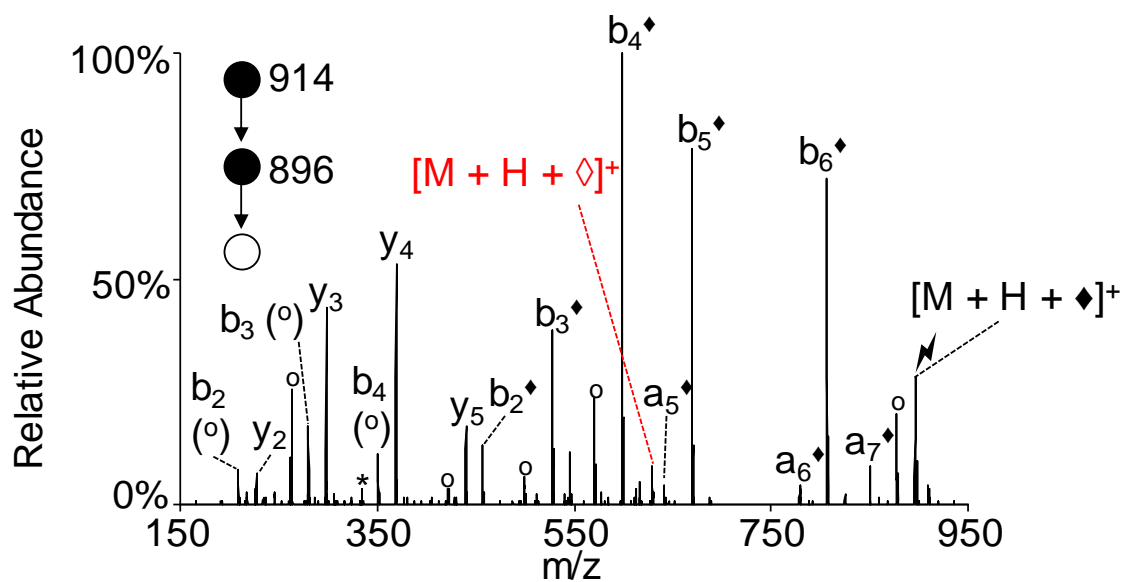
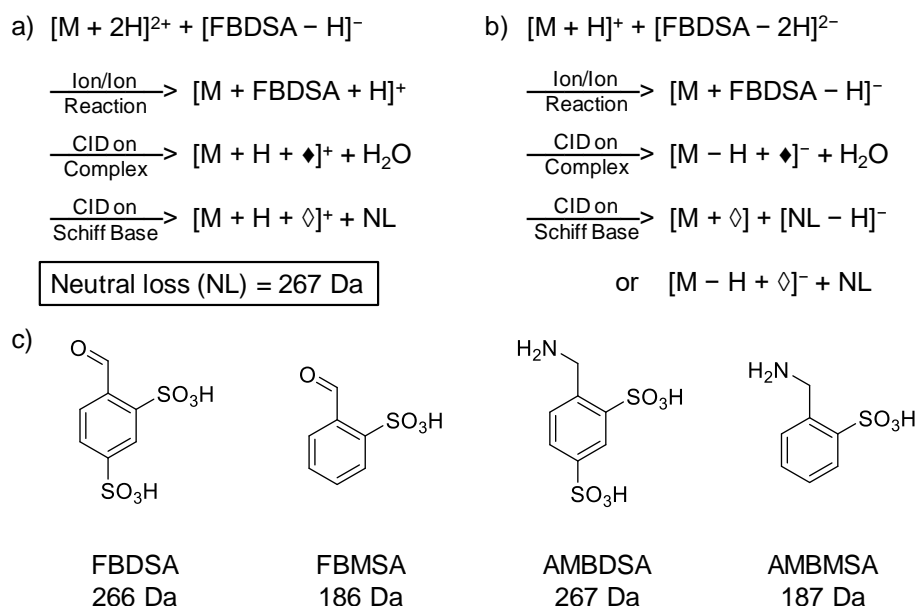
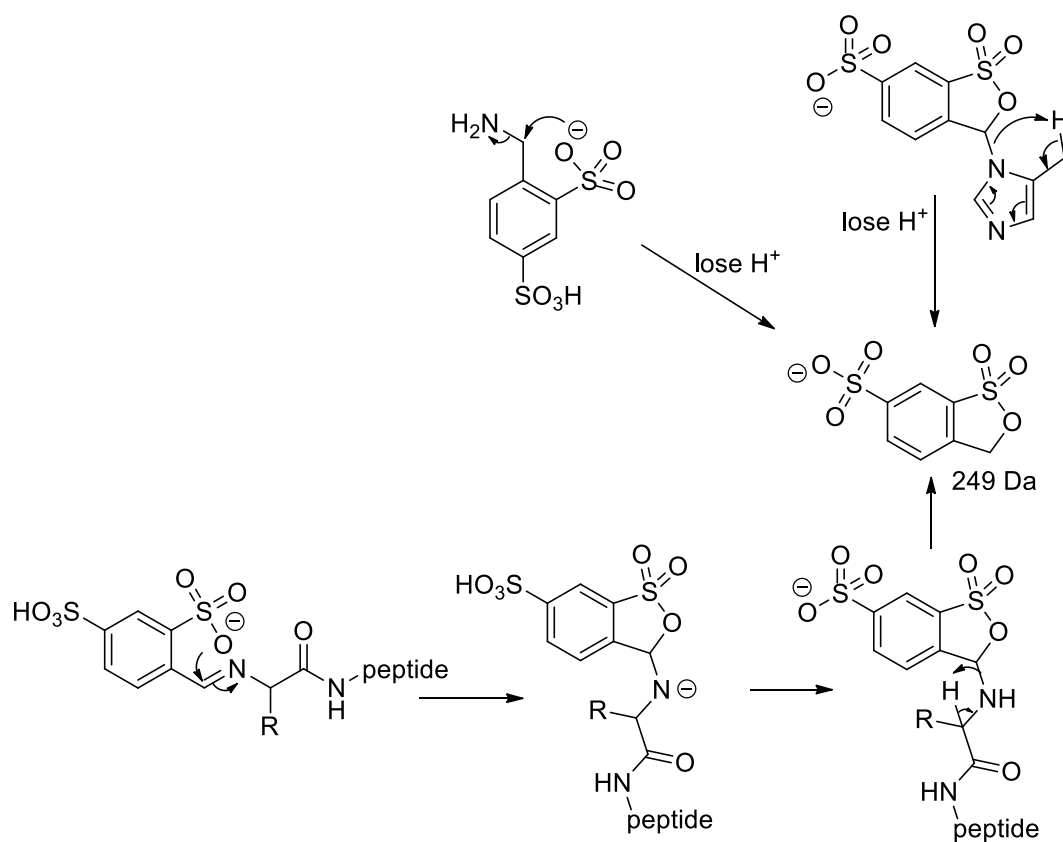


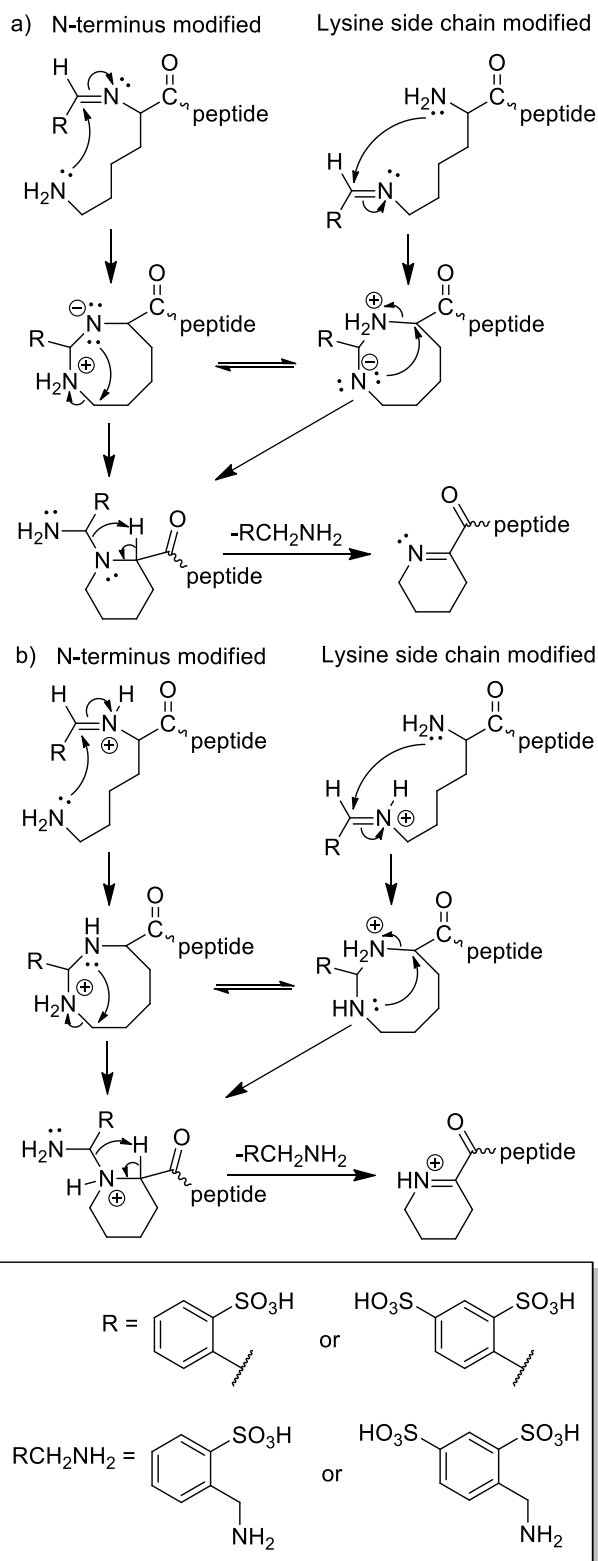
Figure 2.6 Ion trap CID of the gas-phase Schiff-base-modified peptide ions formed using deprotonated FBDSA and doubly protonated AHAAAHA. Degree symbols ($^{\circ}$) denote water losses (-18 Da). Asterisks (*) denote ammonia losses (-17 Da). Black solid diamonds (\blacklozenge) denote ions with Schiff base modification ($+248$ Da). Hollow diamonds (\diamond) denote peptide rearrangement products (-19 Da) and all rearrangement products are labeled in red. The water losses in parentheses denote that the peaks could be assigned both ways and it is not determined which one is the more accurate assignment.



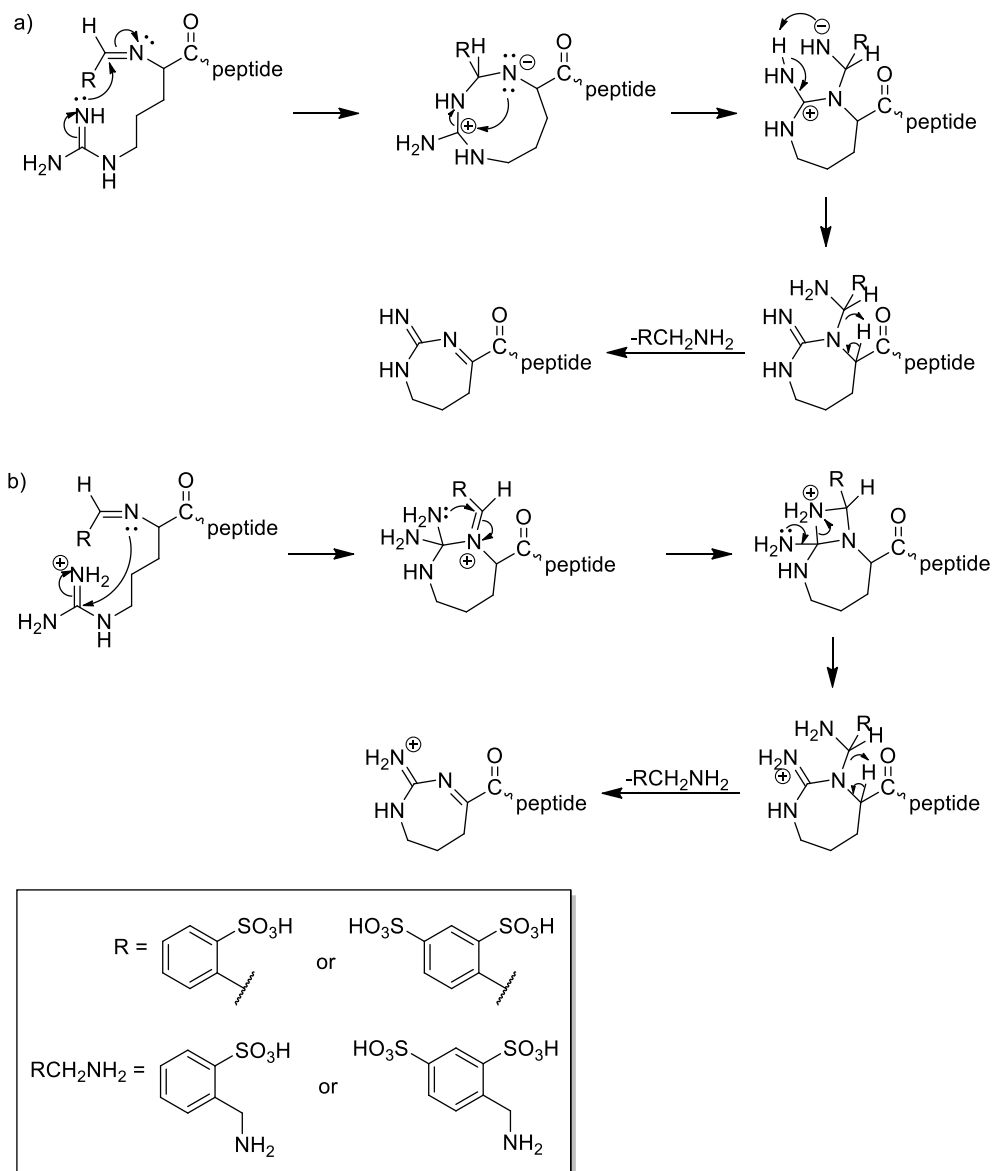
Scheme 2.1 Reactions for Schiff base modification and fragmentation in (a) positive mode and (b) negative mode with FBDSA as an example. (c) Structures of Schiff base modification reagents (FBDSA, FBMSA) and proposed neutral loss structures (AMBDSA and AMBMSA). Solid diamonds (◆) denote ion mass shift with Schiff base modification (+248 Da for FBDSA). Hollow diamonds (◇) denote the mass shift of the special fragmentation products (-19 Da).



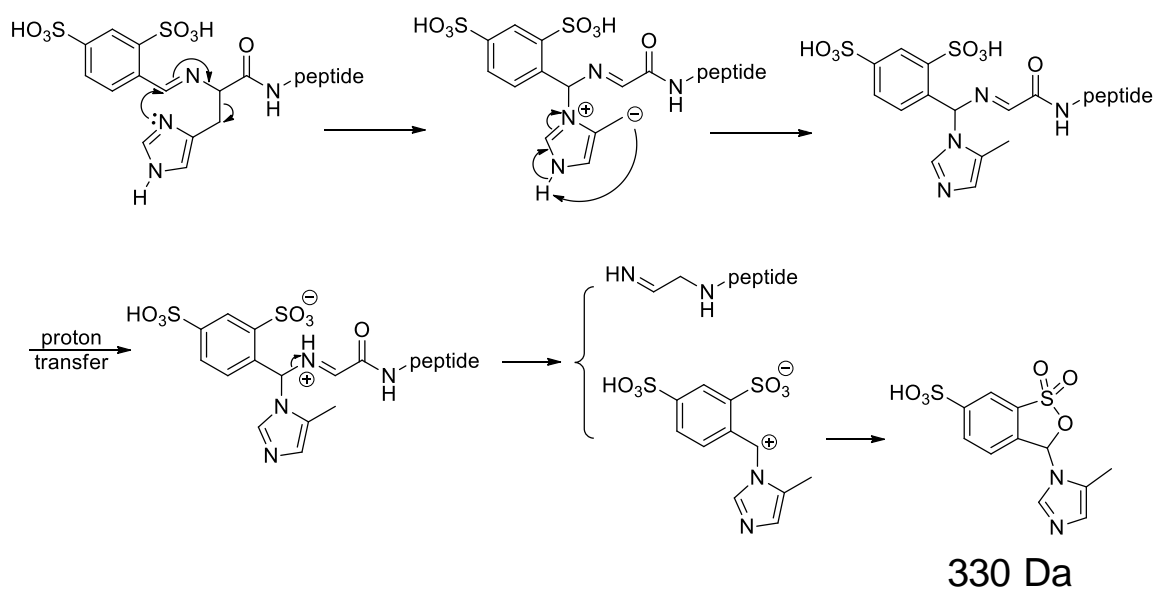
Scheme 2.2 Proposed mechanisms for the formation of the 249 Da peak from the fragmentation of the neutral losses, or from the fragmentation of the Schiff-base-modified peptide itself. N-terminal Schiff base modification was shown here as an example.



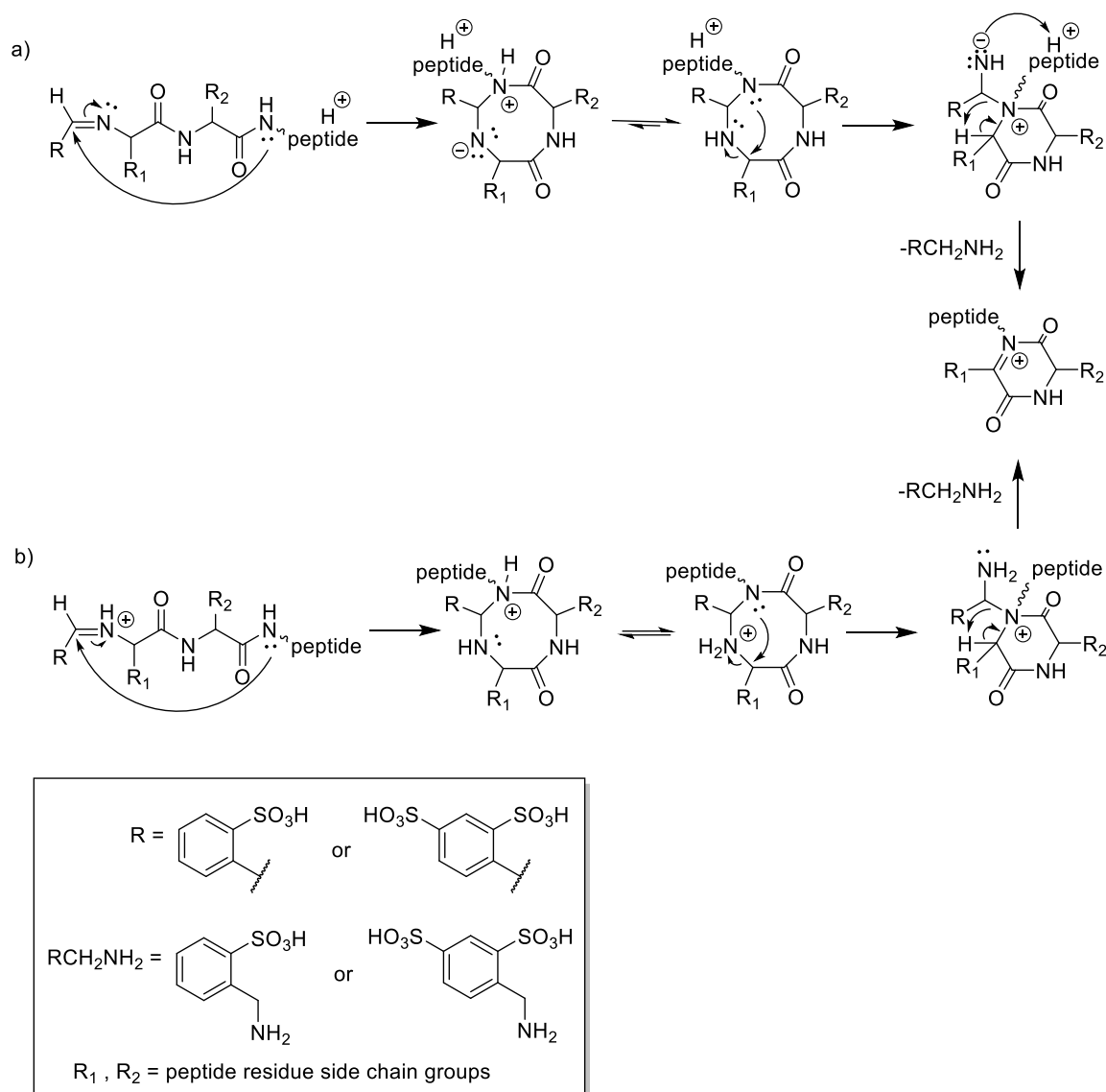
Scheme 2.3 Proposed mechanism for the rearrangement of the lysine-containing Schiff-base-modified peptides between an amino group and (a) a neutral imine group, or (b) a protonated imine group. N-terminal lysine residue is used here as an example.



Scheme 2.4 Proposed mechanism for rearrangement reaction of arginine-containing Schiff-base-modified peptides between an imine group and a) a neutral guanidine group or b) a protonated guanidinium group. N-terminal arginine residue is used here as an example.



Scheme 2.5 Proposed mechanism for rearrangement reaction of histidine-containing Schiff-base-modified peptides between an imine group and a neutral imidazole group. N-terminal histidine residue is used here as an example.



Scheme 2.6 Proposed mechanism for rearrangement reaction of Schiff-base-modified peptides between an amide group and (a) an imine group, or (b) a protonated imine group. Imine formed on the N-terminus is used here as an example.

CHAPTER 3. DISTINCTION OF NON-SPECIFIC AGGREGATION IN ESI FROM SOLUTION-PHASE AGGREGATION: THEORETICAL CONSIDERATIONS

3.1 Introduction

Electrospray ionization mass spectrometry (ESI-MS) has been widely used in biomolecule identification, quantitation and structural analysis. [1] Its potential in aggregation detection is especially promising, because more and more pharmaceuticals are biomolecule solutions that contain biomolecules like peptides and proteins, which can suffer from the aggregation problem in its manufacture, transportation, and storage processes. [2, 3] Since ESI is an ionization method that directly ionize analytes from solutions, and MS directly measures the m/z of the analyte species to know the analyte's oligomeric state, ESI-MS is a competitive approach for aggregation detection. [4]

In the application of ESI-MS to aggregation detection, the non-specific aggregation phenomenon can affect the accuracy of the measurement. [5] Non-specific aggregation in ESI refers to the non-covalent clustering of the analytes in the ESI process. [6] As the charged droplets are formed from the ESI spray, they undergo solvent evaporation and fissions at the Rayleigh limit, which produces smaller progeny droplets. [7] If the analyte ions are ejected from the droplet via Ion Evaporation Model (IEM) or Chain Ejection Model (CEM), it is unlikely for the analytes to be ejected as analyte clusters. [8] However, if the analyte ions are formed through Charge Residue Model (CRM), because the analyte ions stay inside the droplet, there exists the possibility that more than one analyte molecules stay in the same final droplet. [9] The multiple analyte molecules would then get the charges together and show up as an aggregate ion of the analyte on the spectrum.

The non-specific aggregation in the ESI process has been recognized by the ESI-MS society and confirmed by experimental data. [5, 10, 11] Due to the characteristics of the ion generation process via CRM, people have used Poisson statistics to describe the quantitative relationship among the non-specific aggregates. [10] Theoretically, because in CRM analyte molecules tend to stay in the droplet solution phase and are not favorably ejected by other special pathways, the distribution of the analyte molecules in the droplets can be considered as random distribution. [9] Statistically, for a random distribution, the possibility of having a certain number of analytes in a defined volume should follow Poisson statistics. [12]

The application of Poisson statistics to differentiate non-specific aggregation in ESI and solution-phase aggregation has been explored by multiple research groups. The Benesch group used random distribution of analyte to calculate the actual number of analyte molecules in a defined volume via Monte Carlo calculations. [13] Even though they didn't mention Poisson statistics in their paper, their calculation of the number of analyte molecules in a defined volume is actually an attempt to simulate Poisson statistics. [6] The Zachariah group used Poisson statistics to deduce theoretical calculation equations of the ratio among monomer, dimer and trimer generated in the ESI process. [6] Afterwards they applied the theoretical equations to measure the extent of non-specific aggregation in the ESI process versus the solution-phase aggregation. [6, 14] They also applied the theoretical equations to protein concentration measurement. [14, 15]

Here, a new method based on Poisson statistics of the non-specific aggregation for analytes formed by CRM in the ESI process is proposed to distinguish the solution-phase aggregation from the ESI-droplet non-specific aggregation. This method does not require Monte Carlo simulations like the Benesch group, nor does it require the theoretical equation deduction like the Zachariah group.

3.2 Experimental

3.2.1 Materials

Human insulin, zinc acetate, ammonium chloride and ammonium acetate were purchased from Sigma Aldrich (St. Louis, MO, USA). Water (Optima LC/MS grade) and ammonium hydroxide (certified ACS plus grade) was purchased from Fisher Chemical (Waltham, MA, USA). Acetic acid was purchased from Macron Fine Chemicals (Center Valley, PA, USA). Phenol was purchased from Mallinckrodt Chemicals (Center Valley, PA, USA). The insulin hexamer solution was prepared in an aqueous solvent with 20 μM $\text{Zn}(\text{OAc})_2$, 10 μM NH_4Cl , 5 mM phenol and 300 mM NH_4OAc adjusted to a pH of 7.4.

3.2.2 Mass Spectrometry

All mass spectrometric experiments were performed on TripleTOF 5600, a hybrid quadrupole / time of flight (TOF) mass spectrometer (SCIEX, Concord, Canada) previously modified for ion-ion reactions. [16] The sample solutions were sprayed using positive nano-electrospray ionization (nESI). The analyte cations were transferred to q2 and trapped there. If it was a direct analysis of the analyte, the analyte cations would be transferred to the TOF analyzer for m/z determination. If an ion-ion reaction was performed, when the analyte cations were trapped in q2, the reagent anions would be sprayed using negative nESI and transferred to q2. The analyte cations and reagent anions were mutually stored in q2 for 100-500 ms to allow the ions react and then the product ions were transferred to the TOF for m/z analysis. The instrument parameters were adjusted to be as soft as possible (i.e., minimal potential gradients along the ion path) so that the aggregates were not destroyed during the transmission of ions from the ion source to the detector.

3.2.3 Data Analysis

The abundances of ions in the m/z region for the monomer and each aggregate species were each summed to calculate the area of each species with baseline subtraction. For droplet-size-measurement solutions, after obtaining the area of each species, the experimental percentages of the oligomer species were calculated. Then a theoretical Poisson distribution was generated from a guess μ (average number of analyte molecules/droplet, see below in 3.3.2 Theory for Model) value, with the theoretical percentages calculated for each oligomer size. A Poisson fitting was done via minimizing the squares of the differences between the experimental and theoretical percentages by changing the guess μ value. Then the fitted μ value can be used to calculate droplet size using Equation 3.2. A list of symbols and abbreviations are listed in Table 3.1.

For sample aggregation detection, the sum of squares of the differences between theoretical and experimental aggregate distributions was calculated to see if any sample aggregation in solution can be detected. If the sum of squares for the sample solution is larger than that for the droplet-size-measurement solutions, then the sample is considered to have a measurable degree of aggregation in solution.

3.2.4 MATLAB Simulations

3.2.4.1 Droplet Size Distribution

The droplet diameter distribution is assumed to be a Gaussian distribution [17, 18] with an average droplet diameter of μ_G (nm) and a standard deviation of σ_G (nm). The concentration of the non-aggregating solution is set to be c (mol/L). The diameters included in the simulation range from 0 to $2\mu_G$ with a step size of 0.1 nm. For each droplet diameter, a Poisson distribution of aggregates from dimer to hexamer was calculated. The observed aggregate distribution was then obtained by summing together all the Poisson distributions for each droplet size. After that, the

observed aggregate distribution is fitted to a Poisson distribution by least squares fitting to obtain the experimentally measured Poisson distribution parameter μ_p . The experimental droplet diameter d_0 was calculated from μ_p and c .

3.2.4.2 Concentration Error

The observed concentration of solution is set to be c_0 (mol/L). The percentage of the difference between actual concentration and the observed concentration relative to the observed concentration is set to be $A\%$. The true droplet diameter is set to be d . Using the actual concentration in the solution $c_0(1 - A\%)$ and the droplet diameter d , a Poisson distribution was generated as the observed aggregate distribution. Then the observed aggregate distribution was fitted to Poisson distribution by the least squares fitting to obtain the experimentally measured Poisson distribution parameter μ_p . After that the experimental droplet diameter d_0 was calculated from μ_p and c_0 .

3.2.4.3 Aggregation in Droplet-Size-Measurement Solution

The analytical concentration of analyte is set to be c_0 (mol/L). The percentage of the monomers aggregated is set to be $A\%$. The true droplet diameter is set to be d . The aggregation product is set to be either dimer only or trimer only, and its concentration c_{agg} is calculated based on c_0 and $A\%$. Using the actual concentrations of each species in the solution and the droplet diameter d , Poisson distributions of monomer and the aggregated product was generated. For cases of different species staying in the same droplet, the probability was calculated by the multiplication of the possibility of each species because the two species staying in the same droplet are considered independent events. Then the probabilities with the same number of analytes in the droplet were combined to generate the observed aggregate distribution. Later the observed aggregate

distribution was fitted to Poisson distribution by the least squares fitting to obtain the experimentally measured Poisson distribution parameter μ_p . Then the experimental droplet diameter d_0 was calculated from μ_p and c_0 .

3.3 Results and Discussion

3.3.1 Issue of Droplet-Induced Non-specific Aggregation in ESI-MS

ESI-MS analysis works with solution samples. In ESI, a high voltage is applied to the solution to generate charged initial droplets. Due to solvent evaporation and charge repulsion, the droplets shrink in size on their way to the mass spectrometer and will break into smaller progeny droplets. In the end, ions form from the final droplets for subsequent mass analysis. [19]

Ideally, the gas-phase ions detected by the mass spectrometer reflect the identities and abundances of the analyte species in the solution phase. However, as the droplets break down in the ESI process, it is possible to have multiple analytes present in the same final-stage droplet. It is therefore possible for oligomerization to occur via the concentration that occurs as the solvent disappears. An example of the issue is shown in Scheme 3.1. A trimer observed in the mass spectrum can be formed from one trimer in the solution, or from three monomers in the same final droplet. Only when we distinguish the two sources of aggregates will we be able to determine if there is aggregation in the solution.

3.3.2 Theory for Model

3.3.2.1 Poisson Statistics and Its Relationship with ESI Process

Based on the principles of statistics, people have long used Poisson statistics to describe the non-specific aggregation in the ESI droplet. [20, 21] If the analyte ions are formed through the

Charge Residue Model (CRM), i.e., the distribution of the analytes in the droplet is random, then the possibility of having x analytes in the final droplet should follow a Poisson distribution:

$$P(x, \mu) = \frac{e^{-\mu} \mu^x}{x!} \quad (3.1)$$

where $P(x, \mu)$ is the probability of having x analytes in the final droplet, x is the number of analytes in the final droplet and μ is the average number of analytes per droplet. The average number of analytes per droplet is related to the concentration of analyte in the droplet, which is connected with the concentration of analyte in the bulk solution. [22] As a first-order approximation, we use the bulk-solution concentration as an approximation to the analyte concentration in the droplet, such that:

$$\frac{\mu}{V_{drop}} = c_{bulk} \quad (3.2)$$

where V_{drop} is the volume of the final-stage droplet and c_{bulk} is the analyte concentration in the bulk solution. Therefore, the Poisson distribution of the analytes in the final droplet is affected by the bulk solution concentration c_{bulk} and droplet volume V_{drop} via Equation 3.1 and Equation 3.2.

3.3.2.2 Qualitative Application of Poisson Statistics to Aggregation Detection

Since each species in the solution goes through the ESI process generating a Poisson distribution of its droplet-induced aggregates, the final aggregate distribution in the mass spectrum would comprise a convolution of the Poisson distributions of all the species in the solution, including mixed aggregates. (An implicit assumption is that the conditions for sampling and transmission of ions does not destroy aggregates.) If only one analyte exists in the solution, then the mass spectrum would show a Poisson distribution of its aggregate species. On the other hand, if there are aggregates in the solution, the final aggregate distribution would not follow Poisson distribution. In this way, we can determine if there is solution-phase aggregation.

For example, the MS analysis of 5 μM insulin in an aqueous solvent with 20 μM $\text{Zn}(\text{OAc})_2$, 10 μM NH_4Cl , 5 mM phenol and 300 mM NH_4OAc adjusted to a pH of 7.4 showed abundant hexamer peaks aside from the monomer and dimer peaks (Figure 3.1). No intermediate oligomeric states (trimer, tetramer and pentamer) are observed on the spectrum. Compared to common Poisson distributions (Figure 3.2), where a consecutive increase or decrease of the probability is observed with an increase of x , the distribution of monomer, dimer and hexamer in the insulin solution doesn't follow the Poisson distribution and is a good indication of hexamer formation in the solution.

However, in early-stage aggregation, the non-Poisson distribution may not be as apparent as the Figure 3.1 example. Therefore, a quantitative approach of the model is necessary for more accurate determination of solution-phase aggregation.

3.3.2.3 Quantitative Application of Poisson Statistics to Aggregation Detection

For the distinction between solution-phase and ESI-process-induced aggregation, a quantitative model based on Poisson statistics is proposed here. If we obtain the distribution of the aggregates from the experimental data and compare it with the theoretical Poisson distribution from the ESI process, we would know if the distribution of aggregates is considered Poisson or non-Poisson. The comparison can be quantitatively completed by calculating the sum of squares of the differences between the theoretical and experimental distributions for the aggregates.

The experimental distribution of aggregates can be obtained by summing the intensities of peaks that belong to the same oligomeric state. The theoretical Poisson distribution can be calculated from Equation 3.1 if the μ for the analyte is known. To calculate the μ , the concentration of the analyte and the droplet size are needed (Equation 3.2). Usually the concentration is known, so the droplet size needs to be determined first before we obtain the value of μ .

There are multiple methods proposed to measure or to calculate the droplet size for the ESI process, [23, 24] but they are suitable only to the initial droplets and not to the progeny droplets or final-stage droplets. Here, a method that indirectly measures the effective droplet size of the ESI process is proposed. If there is no aggregation in a solution, the aggregate distribution on the mass spectrum is directly the Poisson distribution of the analyte from the ESI process. Therefore, we can fit the experimental distribution to Poisson distribution and obtain the μ value for the non-aggregating solution. With a known concentration, the effective final-stage droplet size V_{drop} of the ESI method can be calculated and used for other solutions.

As a result, the quantitative approach of the model consists of two steps: droplet size determination and sample solution-phase aggregation detection (Scheme 3.2). In the droplet size determination step, we first take the mass spectrum of a non-aggregating solution with known concentration (labeled as c in the flow chart). The aggregates in the mass spectrum of the non-aggregating solution all come from the ESI process. Therefore, the distribution of aggregates from the non-aggregating solution is calculated by summation of the intensities of their corresponding peaks, and then is fit to Equation 3.1 to obtain the μ of the non-aggregating solution. With μ and c of the non-aggregating solution known, Equation 3.2 is used to calculate the droplet size of our method (V_{drop}). A sum of squares of the difference between experimental ESI-induced non-specific aggregate distribution (from experimental data) and the theoretical ESI-induced aggregate distribution (from fitted μ of experimental data) is calculated as the standard value to determine when the system should be considered as non-Poisson statistics.

Then in the solution-phase aggregation detection step, the mass spectrum of the sample solution is obtained. The oligomer distribution is the combination of solution-phase aggregation (if any) and ESI droplet-induced aggregation. The ESI droplet-induced aggregate distribution can

be calculated from the V_{drop} and the sample concentration (c_s) using Equation 3.1 and Equation 3.2. Finally, the actual oligomer distribution and the ESI droplet-induced aggregate distribution are compared by calculating the sum of squares of their differences for each oligomer size. If the difference of the two distributions is larger than the difference for the non-aggregating solution, then solution-phase aggregation in the sample is indicated.

3.3.3 Factors that Affect Droplet Size Determination (MATLAB Simulations)

An accurate droplet size measurement is the key to obtaining the ESI aggregate distribution of the sample solution. Several sources of error are identified and studied using MATLAB simulations, including droplet size distribution, concentration error, and aggregation in the droplet-size-measurement solution. Knowing how each factor plays a role in the droplet size determination assists in the proper design of the experiment for droplet size measurement and aggregation detection.

3.3.3.1 Droplet Size Distribution

Studies have shown that the droplet size is not uniform for different initial droplets [5, 23] and the fissioning process is not identical for each droplet either. [25-27] If the droplet size V_{drop} is different for each droplet, then the analytes in each droplet will have different μ 's and follow different Poisson distributions, leading to a distorted Poisson distribution in the mass spectrum. Often in theoretical discussions, a narrow droplet size distribution is assumed. [5, 6, 14, 15] Here the influence of non-uniform droplet size distribution on the droplet size measurement is discussed using MATLAB simulations.

In the MATLAB simulation, a Gaussian distribution of droplet diameter is assumed. With a set concentration c , an “observed aggregate distribution” was simulated by the sum of all the Poisson distributions of each droplet diameter. Then the “observed aggregate distribution” is fitted

with Poisson distribution, mimicking the actual experimental data analysis process. Using the μ from the Poisson fitting, a droplet diameter is calculated from μ and c based on Equation 3.2. The calculated droplet diameter is compared with the original average droplet diameter to see the effect of droplet size distribution.

In Figure 3.3, the relationship between the width of the droplet size distribution and the accuracy of the calculated droplet size is shown. Based on the simulation results, broader droplet size distribution (i.e., a large σ_G) leads to a larger error in the calculated droplet diameter. Furthermore, measurement of a larger average droplet diameter (μ_G) is less prone to the error caused by the spread of droplet size. For example, for $Error(\mu_G, \sigma_G) = Error(10, 1) = 0.57$ and $Error(\mu_G, \sigma_G) = Error(20, 2) = 0.27$, even when the standard deviation of droplet size distribution is the same relative to the average value (10%), a smaller error in the droplet size measurement is found for a larger average droplet size.

3.3.3.2 Concentration Error

Due to apparatus limitations and dilution errors, there could be concentration error in our analysis. Aggregation in the solution could also lead to concentration error, as we usually consider the analytical concentration as the monomer concentration in the solution. Since concentration is directly involved in the droplet size calculation process, the effect of concentration error is discussed here.

Define the true uniform droplet diameter to be d , the true concentration to be c , the observed concentration to be c_0 , the relative error of that observed concentration value to be $err_c\%$, the calculated μ from the simulated observed distribution to be μ_p , and the measured droplet diameter to be d_0 . The percent error of concentration is calculated to be

$$err\% = \left(\frac{c_0}{c} - 1\right) \times 100\% \quad (3.3)$$

So the relationship between c_0 and c should be

$$c = \frac{c_0}{1 + err_c\%} \quad (3.4)$$

Since the observed distribution is an ideal Poisson distribution generated from d and c , the μ_P would be the same as the μ for the solution with the true concentration, which is

$$\mu_P = c \cdot V_{drop} = \frac{c_0}{1 + err_c\%} \cdot \frac{\pi d^3}{6} \quad (3.5)$$

The experimental droplet volume V_{drop0} was then calculated from μ_P and c_0 by the equation

$$V_{drop0} = \frac{\mu_P}{c_0} = \frac{1}{1 + err_c\%} \cdot \frac{\pi d^3}{6} \quad (3.6)$$

Therefore, the calculated droplet diameter d_0 would be

$$d_0 = \left(\frac{1}{1 + err_c\%}\right)^{\frac{1}{3}} \cdot d \quad (3.7)$$

with the relative error of the droplet diameter measurement to be

$$err_d\% = \left[\left(\frac{1}{1 + err_c\%}\right)^{\frac{1}{3}} - 1 \right] \times 100\% \quad (3.8)$$

With Equation 3.8, we can plot the relationship between $err_d\%$ and $err_c\%$, as shown in Figure 3.4. From the figure, we could see that larger absolute concentration error leads to larger error of droplet size measurement. The increasing rate of the droplet size error is different though with positive or negative concentration error. When the same absolute concentration error is induced, larger error in droplet size measurement is expected from a negative concentration error, i.e., calculated concentration lower than the true concentration. The MATLAB simulation results with different concentration errors match with the results obtained from the equations above.

3.3.3.3 Aggregation in the Droplet-Size-Measurement Solution

The selection of the droplet-size-measurement solution, or the non-aggregating solution, is very important as it sets up a standard on what should be called as an aggregating solution. The analyte and the solvent condition in the non-aggregating solution is preferred to be similar to or the same as the analyte in the sample solution, as that would reduce the ESI-MS response difference between different analytes. [28, 29] In this study, the freshly made solutions of the target aggregation-prone analyte are used as the droplet-size-measurement solutions. However, if there is already aggregation in the droplet-size-measurement solution, then the droplet size measured would not be accurate and it can further influence the aggregation detection.

In the simulation, the analytical concentration of monomer c_0 , the droplet diameter d , the percentage of monomer that aggregated $A\%$, and the ratio of the aggregated species were defined. The observed distribution of aggregates was generated by summation of the Poisson distributions of the different aggregate species. Then the observed distribution was subject to Poisson fitting and droplet size calculation.

The effects of aggregation in droplet-size-measurement solutions are more complicated than the previous two factors. When the monomers aggregate, the apparent error it introduced is the positive error of the monomer concentration, which leads to a negative error on the droplet size measurement as discussed above. On the other hand, the Poisson distributions of the aggregated species would lead to a positive error to the droplet size measurement because it technically increases the percentage of the less likely species.

Both trends are reflected in the MATLAB results (Figure 3.5). The droplet diameter was set to 15 nm. From the figure we can see that the measured droplet size dropped down a little when only considering the monomer concentration change due to aggregation (the $err_c\%$ bars), with a larger decrease on droplet size by the monomer concentration change from the 10% aggregation.

Adding aggregated species in the simulations increases the measured droplet size compared to the ones that only consider the monomer concentration drop. The influence of aggregation in solution on droplet size measurement is more severe in lower concentrations, which indicates that a high concentration solution is preferred for droplet size measurement, while a low concentration solution is better for sample aggregation detection. The aggregation of monomer into larger oligomers lead to a larger error on the measured droplet size, so it is preferred to minimize aggregation in the droplet-size-measurement solutions as much as possible.

3.4 Conclusions

A Poisson-statistics-based model that distinguishes the non-specific aggregation in the ESI process and the solution-phase aggregation was proposed and discussed from a theoretical point of view. Qualitative and quantitative applications of the model are discussed with their detailed steps being developed. As a critical step in the model for aggregation detection, droplet size measurement and its influencing factors are discussed using MATLAB simulations. Based on MATLAB simulation results and theoretical deductions, a larger error of droplet size measurement can be observed with a broad ESI droplet size distribution, a high absolute concentration error (especially when the observed concentration is lower than the actual concentration), and more analyte aggregation in the non-aggregating solution. These theoretical discussions tell us that a uniform droplet spray with an accurate concentration and no solution-phase aggregating is beneficial for droplet size measurement and thus for solution phase aggregation detection. Solutions with high concentrations are less prone to the influence of solution-phase aggregation, which is more suitable to droplet size measurement, while solutions with low concentrations are more sensitive to the solution-phase aggregation and are better used in solution-phase aggregation detection solutions.

3.5 References

1. De Hoffmann, E.; Stroobant, Vincent. *Mass Spectrometry: Principles and Applications* (3rd ed.). John Wiley & Sons, Chichester, UK (2007).
2. Uhlig, T.; Kyprianou, T.; Martinelli, F. G.; Oppici, C. A.; Heiligers, D.; Hills, D.; Calvo, X. R.; Verhaert, P. The Emergence of Peptides in the Pharmaceutical Business: From Exploration to Exploitation. *EuPA Open Proteom.* 4, 58-69 (2014).
3. Costantino, H. R.; Langer, R.; Klivanov, A. M. Aggregation of a Lyophilized Pharmaceutical Protein, Recombinant Human Albumin: Effect of Moisture and Stabilization by Excipients. *Bio/Technol.* 13, 493-496 (1995).
4. Young, L. M.; Saunders, J. C.; Mahood, R. A.; Revill, C. H.; Foster, R. J.; Ashcroft, A. E.; Radford, S. E. ESI-IMS-MS: A Method for Rapid Analysis of Protein Aggregation and Its Inhibition by Small Molecules. *Methods* 95, 62-69 (2016).
5. Davidson, K. L.; Oberreit, D. R.; Hogan, C. J., Jr.; Bush, M. F. Nonspecific Aggregation in Native Electrokinetic Nanoelectrospray Ionization. *Int. J. Mass Spectrom.* 420, 35-42 (2017).
6. Li, M.; Guha, S.; Zangmeister, R.; Tarlov, M. J.; Zachariah, M. R. Quantification and Compensation of Nonspecific Analyte Aggregation in Electrospray Sampling. *Aerosol Sci. Technol.* 45, 849-860 (2011).
7. Siuzdak, G. An Introduction to Mass Spectrometry Ionization: An Excerpt from The Expanding Role of Mass Spectrometry in Biotechnology, 2nd ed.; MCC Press: San Diego, 2005. *JALA – J. Assoc. Lab. Autom.* 9, 50-63 (2004).
8. Konermann, L.; Ahadi, E.; Rodriguez, A. D.; Vahidi, S. Unraveling the Mechanism of Electrospray Ionization. *Anal. Chem.* 85, 2-9 (2013).
9. Kitova, E. N.; El-Hawiet, A.; Schnier, P. D.; Klassen, J. S. Reliable Determinations of Protein-Ligand Interactions by Direct ESI-MS Measurements. Are We There Yet? *J. Am. Soc. Mass Spectrom.* 23, 431-441 (2012).
10. Sun, J.; Kitova, E. N.; Wang, W.; Klassen, J. Method for Distinguishing Specific from Nonspecific Protein-Ligand Complexes in Nanoelectrospray Ionization Mass Spectrometry. *Anal. Chem.* 78, 3010-3018 (2006).
11. Wang, W.; Kitova, E. N.; Klassen, J. S. Influence of Solution and Gas Phase Processes on Protein-Carbohydrate Binding Affinities Determined by Nanoelectrospray Fourier Transform Ion Cyclotron Resonance Mass Spectrometry. *Anal. Chem.* 75, 4945-4955 (2003).
12. Grimmett, G.; Stirzaker, D. *Probability and Random Processes* (3rd ed.). Oxford University Press, Oxford, UK (2001).

13. Lane, L. A.; Ruotolo, B. T.; Robinson, C. V.; Favrin, G.; Benesch, J. L. P. A Monte Carlo Approach for Assessing the Specificity of Protein Oligomers Observed in Nano-Electrospray Mass Spectra. *Int. J. Mass Spectrom.* 283, 169-177 (2009).
14. Li, M.; Tan, J.; Tarlov, M. J.; Zachariah, M. R. Absolute Quantification Method for Protein Concentration. *Anal. Chem.* 86, 12130-12137 (2014).
15. Li, M.; Guha, S.; Zangmeister, R.; Tarlov, M. J.; Zachariah, M. R. Method for Determining the Absolute Number Concentration of Nanoparticles from Electrospray Sources. *Langmuir* 27, 14732-14739 (2011).
16. Rojas-Betancourt, S.; Stutzman, J. R.; Londry, F. A.; Blanksby, S. J.; McLuckey, S. A. Gas-Phase Chemical Separation of Phosphatidylcholine and Phosphatidylethanolamine Cations via Charge Inversion Ion/Ion Chemistry. *Anal. Chem.* 87, 11255-11262 (2015).
17. Majewski, J. Measurement Techniques Concerning Droplet Size Distribution of Electrosprayed Water. *Przeegląd Elektrotechniczny.* 89.3b, 300-302 (2013).
18. De Juan, L.; de la Mora, J. F. Charge and Size Distributions of Electrospray Drops. *J. Colloid Interface Sci.* 186, 280-293 (1997).
19. Kebarle, P.; Verkerk, U. H.: Electrospray: From Ion in Solution to Ion in the Gas Phase, What We Know Now. *Mass Spectrom. Rev.* 28, 898-917 (2009).
20. Lewis, K. C.; Dohmeier, D. M.; Jorgenson, J. W.; Kaufman, S. L.; Zarrin, F.; Dorman, F. D. Electrospray-Condensation Particle Counter: A Molecule-Counting LC Detector for Macromolecules. *Anal. Chem.* 66, 2285-2292 (1994).
21. Hogan, C. J., Jr.; Biswas, P. Porous Film Deposition by Electrohydrodynamic Atomization of Nanoparticle Sols. *Aerosol Sci. Technol.* 42, 75-85 (2008).
22. Constantopoulos, T. L.; Jackson, G. S.; Enke, C. G. Effects of Salt Concentration on Analyte Response Using Electrospray Ionization Mass Spectrometry. *J. Am. Soc. Mass Spectrom.* 10, 625-634 (1999).
23. Wortmann, A.; Kistler-Momotova, A.; Zenobi, R.; Heine, M. C.; Wilhelm, O.; Pratsinis, S. E. Shrinking Droplets in Electrospray Ionization and Their Influence on Chemical Equilibria. *J. Am. Soc. Mass Spectrom.* 18, 385-393 (2007).
24. Schmidt, A.; Karas, M.; Dülcks, T. Effect of Different Solution Flow Rates on Analyte Ion Signals in Nano-ESI MS, or: When Does ESI Turn into Nano-ESI? *J. Am. Soc. Mass Spectrom.* 14, 492-500 (2003).
25. Kebarle, P.; Tang, L. From Ions in Solution to Ions in the Gas Phase: The Mechanism of Electrospray Mass Spectrometry. *Anal. Chem.* 65, 972-986 (1993).

26. Peschke, M.; Verkerk, U. H.; Kebarle, P.: Features of the ESI Mechanism that Affect the Observation of Multiply Charged Noncovalent Protein Complexes and the Determination of the Association Constant by the Titration Method. *J. Am. Soc. Mass Spectrom.* 15, 1424-1434 (2004).
27. Kebarle, P.; Peschke, M.: On the Mechanism by which the Charged Droplets Produced by Electrospray Lead to Gas Phase Ions. *Anal. Chim. Acta* 406, 11-35 (2000).
28. Bronsema, K. J.; Bischoff, R.; van de Merbel, N. C. Internal Standards in the Quantitative Determination of Protein Biopharmaceuticals Using Liquid Chromatography Coupled to Mass Spectrometry. *J. Chromatogr. B* 893-894, 1-14 (2012).
29. Du, L.; White, R. L. Improved Partition Equilibrium Model for Predicting Analyte Response in Electrospray Ionization Mass Spectrometry. *J. Mass Spectrom.* 44, 222-229 (2009).

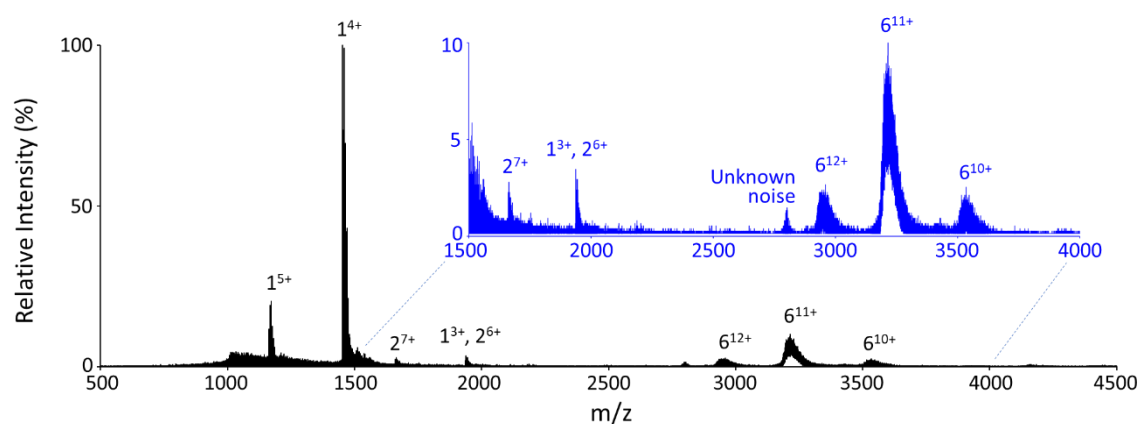


Figure 3.1 Mass spectrum of 5 μM insulin in an aqueous solvent with 20 μM $\text{Zn}(\text{OAc})_2$, 10 μM NH_4Cl , 5 mM phenol and 300 mM NH_4OAc adjusted to a pH of 7.4 to show the non-Poisson distribution of monomer, dimer and hexamer. The inset is a zoomed-in mass spectrum for the m/z range of 1500 – 4000 to show that no intermediate oligomer sizes (i.e., trimer, tetramer or pentamer) were observed on the spectrum.

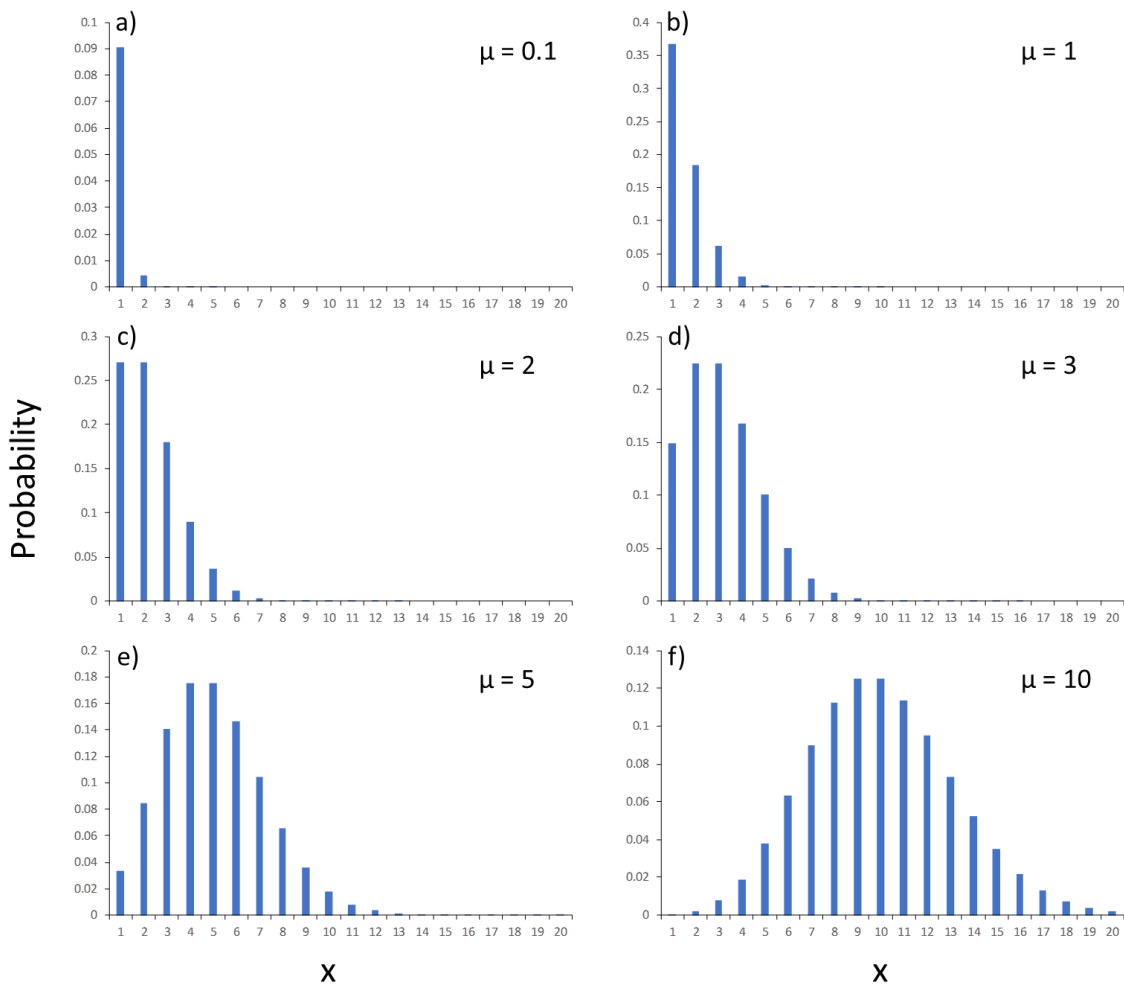


Figure 3.2 Poisson distributions at different μ values.

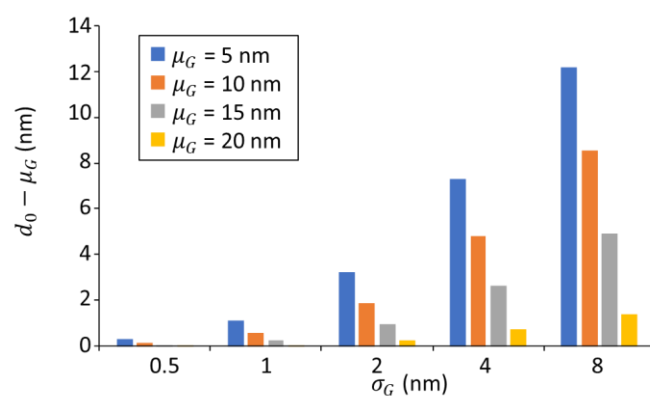


Figure 3.3 The relationship between the spread of droplet size distribution and the error of the calculated diameter. μ_G denotes the average droplet diameter for the Gaussian distribution of droplet size. $(d_0 - \mu_G)$ denotes the error of the calculated diameter from the true average droplet diameter. σ_G refers to the standard deviation of the Gaussian droplet diameter distribution.

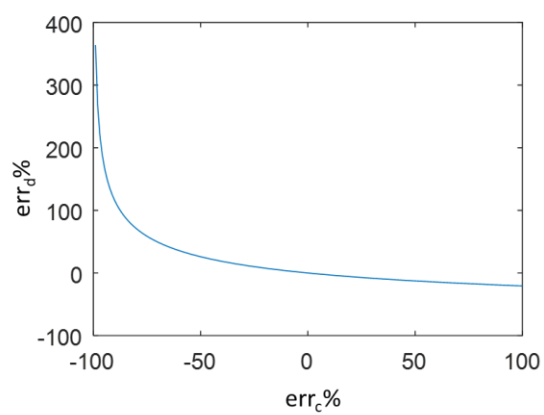


Figure 3.4. Relationship between relative error of concentration ($err_c\%$) and that of droplet diameter measurement ($err_d\%$). The curve was plotted from Equation 3.8.

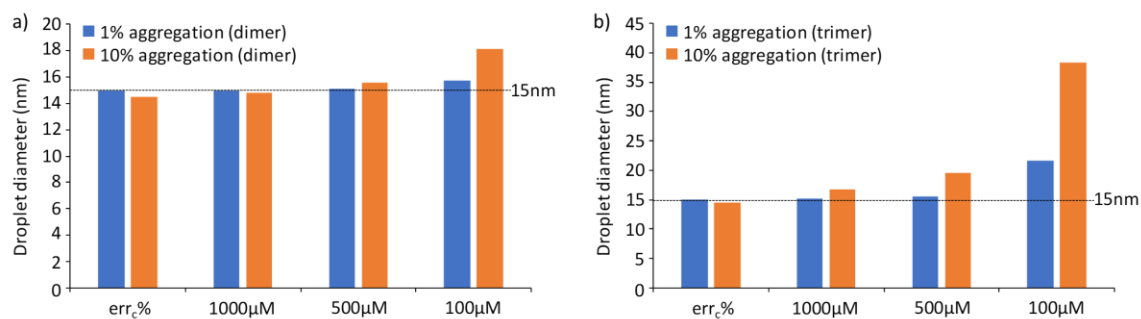
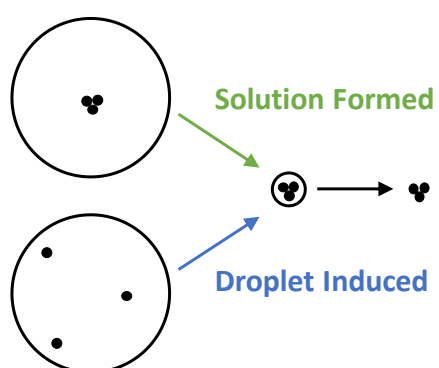
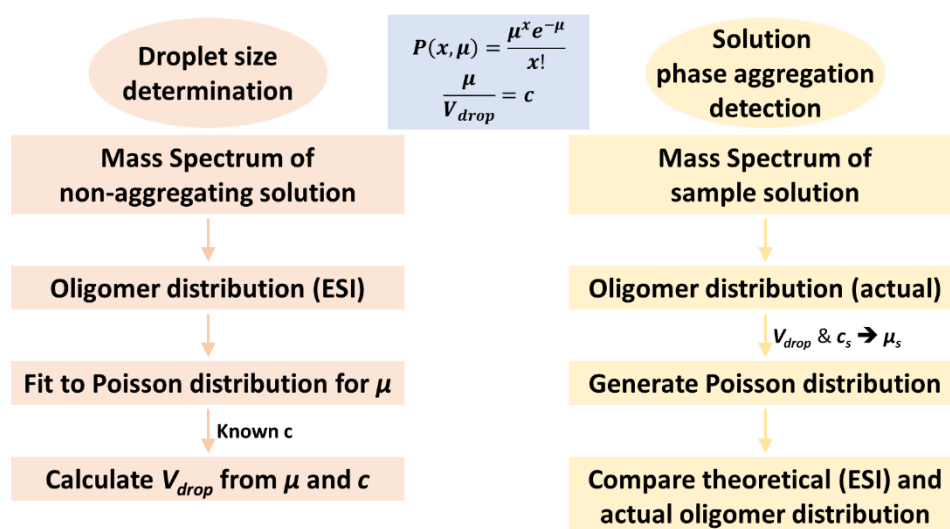


Figure 3.5 Simulated measured droplet diameter when 1% and 10% monomers aggregated into (a) dimers or (b) trimers. The analytical concentration of the solution is 1000μM, 500μM and 100μM respectively. The measured droplet sizes with the same monomer concentration error but no aggregation are listed on the left to show how aggregation-caused concentration change affects the measured droplet size.



Scheme 3.1 A demonstration of solution-phase aggregation and droplet-induced aggregation. Each black dot in the scheme denotes one analyte molecule. The charges on the droplet or the analytes are not drawn for simplicity.



Scheme 3.2 Flow chart of the quantitative approach of solution-phase aggregation detection. μ and c are the average number of analytes per droplet and the analyte concentration (no subscript: non-aggregating solution; subscript s: sample solution). V_{drop} is the droplet volume for the ESI-MS method.

Table 3.1 List of symbols and abbreviations and their definitions

Symbol or abbreviation	Definition	Example / Comment
size ^{charge}	Monomer or oligomer with n monomers and m charges, which has an m/z of $[n \cdot M(\text{monomer}) + m \cdot H]^{m+}$	1 ³⁺ : $[M+3H]^{3+}$ 2 ⁶⁺ : $[2M+6H]^{6+}$
μ_G	Average of the simulated Gaussian droplet diameter distribution (nm)	/
σ_G	Standard deviation of the simulated Gaussian droplet diameter distribution (nm)	/
A%	The difference between actual concentration and the observed concentration relative to the observed concentration, i.e., $\frac{c - c_0}{c_0} \times 100\%$ A% could also be the percentage of the monomers that aggregate in the solution	$c = c_0(1 - A\%)$
c	True concentration of the non-aggregating solution, or the true concentration of the analyte monomer (mol/L)	/
c_0	Observed solution concentration, or the analytical concentration of the analyte (mol/L)	/
c_{agg}	True concentration of aggregate species with an oligomer size of n (M_n)	$c_{agg} = \frac{c_0 \times A\%}{n}$
c_{bulk}	Analyte concentration in the bulk solution	/
c_s	Sample concentration	/
d	True droplet diameter (no droplet size distribution considered)	/
d_0	Calculated droplet diameter from the Poisson fitting in the simulation (nm)	/

Table 3.1 List of symbols and abbreviations and their definitions (continued)

$Error(\mu_G, \sigma_G)$	The error of obtained droplet diameter compared to the true average droplet diameter when the Gaussian distribution of droplet diameter has an average diameter of μ_G and a standard deviation of σ_G	$Error(\mu_G, \sigma_G) = Error(10,1) = 0.57$ means when $\mu_G = 10$ nm and $\sigma_G = 1$ nm, the measured diameter is 10.57 nm, with an error of 0.57 nm compared to the true value of 10 nm
$err_c\%$	Relative error of the observed concentration to the true value, i.e., $\frac{c_0 - c}{c} \times 100\%$	$c = \frac{c_0}{1 + err_c\%}$
$err_d\%$	Relative error of the measured droplet diameter to the true value, i.e., $\frac{d_0 - d}{d} \times 100\%$	$d = \frac{d_0}{1 + err_c\%}$
$P(x, \mu)$	The possibility of having x analytes in the final droplet	$P(x, \mu) = \frac{e^{-\mu} \mu^x}{x!}$
x	Number of analytes in the final droplets	/
μ	Average number of analytes per droplet	/
μ_P	Fitted Poisson statistics parameter to the simulated experimental distribution, which means the experimental average number of analytes per droplet in the simulation	/
μ_s	Average number of analytes per droplet for the sample solution	/
V_{drop}	Volume of the final droplet	$\frac{\mu}{V_{drop}} = c_{bulk}$
ESI-MS	Electrospray Ionization Mass Spectrometry	/

CHAPTER 4. EARLY DETECTION OF SOLUTION-PHASE AGGREGATION OF SMALL PEPTIDES AND PROTEINS

4.1 Introduction

Peptide and protein aggregation is an important process in pathology and pharmaceutical development. For example, amyloid-related diseases, such as Alzheimer's disease and Parkinson's disease, are characterized by amyloid fibril formation from misfolding proteins. [1] To decipher the mechanism and to develop early diagnosis and treatment of such diseases, the aggregation mechanism(s) of related proteins and peptides are widely studied. [2] On the other hand, aggregation of peptide and protein pharmaceuticals leads to low drug efficiency. For example, since insulin is only active in monomeric form, the aggregation of insulin would lead to lower drug efficiency. [3] The larger size of drug aggregates also causes lower drug delivery efficiency and a higher risk of inducing immune responses. Both cases point to the need for methods to detect early-stage aggregation.

Multiple techniques are used to study aggregation. For example, imaging methods like X-ray crystallography, AFM and TEM have been applied to study the structure of fibrils or crystals, [4-6] which are relevant to late-stage aggregation. Fluorescence measurements [7] and laser light scattering techniques [8] can be used to detect smaller aggregates, but remain limited for early stage aggregation due to insufficient detection limits. Mass spectrometry, with its ability to observe monomer and small oligomeric species with relatively high sensitivity, high specificity, and wide dynamic range, lends itself as a strong candidate to study the early-stage aggregation process.

Electrospray ionization mass spectrometry (ESI-MS) is widely used for biomolecule samples due to the ability to detect high mass molecules and non-covalently-bound complexes thereof as well as direct compatibility with solution samples. [9] Multiply charged ions are

commonly formed from polymeric species in the ESI process, which enables the detection of large molecules in solution. [9] However, two main issues remain for ESI-MS in its application to aggregation detection. First, since ions are multiply charged, different aggregates can have the same mass to charge (m/z) ratio after ESI and appear at the same position on the m/z scale, which produces overlap peaks [10] that complicate oligomer size assignment. The other issue is that non-specific aggregation can take place during the ESI process itself as the ESI droplets shrink and break into smaller droplets, [11] which further complicates the determination of solution-phase aggregation from mass spectra. In this project, we explore the use of ion-ion proton transfer reactions to reduce or eliminate the charge state overlap issue, and application of the statistical model to differentiation of the aggregation in the solution from that in the ESI process.

4.2 Experimental

4.2.1 Materials

Peptide NNQQNY was synthesized by GenScript (Piscataway, NJ, USA). Human insulin, glucagon, ammonium acetate and 2,2,3,3,4,4,5,5,6,6,7,7,8,8,8-pentadecafluoro-1-octanol (PFO) were purchased from Sigma Aldrich (St. Louis, MO, USA). Water (Optima LC/MS grade), acetonitrile (Optima grade), methanol (Optima grade) and ammonium hydroxide (certified ACS plus grade) was purchased from Fisher Chemical (Waltham, MA, USA). Acetic acid was purchased from Macron Fine Chemicals (Center Valley, PA, USA). Sodium chloride was purchased from Mallinckrodt Chemicals (Center Valley, PA, USA). Hydrochloric acid was purchased from J. T. Baker (Center Valley, PA, USA). NNQQNY solution was prepared in water/methanol 50/50. Insulin and glucagon solutions were prepared in 4% acetic acid (aqueous) unless particularly specified. PFO solutions were prepared to be 5 mM in water/methanol/ammonium hydroxide 49.5/49.5/1.

4.2.2 Mass Spectrometry

All mass spectrometric experiments were performed on TripleTOF 5600, [12] a hybrid triple quadrupole / time of flight (TOF) mass spectrometer (SCIEX, Concord, Canada) previously modified for ion-ion reactions. [13] Droplet-size-measurement solutions or sample solutions were sprayed using positive nano-electrospray ionization (nESI). The analyte cations were transferred to q2 and trapped there. If it was a direct analysis of the analyte, the analyte cations would be transferred to the TOF analyzer for m/z determination. If an ion-ion reaction was performed, when the analyte cations were trapped in q2, the reagent PFO anions would be sprayed using negative nESI and transferred to q2. The analyte cations and reagent anions were mutually stored in q2 for 100-500 ms to allow the ions react and then the product ions were transferred to the TOF for m/z analysis. The instrument parameters were adjusted to be as soft as possible (i.e., minimal potential gradients along the ion path) so that the aggregates were not destroyed during the transmission of ions from the ion source to the detector.

4.2.3 Data Analysis

The abundances of ions in the m/z region for the monomer and each aggregate species were each summed to calculate the area of each species with baseline subtraction. If peak overlap happened, a correction described under “Mass spectrum overlap correction” would be performed.

For droplet-size-measurement solutions, after obtaining the area of each species, the experimental percentages of the oligomer species were calculated. Then a theoretical Poisson distribution was generated from a guess μ (average number of analyte molecules/droplet, see below in Section 4.3.2.2) value, with the theoretical percentages calculated for each oligomer size. A Poisson fitting was done via minimizing the squares of the differences between the experimental and theoretical percentages by changing the guess μ value. Then the fitted μ value can be used to

calculate droplet size using Equation 4.2. A list of symbols and abbreviations are listed in Table 4.2.

For sample aggregation detection, the sum of squares of the differences between theoretical and experimental aggregate distributions was calculated to see if any sample aggregation in solution can be detected. If the sum of squares for the sample solution is larger than that for the droplet-size-measurement solutions, then the sample is considered to have a measurable degree of aggregation in solution.

4.2.4 Mass Spectrum Overlap Correction

The overlap peaks were processed through averaging the non-overlap isotopic peaks to recover the area of overlapped oligomer. Figure 4.1 presents an example of the overlap of monomer and dimer peaks. Usually in the overlap region, there are two cases: peaks with overlap (blue shading) and without overlap (yellow shading). The peaks without overlap would be directly assigned, as in this example to be 2^{6+} (dimer at 6+ charge state) adduct peaks. For the peaks with overlap, the overlap peak area of 2^{6+} under the 1^{3+} isotopic peaks is approximated by the average of neighboring 2^{6+} non-overlap isotopic peaks (labeled as 1-8 on the spectrum). Therefore, the 2^{6+} peak area in the blue shade would be calculated as

$$\begin{aligned} & \frac{\textcircled{1}}{2} + \textcircled{1} + \frac{\textcircled{1} + \textcircled{2}}{2} + \textcircled{2} + \frac{\textcircled{2} + \textcircled{3}}{2} + \textcircled{3} + \dots + \textcircled{7} + \frac{\textcircled{7} + \textcircled{8}}{2} + \frac{\textcircled{8}}{2} \\ & = 2(\textcircled{1} + \textcircled{2} + \textcircled{3} + \textcircled{4} + \textcircled{5} + \textcircled{6} + \textcircled{7} + \textcircled{8}) \end{aligned}$$

with the non-overlap isotopic peak area denoted by peak number in circle. Similarly, if the overlap peaks are 1^{3+} and 3^{9+} peaks, then the 3^{9+} peak area would be 3/2 of the non-overlap isotopic peak area.

4.2.5 Size-Exclusion Chromatography (SEC) Protocol

Agilent 1200 Series HPLC system and Agilent Advanced Bio 130Å SEC column (MW range 100 Da – 120 kDa) were used for SEC separation. The mobile phase was prepared with 16.7% acetic acid, 25% acetonitrile, 1.67% concentrated ammonium hydroxide (to adjust the pH to 3) and water, based on Agilent application note conditions. [14] The flow rate was set to 0.5 mL/min. Mobile phase and samples were filtered with 0.45- μ m filter before use.

4.2.6 Insulin Stress Conditions

Three insulin stress conditions were used in this project, including: a) 3.4 mg/mL insulin in SEC mobile phase in 60°C for 6 hours; [14] b) 1 mg/mL insulin in 10 mM HCl in room temperature for 5 days; and c) 10 mg/mL insulin in 0.1 M NaCl and 10 mM HCl at 300 rpm at 37°C for 48 hours. These conditions are mainly used for SEC experiment, as they are not all MS-compatible.

The adjusted MS-compatible stress conditions are: a) 3.4 mg/mL insulin in 4% acetic acid in 60°C for 6 hours, b) 3.4 mg/mL insulin in a mobile-phase-like solvent (20% acetic acid, 30% acetonitrile and some ammonium hydroxide to adjust the pH to 3); c) 10 mg/mL insulin in 97mM ammonium acetate and 6.8% acetic acid at 300 rpm at 37°C for 48 hours.

4.3 Results and Discussion

4.3.1 Peak Overlap Reduced or Eliminated by Ion/Ion Reaction

When the sample is directly analyzed using ESI-MS, the analyte monomers and oligomers of different sizes, which may have the same m/z , can overlap in the spectrum. For example, in Figure 4.2(a), the mass spectrum of peptide NNQQNY has overlap peaks that are assigned with multiple species. The peaks are assigned based on the isotope spacings, as shown in Figure 4.2(b).

The m/z spacings between adjacent isotope peaks, which differ in mass nominally by 1 Da, indicates the charge of the species. The size of the oligomer can then be deduced from the mass calculated from the m/z and charge. From the NNQQNY example, we can see that the assignment of the overlap peaks requires the overlap species to be abundant enough so that they can be distinguished from the dominant peak. The ESI-MS instrument also must have a high resolution sufficient to resolve the overlap isotope peaks for peak assignment.

Upon ion-ion reaction with deprotonated PFO, [15] a proton transfer reagent, charge states of the NNQQNY cations are reduced and initially overlapped peaks are separated in m/z space (Figure 4.2(c)). Low charge states obtained from the ion-ion reaction (such as +1 or +2 charge states) can be easily assigned on instruments with lower resolution. Since the peaks are no longer overlapping, the species with lower abundances are apparent, such as the octadecamer in Figure 4.2(c). Therefore, more confident peak assignment and better quantitation can be achieved for the mass spectra after ion-ion reaction.

4.3.2 Differentiation between Solution-Phase and Droplet-Induced Aggregation

4.3.2.1 Non-Specific Aggregation in ESI-MS

Non-specific aggregation refers to the non-covalent clustering of analytes in the ESI process. The non-specific aggregation phenomenon is largely related to the ESI mechanism. In ESI-MS, charged droplets are formed from the high voltage applied to the sample solution. As the droplets fly closer to the mass spectrometer, solvent evaporates from the droplet, and the increasing Coulomb repulsion from the charges on the droplet surface makes the droplet fission into smaller progeny droplets. [9] At last ions form from the final droplets and enter the mass spectrometer. When there are more than one analyte molecules in the final droplets, the analyte cluster would have all the charges on the final droplet and get detected as an “aggregate” of the analyte.

The non-specific aggregation in ESI-MS is problematic especially for aggregation detection using ESI-MS. When an oligomer is observed on the mass spectrum, people need to identify the source of the aggregate before making conclusions on the aggregation status of the solution.

4.3.2.2 Poisson-Statistics Based Model to Analyze Solution-Phase Aggregation

For the distinction between solution-phase and ESI-process-induced aggregation, the statistical model proposed in CHAPTER 3 can be used. Here is a brief introduction to the statistical model in CHAPTER 3. Poisson statistics (Equation 4.1) can be used to describe the non-specific aggregation in the ESI process:

$$P(x, \mu) = \frac{e^{-\mu} \mu^x}{x!} \quad (4.1)$$

where $P(x, \mu)$ is the probability of having x analytes in the final droplet, x is the number of analytes in the final droplet and μ is the average number of analytes per droplet. The average number of analytes per droplet μ in the Poisson statistics equation is related to the concentration of analyte in the bulk solution under first order approximation:

$$\frac{\mu}{V_{drop}} = c_{bulk} \quad (4.2)$$

where V_{drop} is the volume of the final-stage droplet and c_{bulk} is the analyte concentration in the bulk solution.

If the droplet size and the analyte concentration is known, a theoretical Poisson distribution from the ESI process can be generated and compared with the experimental data to determine if there is solution-phase aggregation. This can be done quantitatively through two steps: droplet size determination and sample solution-phase aggregation detection (Scheme 3.2).

In the droplet size determination step, we first take the mass spectrum of a non-aggregating solution with known concentration (labeled as c in the flow chart). The distribution of aggregates is fit to Equation 4.1 to obtain the μ of the non-aggregating solution, because all the aggregates come from the ESI process. Using fitted μ and known c of the non-aggregating solution, the droplet size of our method (V_{drop}) can be calculated from Equation 4.2. A sum of squares between the Poisson distribution calculated from fitted μ and the experimental distribution obtained from the mass spectrum of the non-aggregating solution is calculated as the standard to determine the aggregation status of the sample solution below.

Then in the solution-phase aggregation detection step, the mass spectrum of the sample solution is obtained. The oligomer distribution on the mass spectrum is the convolution of solution-phase aggregation (if any) and ESI droplet-induced aggregation. The theoretical non-specific aggregate distribution can be calculated from the V_{drop} and the sample concentration (c_s) using Equation 4.1 and Equation 4.2. Finally, the actual oligomer distribution and the theoretical non-specific aggregate distribution are compared by calculating the sum of squares of their differences for each oligomer size. If the difference of the two distributions is larger than that of the non-aggregating solution, then solution-phase aggregation exists in the sample.

4.3.2.3 Experimental Droplet Size Determination

The droplet size determination with the method proposed above was done with freshly made insulin solutions, because insulin is the model molecule to study the aggregation process. Based on the simulation results (Section 3.3.3), high concentrations (100 to 1000 μM) were used for droplet size determination. The mass spectra of the analyte (insulin) solutions with different concentrations were taken. Then the summation of the peaks of each monomer or oligomer species were calculated from the spectrum. For example, the intensities between 968 Th and 1043 Th were

summed to get the ion count of monomer and its adducts at +6 charge state. If there are overlap peaks in the spectrum and could be identified from isotope spacing, the overlap peak intensities were recovered by the summation of the non-overlap isotopic peaks (details in Experimental section 4.2.4). Percentage of each species were calculated based on the peak intensity summation. Then the percentage was fitted with Poisson distribution to obtain the μ value of the system, after which the droplet size was calculated with Equation 4.2.

The results for insulin and glucagon droplet size measurement are listed in Table 4.1. For insulin solutions in 4% acetic acid, the droplet size was determined to be 16 ± 2 nm in diameter when using the nanoelectrospray ionization (nESI) source and 4- μ m nESI tips. The scale of measured droplet diameter matches with calculation models for ESI mechanism studies. [16] For 10- μ m nESI tips and the same solution condition, the droplet size was measured to be 22 ± 1 nm, which makes sense since larger initial droplets are generated from larger tips.

To test if a measured droplet size can be applied to another system, a cross-system measurement was made between insulin and glucagon (results in Table 4.1). For 3- μ m nESI tips and 4% acetic acid as solvent, droplet diameters for insulin and glucagon were measured to be 17 ± 2 nm and 14 ± 2 nm respectively, which is very close and shows the possibility of applying measured droplet size of one analyte to another system.

4.3.2.4 Application of Model on Stressed Insulin System

To verify the practicality of the proposed method, insulin under different stress conditions were monitored with both MS and size exclusion chromatography (SEC, as an orthogonal method). Three stress conditions of low pH, high temperature and elevated temperature with agitation were tested, with detailed stress conditions described in the Experimental section 4.2.6. The MS and

SEC results both showed insulin signal decrease, but no apparent aggregate ratio change was observed.

For the low pH stressing at pH 2 with acetic acid, no change was observed. For high temperature stressing at 60°C, the decrease of insulin signal and the appearance of insulin fragments was observed, as flocculent precipitate was observed during the stressing process. However, no apparent aggregate ratio change was observed in the MS data. Under the condition of elevated temperature with agitation, insulin solution would gradually become opaque and hard to be filtered by the 0.45- μ m filter. Insulin signal decrease was observed but still with no apparent aggregate ratio change.

In the SEC separation, only covalent insulin dimer was separated from the insulin monomer, as shown in Figure 4.3. Two insulin species were separated on the SEC. MS analysis of the two insulin fractions show one species to be monomer and the other species to be dimer with ammonia loss (Figure 4.3 (c)-(f)). The insulin dimer with the loss of ammonia was assigned as a covalent dimer based on the support from literature [18] and the fact that it is not easy to break apart upon collisional activation in the mass spectrometer. No non-covalent aggregates were separated by the SEC yet. The ratio between the covalent dimer and the monomer remains almost constant in the stressing process.

This is probably due to the aggregation reaction being too fast and we failed to catch the very early stage of aggregation. When the late-stage aggregation starts, the monomers will directly attach to the large aggregates and they will soon become precipitates and not suitable for ESI-MS or SEC detection.

4.3.2.5 Application of Model on Concentration Recovery from ESI-MS Spectra

To test if the MS result is similar to SEC result quantitatively, the ratio of the covalent dimer to the monomer was calculated based on MS result. On the mass spectrum, for the peaks of the covalent dimer (two insulin molecules minus ammonia), it may come from solution-phase covalent dimer, but it can also be a non-specific aggregation in the droplet by one insulin and one insulin with ammonia loss. Therefore, the droplet-induced non-specific aggregation needs to be subtracted from the experimental result to determine the actual ratio of the covalent dimer to the monomer in the solution.

If we assume that the occurrences of monomer and monomer-NH₃ in the droplet are independent events, then the probability of having droplet-induced dimer-NH₃ would be

$$P(\text{dimer} - \text{NH}_3) = P(\text{monomer}) \cdot P(\text{monomer} - \text{NH}_3) \quad (4.3)$$

Then if we assume that both insulin monomer and monomer-NH₃ molecules are following the Poisson statistics model, and only their concentrations are affecting their μ in the Poisson statistics, then the areas of them on the mass spectrum would be a direct reflection of their actual probability:

$$\frac{P(\text{monomer} - \text{NH}_3)}{P(\text{monomer})} = \frac{A(\text{monomer} - \text{NH}_3)}{A(\text{monomer})} \quad (4.4)$$

And since the Equation 4.3 could be rewritten as

$$P(\text{dimer} - \text{NH}_3) = \frac{P(\text{monomer} - \text{NH}_3)}{P(\text{monomer})} \cdot P^2(\text{monomer}) \quad (4.5)$$

After plugging in the Equation 4.4 expression, the probability of having droplet-induced dimer-NH₃ is

$$P(\text{dimer} - \text{NH}_3) = \frac{A(\text{monomer} - \text{NH}_3)}{A(\text{monomer})} \cdot P^2(\text{monomer}) \quad (4.6)$$

Therefore, as long as we have the probability of insulin monomer and the area ratio between the monomer-NH₃ and monomer, we could calculate the probability of droplet-induced dimer-NH₃.

On the mass spectrum of human insulin in 4% acetic acid, peak areas of monomer, dimer, trimer, monomer-NH₃, and dimer-NH₃ were calculated. A Poisson distribution fitting of the area percentage of monomer, dimer and trimer was performed to obtain μ value. The probability of monomer $P(\text{monomer})$ was calculated using Equation 4.1. Then using Equation 4.6 the probability of droplet-induced dimer-NH₃ was calculated, and $\frac{P(\text{dimer-NH}_3)}{P(\text{monomer})}$ was obtained. Then it was compared with experimental value of $\frac{P(\text{dimer-NH}_3)}{P(\text{monomer})}$ to calculate the solution portion of $\frac{P(\text{dimer-NH}_3)}{P(\text{monomer})}$. Since the solution-phase dimer-NH₃ would still show up as Poisson distribution on the mass spectrum, the actual concentration ratio of dimer-NH₃ to monomer was calculated using the model and it was determined to be 0.00146.

On the SEC chromatogram, the area ratio between the dimer-NH₃ and the monomer was 0.00273. Considering a theoretically twice absorbance of the dimer-NH₃ than the monomer, the concentration ratio of dimer-NH₃ to monomer would be 0.00137. The obtained concentration ratios were very close for MS and SEC results, which supports the consistency between MS and SEC analysis. It also confirmed the possibility of applying the Poisson distribution model to quantify the species in the solution phase.

4.4 Conclusions

ESI-MS is a promising tool for early-stage aggregation detection, because it measures the mass of the analyte and it works with solution samples. Two issues have been identified in the application of ESI-MS to aggregation detection: the peak overlap issue and the non-specific droplet-induced aggregation issue. Ion-ion reaction was found to help reduce or eliminate peak overlap. A model based on Poisson distribution of the ESI droplet-induced aggregation was proposed and tested with experimental data. Future work will focus on the exploration of

aggregation conditions and systems so that we can capture the very early stage of aggregation with MS and SEC. Theoretical discussion of the droplet partitioning and the effect of concentration difference between the bulk solution and the droplets will be further explored. The application of the Poisson statistics model to analyte concentration determination, binding constant measurement and ESI mechanism studies will also be investigated.

4.5 References

1. Dobson, C. M.: Protein Misfolding, Evolution and Disease. *Trends Biochem. Sci.* 24, 329-332 (1999).
2. Bleiholder, C., Dupuis, N. F., Wyttenbach, T., Bowers, M. T.: Ion Mobility-Mass Spectrometry Reveals a Conformational Conversion from Random Assembly to β -Sheet in Amyloid Fibril Formation. *Nat. Chem.* 3, 172-177 (2011).
3. Sharma, V. K., Bajaj, H., Kalonia, D. S.: Reversible Self-Association of Pharmaceutical Proteins: Characterization and Case Studies. In: Jameel, F., Hershenson, S.(eds.) *Formulation and Process Development Strategies for Manufacturing Biopharmaceuticals*, p. 429. John Wiley & Sons, Hoboken, NJ (2010).
4. Nelson, R., Sawaya, M., Balbirnie, M., Madsen, A., Riek, C., Grothe, R., Eisenberg, D.: Structure of the Cross- β Spine of Amyloid-like Fibrils. *Nature* 435, 773–778 (2005).
5. Marshall, K., Hicks, M., Williams, T., Hoffmann, S., Rodger, A., Dafforn, T., Serpell, L.: Characterizing the Assembly of the Sup35 Yeast Prion Fragment, GNNQQNY: Structural Changes Accompany a Fiber-to-Crystal Switch. *Biophys. J.* 98, 330–338 (2010).
6. Portillo, A., Krasnoslobodtsev, A., Lyubchenko, Y.: Effect of Electrostatics on Aggregation of Prion Protein Sup35 Peptide. *J. Phys. Condens. Matter* 24, 164205 (2012).
7. Do, T. D.; Economou, N. J.; LaPointe, N. E.; Kincannon, W. M.; Bleiholder, C.; Feinstein, S. C.; Teplow, D. B.; Buratto, S. K.; Bowers, M. T.: Factors that Drive Peptide Assembly and Fibril Formation: Experimental and Theoretical Analysis of Sup35 NNQQNY. *J. Phys. Chem. B* 117, 8436-8446 (2013).
8. Folta-Stogniew, E.: Oligomeric States of Proteins Determined by Size-Exclusion Chromatography Coupled with Light Scattering, Absorbance, and Refractive Index Detectors. *Methods Mol. Biol.* 328, 97–112 (2006).
9. Kebarle, P.; Verkerk, U. H.: Electrospray: From Ion in Solution to Ion in the Gas Phase, What We Know Now. *Mass Spectrom. Rev.* 28, 898-917 (2009).
10. Wang, J. S. H.; Whitehead, S. N.; Yeung, K. K. C.: Detection of Amyloid Beta ($A\beta$) Oligomeric Composition Using Matrix-Assisted Laser Desorption Ionization Mass Spectrometry (MALDI MS). *J. Am. Soc. Mass Spectrom.* 29, 786-795 (2018).
11. Li, M.; Guha, S.; Zangmeister, R.; Tarlov, M. J.; Zachariah, M. R.: Quantification and Compensation of Nonspecific Analyte Aggregation in Electrospray Sampling. *Aerosol Sci. Technol.* 45, 849-860 (2011).
12. Andrews, G. L.; Simons, B. L.; Young, J. B.; Hawkridge, A. M.; Muddiman, D. C.: Performance Characteristics of a New Hybrid Quadrupole Time-of-Flight Tandem Mass Spectrometer (TripleTOF 5600). *Anal. Chem.* 83, 5442-5446 (2011).

13. Rojas-Betancourt, S.; Stutzman, J. R.; Londry, F. A.; Blanksby, S. J.; McLuckey, S. A.: Gas-Phase Chemical Separation of Phosphatidylcholine and Phosphatidylethanolamine Cations via Charge Inversion Ion/Ion Chemistry. *Anal. Chem.* 87, 11255-11262 (2015).
14. Palaniswamy, M. S.; Coffey, A.: Size Exclusion Chromatography of Biosimilar and Innovator Insulin Using the Agilent AdvanceBio SEC Column (Application Note 5991-6872EN, 2016). Retrieved from Agilent Technologies website: <https://www.agilent.com/cs/library/applications/5991-6872EN.pdf>
15. Xia, Y.; Liang, X.; McLuckey, S. A.: Pulsed Dual Electrospray Ionization for Ion/Ion Reactions. *J. Am. Soc. Mass Spectrom.* 16, 1750-1756 (2005).
16. Davidson, K. L.; Oberreit, D. R.; Hogan Jr., C. J.; Bush, M. F.: Nonspecific Aggregation in Native Electrokinetic Nanoelectrospray Ionization. *Int. J. Mass Spectrom.* 420, 35-42 (2017).
17. Lane, L. A.; Ruotolo, B. T.; Robinson, C. V.; Favrin, G.; Benesch, J. L. P.: A Monte Carlo Approach for Assessing the Specificity of Protein Oligomers Observed in Nanoelectrospray Mass Spectra. *Int. J. Mass Spectrom.* 283, 169-177 (2009).
18. Darrington, R. T.; Anderson, B. D.: Evidence for a Common Intermediate in Insulin Deamidation and Covalent Dimer Formation: Effects of pH and Aniline Trapping in Dilute Acidic Solutions. *J. Pharm. Sci.* 84, 275-282 (1995).

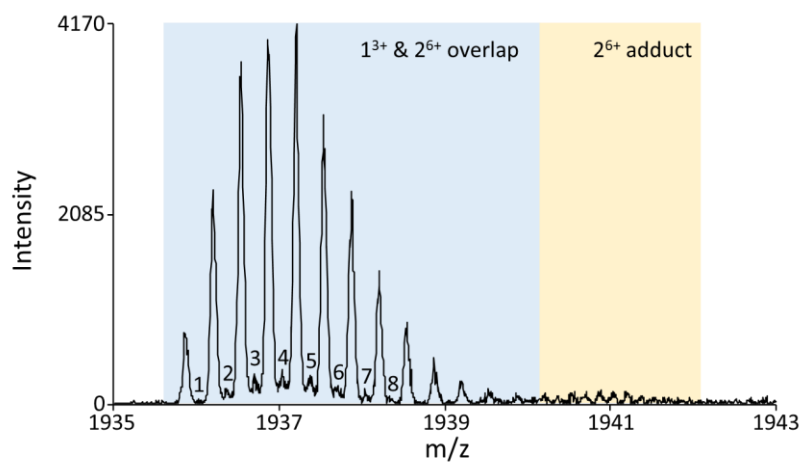


Figure 4.1 Zoomed-in mass spectrum of 196 μM insulin solution. The region in blue shading has overlap peaks of 1^{3+} (oligomer size^{charge}) and 2^{6+} , with the non-overlap isotopic peaks of 2^{6+} labelled in number. The region in yellow shading has 2^{6+} adduct peaks only.

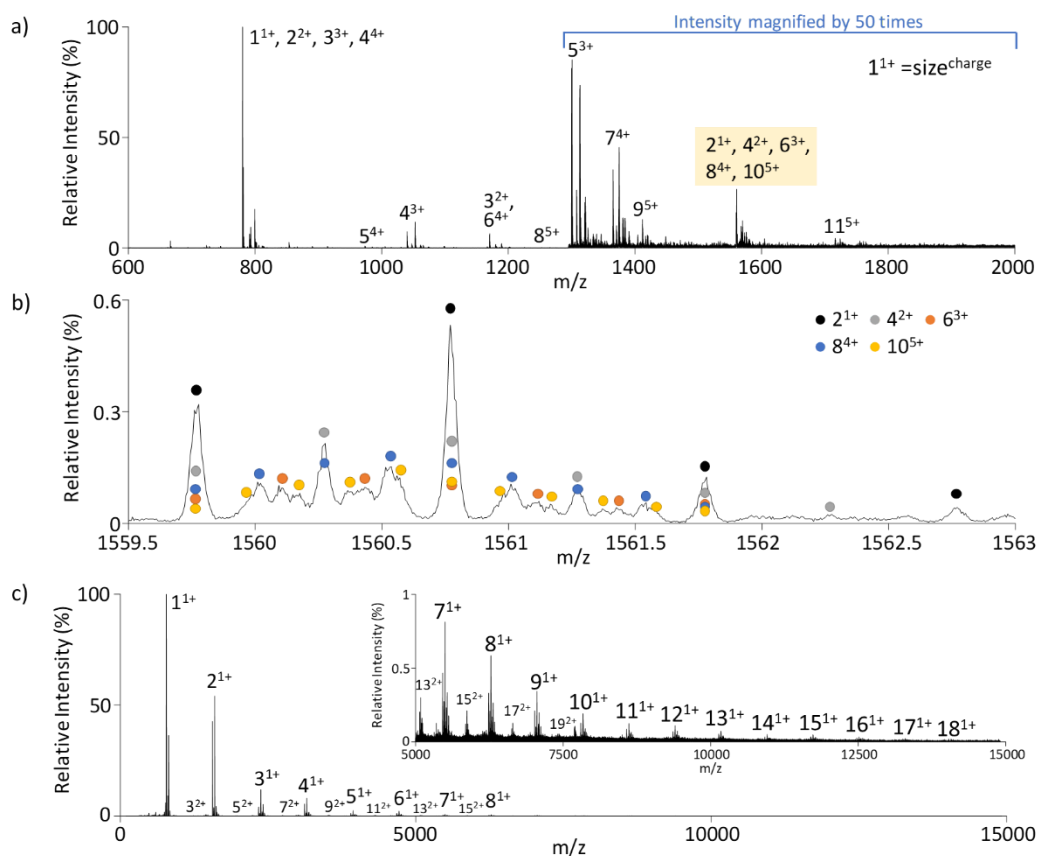


Figure 4.2 Comparison between mass spectra before and after ion-ion reaction. (a) mass spectrum of peptide NNQQNY not subjected to ion-ion reaction with PFO, with the peak assignment labeled as (oligomer size)^{charge}; (b) zoomed-in mass spectrum of the shaded labeled peak in spectrum (a) to show how overlap peaks are assigned based on isotope spacing; (c) mass spectrum of peptide NNQQNY subjected to ion-ion reaction with PFO, with an inset showing the zoomed-in spectrum for m/z range 5000 to 15000.

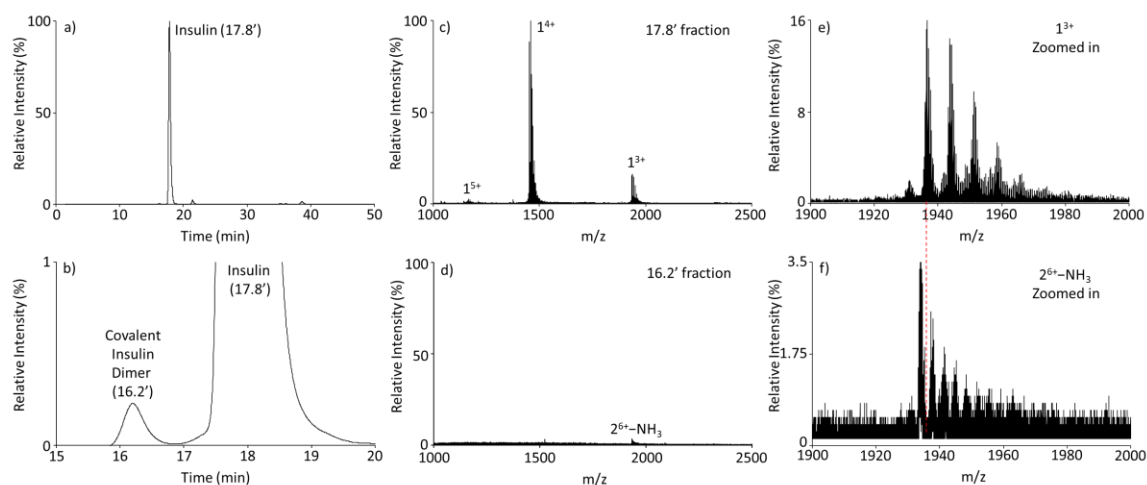


Figure 4.3 SEC separation of 3.4 mg/mL insulin in mobile phase and its corresponding MS spectra of the SEC fractions. (a) SEC separation of insulin (zoomed-out). (b) Zoomed-in SEC chromatogram highlighting the main insulin fraction at 17.8 min and the small covalent insulin dimer fraction at 16.2 min. (c) MS spectrum of the 17.8-min fraction, with only monomers at different charge states observed. (d) MS spectrum of the 16.2-min fraction, with a tiny peak of covalent dimer (2^{6+} -NH₃) observed. (e) Zoomed-in spectrum of the monomer at 3+ charge state from spectrum (c). (f) Zoomed-in spectrum of the covalent dimer at 6+ charge state from spectrum (d), with the peak position of the noncovalent insulin dimer labeled by the red dash line.

Table 4.1 Droplet size measurement results summary for insulin and glucagon

Analyte	Condition	Droplet diameter (nm)
human insulin	4% AcOH; 4- μ m nESI tips	16 \pm 2
human insulin	4% AcOH; 10- μ m nESI tips	22 \pm 1
human insulin	4% AcOH; 3- μ m nESI tips	17 \pm 2
glucagon	4% AcOH; 3- μ m nESI tips	14 \pm 2

Table 4.2 List of symbols and abbreviations and their definitions

Symbol or abbreviation	Definition	Example / Comment
size ^{charge}	Monomer or oligomer with n monomers and m charges, which has an m/z of $[n * M(\text{monomer}) + m * H]^{m+}$	1 ³⁺ : $[M+3H]^{3+}$ 2 ⁶⁺ : $[2M+6H]^{6+}$
<i>c</i>	True concentration of the non-aggregating solution, or the true concentration of the analyte monomer (mol/L)	/
<i>c_{bulk}</i>	Analyte concentration in the bulk solution	/
<i>c_s</i>	Sample concentration	/
$P(x, \mu)$	The possibility of having <i>x</i> analytes in the final droplet	$P(x, \mu) = \frac{e^{-\mu} \mu^x}{x!}$
<i>x</i>	Number of analytes in the final droplets	/
μ	Average number of analytes per droplet	/
μ_s	Average number of analytes per droplet for the sample solution	/
<i>V_{drop}</i>	Volume of the final droplet	$\frac{\mu}{V_{drop}} = c_{bulk}$
PFO	2,2,3,3,4,4,5,5,6,6,7,7,8,8,8-pentadecafluoro-1-octanol	/
ESI-MS	Electrospray Ionization Mass Spectrometry	/

CHAPTER 5. FACILITATED ISOMER DETECTION WITH DIFFERENTIAL MOBILITY SPECTROSCOPY AND ION-ION REACTION

5.1 Introduction

Proteomics, [1] lipidomics [2] and metabolomics [3] are the three frontier areas that rapidly grow in the last three decades. One important aim for the development of the three areas above is to directly analyze the biomolecules in their native environment so that accurate description of biological processes is obtained. [4] Mass spectrometry (MS) is a powerful tool in biomolecule analysis due to its high sensitivity, fast speed, and versatile applications. [5] With the help of soft ionization methods such as electrospray ionization (ESI), samples can be directly analyzed from solution phase, where most biomolecules exist in nature. [6] However, sample matrix often affects the ionization efficiency of target analytes or complicates the mass spectrum by contaminant noise like salt cluster peaks. [7, 8] Not only sample matrix creates a dimension of sample complexity, but also the analyte itself is a source of complexity. Take proteomics as an example. The protein database SWISS-PROT contains 559228 entries (checked on 2/25/2019) for all the proteins with reviewed known sequence, among which human-source proteins have 20417 entries. [9] Proteins without known sequence are not even counted in the numbers above. There are also many structural variations for the same protein species, such as immunoglobulin G (IgG). [10] Moreover, the analysis methods can introduce sample complexity as well. For example, the enzyme digestion of one protein can generate tens to hundreds of peptide fragments. [11] Therefore, in order to analyze biological samples and to study biological processes, the sample complexity is an issue that everyone needs to confront. [12]

Separation of analytes before they enter the mass spectrometer is a good way to deal with the issue of sample complexity. Various techniques have been developed to separate the analytes outside the mass spectrometer. As a representative chromatography method, High Pressure Liquid Chromatography (HPLC) is widely used in biological sample preparation and separation. [13] Based on their separation mechanism, HPLC can be further categorized into normal-phase HPLC (NP-HPLC), reverse-phase HPLC (RP-HPLC), Hydrophilic Interaction Chromatography (HILIC), Hydrophobic Interaction Chromatography (HIC), Size Exclusion Chromatography (SEC), and Ion Exchange Chromatography (IEC). [14] The categories above are achieved by a great selection of HPLC columns and mobile phases, and different dimensions of separation are provided. Despite the various types of separation dimensions and applications, HPLC still has its drawbacks when it's coupled to MS. The time it takes to do HPLC separation is much longer (in minutes to hours) compared to MS analysis timeframe (in seconds to minutes). The compatibility of the HPLC mobile phase with MS methods may be another issue.

Differential Mobility Spectrometry (DMS), also called High Field Asymmetric Waveform Ion Mobility Spectrometry (FAIMS), is an uprising separation technique coupled to mass spectrometers. [15] It is an analytical technique that separates ions in the carrier gas based on their mobility difference in high electrical field and low electrical field, [16] so there is no solvent compatibility issue. The DMS separation is very fast (in seconds) [17] and its apparatus is small. [18] Because it's an ambient separation technique, the DMS apparatus can be directly coupled to the mass spectrometer interface. Up to now DMS has been mostly applied to separate peptides, [19] proteins, [20] lipids, [21] isomers [22] and molecules with different conformations. [23]

The other route to solve the sample complexity issue is to increase the separation capability inside the mass spectrometer. On top of the analytes' mass-to-charge ratio (m/z) difference, which

is the first dimension of separation inside the mass spectrometer, tandem mass spectrometry (MSⁿ) provides a second dimension of separation through the fragmentation of analytes upon ion activation. [24] For isobaric or isomeric analytes, they can be distinguished by their different fragmentation patterns. The fragmentation pattern of the analyte can be altered by the ion structure, ion type and the activation method. [25] For an MS with fixed capability of activation method, the separation by tandem mass spectrometry can be further facilitated by altering the ion's structure and ion type through charge state manipulation and covalent modification. [25, 26]

Ion/ion reaction is a great way to change ion type and alter ion structure in the gas phase. [27] It's fast compared to solution-phase reactions, and it's thermodynamically and kinetically favored compared to ion/molecule reaction in the gas phase. [28] Charge transfer and charge exchange ion/ion reactions, such as proton transfer reaction, [29] electron transfer reaction, [30] and metal cation exchange reaction, [31] have been extensively used for spectrum simplification, reactant ion concentration, and complementary structural information probing. Covalent modification ion/ion reactions have also been applied to locate specific functional group in the analyte and to obtain more structural information by altering fragmentation pathways. [32]

As the complexity of the system studied increases, more and more samples require both ways of separation (outside / inside MS) to be analyzed. Taking advantage of the two techniques, the hyphenation of DMS and ion/ion can meet the need of more complicated systems and get the different species identified. Here, the DMS-Ion/Ion coupling method is developed and a model isomeric peptide system is used to demonstrate its capability in complex sample analysis.

5.2 Experimental

5.2.1 Materials

Methanol was purchased from Mallinckrodt (Phillipsburg, NJ). Peptides KAGK(AG)₃ and K(AG)₄K were custom synthesized by CSC Scientific (Fairfax, VA). Reagent 4-formyl-benzene-1,3-disulfonic acid (FBDSA) was obtained from Sigma-Aldrich (St. Louis, MO). All peptide solutions were prepared in 50/50 (v/v) methanol/water (~ 0.2 mM). The FBDSA reagent was dissolved in water (~ 3 mM).

5.2.2 Mass Spectrometry

Analyses of peptides were performed on QTRAP[®] 4000, a hybrid triple quadrupole / linear ion trap mass spectrometer (SCIEX, Concord, ON, Canada), previously modified for ion/ion reactions. [33] Alternately pulsed nano-electrospray ionization (nESI) sources allow for sequential injections of reagent and analyte ions, which are sequentially isolated in the Q1-mass filter prior to their injection into the q2 reaction cell. After a defined mutual storage reaction time, the product ions are then transferred to Q3, where the ions undergo further mass analysis via MSⁿ and get detected by mass-selective axial ejection (MSAE).

DMS related experiments were performed on TripleTOF[®] 5600, a hybrid quadrupole / time of flight (TOF) mass spectrometer (SCIEX, Concord, ON, Canada), previously modified for ion/ion reactions. [34] After injections of analyte or reagent ions by alternately pulsed nESI, the ions are first separated by the DMS device, then isolated in the Q1 mass filter and injected into the q2 reaction cell. Mutual storage time in q2 allows for ion/ion reaction. The ions then undergo further mass analysis via MSⁿ and get detected by TOF analysis. For details of the DMS-Ion/Ion setup, please refer to section 5.3.1.

5.3 Results and Discussion

5.3.1 Setup of DMS-Ion/Ion Scan Function

Since the DMS-Ion/Ion experimental procedure is different from conventional DMS experiment or conventional ion/ion experiment, a detailed explanation on the setup of DMS-Ion/Ion is described here. The DMS device in use is a commercial SelexION[®] DMS cell (SCIEX, Concord, ON, Canada), which is directly coupled with the interface of the TripleTOF[®] 5600 mass spectrometer (SCIEX, Concord, ON, Canada), a QqTOF system modified for ion/ion reactions. The DMS cell consists of two planar electrodes, two gas sources, a temperature control module, and a power supply (Figure 1.7(a)). [35, 36]

Under normal operation conditions, when the DMS is in use, the DMS cell would be mounted onto the instrument interface. A constant spray of sample, either by electrospray ionization (ESI) or nano-electrospray ionization (nESI), is provided to the entrance inlet of DMS. A separation voltage (SV) of periodically alternating V_{high} and V_{low} is constantly applied to the two electrodes in order to separate the ions based on their different ion mobility in high and low electric fields. The compensation voltage (CV) is applied to the electrodes to compensate for the vertical displacement caused by SV. The CV can either be applied at a constant value to allow for only one type of ions to go through, or be a ramp from a low value (CV_{low}) to a high value (CV_{high}) with a certain step size. At each CV step, ions that can go through the DMS cell will be detected, and a total ion current (TIC) shall be calculated and saved with the mass spectrum at that CV step. After the completion of the CV ramp, an array of mass spectra with their TIC values is saved with their corresponding CV voltages. From the array of mass spectra, and their corresponding TIC values and CV voltages, three types of spectrum can be obtained. The overall ionogram can be obtained by plotting the TIC values at different CV steps with the CV voltages. The averaged mass spectrum can be calculated by averaging the array of mass spectra. The extracted ionogram for an

m/z range can also be calculated from the array of mass spectra, where the sum of intensities for that specific m/z range from each mass spectrum are plotted with their corresponding CV voltages.

Typically, ion/ion reactions are performed using the following procedure. The analyte ions are sprayed by source A, injected into the mass spectrometer, isolated in Q1 if necessary, transferred to q2 and trapped there. Then the reagent ions are sprayed by source B, injected into the mass spectrometer, isolated in Q1 if necessary, transferred to q2 and react with analyte ions when they are mutually trapped in q2. Then the product ions from the ion/ion reaction undergo MS^n and get detected.

To establish the DMS-Ion/Ion method, we need to consider where the DMS can be incorporated into the ion/ion scan function. To start with, since the reagent ion for ion/ion reaction is usually fixed, only the DMS for the analyte ions is needed. Therefore, in the analyte injection step, a fixed DMS SV and a CV ramp is needed. For the injection of reagent, the DMS voltages can be changed to ground so that the injection of reagent is the same as a conventional ion/ion experiment process, which will be called 1D DMS-Ion/Ion process. Another way to do this is to set the DMS voltages to certain values in the reagent injection step so that the reagent ion can go through efficiently, which will be called 1.5D DMS-Ion/Ion process.

In the 1D DMS-Ion/Ion process, the experiment is done with the following steps:

1. Set DMS SV to be V_{SV} . Set DMS CV to be $V_{CV} = CV_1$. CV_1 means the first CV voltage in the CV voltage ramp.
2. Spray analyte ions (e.g., cations) using nESI with the instrument parameters set to transmit analyte ions (e.g., parameters for cation transmission).
3. Analyte ions that can go through the DMS device are trapped in q2.
4. Change SV and CV settings to zero.

5. Spray reagent ions (e.g., anions) using nESI with the instrument parameters set to transmit reagent ions (e.g., parameters for anion transmission).
6. All reagent ions can go through the DMS device. They are subject to Q1 isolation and then mutually trapped with analyte ions in q2, where ion/ion reaction happens.
7. The ions in q2 are subject to tandem MS operations and the final product ions are detected by TOF. The mass spectrum is saved with its TIC and CV values.
8. Repeat Step 1 to Step 7 with the CV voltage set to the next voltage in the CV ramp (e.g., $V_{CV} = CV_2$ for the second round, $V_{CV} = CV_3$ for the third round, etc.), until all the voltages in the CV ramp are completed.

In the 1.5D DMS-Ion/Ion process, the experiment is done with the following steps:

1. Run a normal DMS scan for the reagent ions to learn at what CV voltage the reagent ions are best transmitted through the DMS device. The CV voltage with the climax reagent ion transmission is called $CV_{reagent}$ in the following steps.
2. Set DMS SV to be V_{SV} . Set DMS CV to be $V_{CV} = CV_1$. CV_1 means the first CV voltage in the analyte CV voltage ramp.
3. Spray analyte ions (e.g., cations) using nESI with the instrument parameters set to transmit analyte ions (e.g., parameters for cation transmission).
4. Analyte ions that can go through the DMS device are trapped in q2.
5. Keep SV the same. Change CV voltage to $CV_{reagent}$.
6. Spray reagent ions (e.g., anions) using nESI with the instrument parameters set to transmit reagent ions (e.g., parameters for anion transmission).
7. The reagent ions that can go through the DMS device at $CV_{reagent}$ shall enter the mass spectrometer. They are subject to Q1 isolation and then mutually trapped with analyte ions in q2,

where ion/ion reaction happens.

8. The ions in q_2 are subject to tandem MS operations and the final product ions are detected by TOF. The mass spectrum is saved with its TIC and CV values.

9. Repeat Step 1 to Step 7 with the analyte CV voltage set to the next voltage in the CV ramp (e.g., $V_{CV} = CV_2$ for the second round, $V_{CV} = CV_3$ for the third round, etc.), until all the voltages in the analyte CV ramp are completed.

Although the 1D DMS-Ion/Ion experiment is very similar to 1.5D DMS-Ion/Ion one, each of them has their own advantages and disadvantages. For 1D DMS-Ion/Ion, because the SV and CV voltages are grounded when the reagent ions are injected, there is no reagent ion loss in this process. However, the electronics that apply SV voltage may require some warm-up time to provide a stable SV output, [36] so grounding the SV in the middle of the experiment may affect the SV output in the following CV ramp steps. Similarly, for 1.5D DMS-Ion/Ion experiment, the advantage is a stable SV output, but there could be reagent ion loss due to the DMS separation of the reagent ions.

5.3.2 Application of 1D DMS-Ion/Ion Method to a Model Peptide Isomer System

One application of the DMS-Ion/Ion method is to distinguish isomers in a sample, using both the separation capability of DMS and that of the ion/ion reaction. Isomeric peptides KAGK(AG)₃ and K(AG)₄K are chosen as the model system to demonstrate the need of combining DMS and ion/ion reaction in order to separate and identify each of the component in a mixture.

5.3.2.1 Exploration on Isomer Identification by CID Only

The two isomeric peptides are very similar in structure. Their only difference is the position of the second lysine residue in the peptide sequence, one in the fourth position to the N-terminus, and the other in the tenth position to the N-terminus. One common solution to the identification of

the two isomers with mass spectrometer is to apply CID on the two species, and they should be distinguished by their unique fragmentation. However, these two isomeric model peptides are not easily distinguished with only mass isolation and CID. The complexity of the system not only comes from their similarity in the peptide sequence, but also relates to the coincidence that the mass of peptide residue AG is isobaric to the residue K. Those two factors result in very little difference in the mass of their fragment ions (Table 5.1) and hence their CID spectra (Figure 5.1).

Table 5.1 compares the mass of common CID fragment ions (b/y ions) of the two peptides. Fragment ions with the same exact mass between the two peptides are filled with red shade and they cannot be used for isomer identification. Fragment ions that have isobaric mass between the two peptides are filled with yellow shade. The isobaric fragment ions in yellow shade have less than 0.05 Da mass difference, which is not preferred for general identification of the two isomers because they can only be distinguished with high resolution instrument. For the fragment ion in green shade (b_4 fragment ion of $K(AG)_4K$), even though it seems unique to the peptide $K(AG)_4K$, the other peptide $KAGK(AG)_3$ can still form this fragment through sequential fragmentation of its scrambled b ions, so it's not safe to distinguish one peptide from another through the fragment ion in green shade. Therefore, only the fragment ions without shade are easily distinguishable on the spectrum, which leaves b_9 and y_1 for $KAGK(AG)_3$ and y_6 for $K(AG)_4K$ as the unique peaks in the CID spectrum. Since y_1 of $KAGK(AG)_3$ is usually below the low mass cutoff setting of the instrument and barely seen on the spectrum, there are only two unique fragment ions left: the b_9 of $KAGK(AG)_3$ and y_6 of $K(AG)_4K$.

Figure 5.1 demonstrates the CID spectra of the two peptide isomers respectively. In aqueous solution under neutral pH, the two peptides are mainly in doubly protonated form, though singly protonated peptide ions are also observable with lower intensities. As a result, CID on the

doubly protonated peptide $[M+2H]^{2+}$ and singly protonated peptide $[M+H]^+$ are performed. The comparison of the CID spectrum on the doubly protonated peptides is shown on the left two panels ((a) and (c)) in Figure 5.1. The two spectra are very similar in overall pattern. The unique fragment peaks are labeled with a red dot, which are much lower in intensity than the other dominant fragment ions and may not be good for peptide identification in a mixture. The CID spectra on the singly protonated peptides are shown in the right panel ((b) and (d)) of Figure 5.1. Similar to the previous comparison spectra, the unique peaks are labeled with red dots. From the spectra we can see that the y_6 fragment ion of $K(AG)_4K$ still has a low intensity. Even though the b_9 fragment ions and its water loss peaks in the CID spectrum of singly protonated $KAGK(AG)_3$ is quite obvious, it is not straightforward to tell whether there is a low concentration of $K(AG)_4K$ in the $KAGK(AG)_3$ sample. Therefore, a direct distinction of the two peptides is not easy to achieve with mere CID fragmentation.

5.3.2.2 Exploration on Isomer Identification by Ion/Ion Reaction

Gas-phase Schiff-base modification can be applied to the two model peptides via ion/ion reaction. After mutual storage of the doubly protonated analyte ions $[M+2H]^{2+}$ with the singly deprotonated FBDSA ions $[FBDSA-H]^-$, an electrostatic complex $[M+FBDSA+H]^+$ would form. CID on the electrostatic complex ions generates a signature water loss peak, which indicates the formation of Schiff-base modified peptide ions $[M+H+\blacklozenge]^+$ (\blacklozenge denotes the +248 Da mass shift caused by the Schiff-base modification). [37] The fragmentation patterns of the two Schiff-base modified peptide ions show more difference than the CID spectrum of their unmodified counterparts, as shown in Figure 5.2. Due to the covalent modification to the amine group (either on the N-terminus or the lysine side chain) on the isomeric peptides, more unique fragment ions can be identified with $K(AG)_4K$. Compared to peptide $KAGK(AG)_3$, the second lysine being the

C-terminus residue makes all the modified y ions after y_6 (including modified y_6) and unmodified b ions after b_6 (including unmodified b_6) unique fragments for FBDSA-modified $K(AG)_4K$, as shown in Figure 5.2(a). For peptide $KAGK(AG)_3$, no new unique fragment ion species are added. The only unique fragment ions are still b_9 related, and since all the amine groups are on the N-terminal side of b_9 position for $KAGK(AG)_3$, all the b_9 ions should be modified ions, as shown in Figure 5.2(b).

Although with the help of ion/ion reaction, the two peptide isomers can be better identified, there are still cases where one of the isomers may be not easily distinguished from the other peptide. For example, since the unique fragment ions for $K(AG)_4K$ are still not the dominant fragment ions, chances are when the concentration of $K(AG)_4K$ is very low in a mixture of $K(AG)_4K$ and $KAGK(AG)_3$, its unique fragment ions may not be apparent enough for its identification.

5.3.2.3 Exploration on Isomer Identification with DMS Only

With DMS only, where no tandem MS or ion/ion reaction is involved, the two peptide isomers can be separated well at an SV setting of 4000V, as shown in Figure 5.3. Isomer standard solution of each peptide is sprayed, and the ions are separated with normal DMS. The extracted CV ionograms of the doubly protonated peptide peak are shown in Figure 5.3. The peptide $K(AG)_4K$ go through the DMS at a CV voltage of 20.3V (Figure 5.3(a)), while its isomer $KAGK(AG)_3$ go through the DMS at a CV voltage of 27.7V (Figure 5.3(b)). For a mixture of the two isomers, the $[M+2H]^{2+}$ ions for each isomer are still well separated, as what they do in the standard solutions. The two CV traces are well separated for each ion, and their corresponding CV at climax DMS transmission stay in the same position as the two standard solutions, which allows for the unambiguous assignment of each species in the peptide mixture.

Clearly if we have the standard solutions of the two isomers, the DMS by itself can identify the two isomeric species by comparing the DMS CV ionograms. However, not all of the isomers in real life have standard solutions, which makes it harder to do isomer identification by DMS only. It also complicates the sample preparation process, since each of the isomers need a standard solution. Besides, with the powerful capability of tandem MS to decipher the structural information of molecules, the dissociation spectra of the isomers are a good way of structural confirmation and they may provide further explanations on their separation by the DMS device.

5.3.2.4 Exploration on Isomer Identification with 1D DMS-Ion/Ion

Following the steps in Section 5.3.1 for 1D DMS-Ion/Ion experiment, the K(AG)₄K and KAGK(AG)₃ standard solutions are sprayed and separated with DMS. The K(AG)₄K and KAGK(AG)₃ still have their climax DMS transmission at a CV voltage of 20.3V and 27.7V respectively, when the SV is set to 4000V. Their DMS separation is followed by ion/ion reaction with isolated FBDSA reagent ions, isolation of the electrostatic complex, and fragmentation of the electrostatic complex to generate the MS³ mass spectrum. One limitation for our current DMS setting is that under the DMS CV scanning mode, the DMS data cannot be averaged. Therefore, due to the low ion statistics in the MS³ experiment, the MS³ mass spectra in Figure 5.4 were taken with a fixed CV for the analyte peptide and a fixed CV for the reagent, in which the mass spectrum can be saved after 100 averages for better ion statistics. On the mass spectra, the unique fragment peaks (labeled with red dots) remain on the mass spectrum for clear isomer identification, though the ions are fragmented at a higher pressure in q2 of TripleTOF[®] 5600 for the DMS experiments than the CID in the low pressure Q3 of QTRAP[®] 4000 in Section 5.3.2.2.

For the isomer mixture, they are well separated by DMS, with their corresponding climax DMS transmission CV voltages at 20.0V and 28.0V (SV=4000V). Similar to the standard solutions,

the MS³ mass spectra were taken for 100 averages with a fixed CV for both analyte and reagent ions. The MS³ mass spectrum for the CV=20.0V isomer in the mixture experiment (Figure 5.4(c)) matches with that of the K(AG)₄K isomer (Figure 5.4(a)) with the unique fragment ions clearly shown on the spectrum. Similarly, the CV=28.0V isomer in the mixture (Figure 5.4(d)) can be identified to be KAGK(AG)₃ from its identical fragmentation pattern to the standard solution (Figure 5.4(b)) and the existence of the unique b₉⁺ ion on the mass spectrum.

From the application of DMS-Ion/Ion to the model peptide isomer system of K(AG)₄K and KAGKAGAGAG, it can be inferred that the combination of DMS and ion/ion is suitable for the identification of complex isomer system, especially when they are not easy to be distinguished by only one of the techniques. Compared to mere CID, ion/ion reaction can facilitate the analyte identification by adding more structural features to the analytes. With DMS, the separation of the analyte isomers can be achieved to simplify the subsequent tandem MS spectrum. As for the 1D DMS-Ion/Ion experiment, the possible drawback of unstable SV voltage is not reflected on the mass spectra, which show reproducible CV voltages at the climax DMS transmission.

5.3.3 Application of 1.5D DMS-Ion/Ion Method to a Peptide Mixture System

Another possible application of DMS-Ion/Ion is to simplify the post-ion/ion mass spectrum for the ion/ion reaction of a mixture. The ion/ion reaction applied to a mixture can be used for isomer identification, analyte labeling in a complex sample, and rapid reactivity examination of ion/ion reaction. Here a peptide mixture of ARAAKA, AHAAHA, GRGMGRGMGRL and K(AG)₄K and a reagent ion of periodate (IO₄⁻) is used as an example to perform 1.5D DMS-Ion/Ion experiment.

The ion/ion reagent periodate can be applied to selectively oxidize antioxidant residues (such as methionine and tryptophan), neutral basic residues (lysine, arginine and histidine) and

disulfide bond linkage in the peptide by adding an oxygen to the residue after activation of the electrostatic complex ion. [38-40] In the peptide mixture, we intentionally selected peptides that contain antioxidant residues (GRGMGRGMGRL) and peptides that contain basic residues (ARAAKA, AHAAAHA, K(AG)₄K) so that a comparison of the reactivity between the periodate and different peptide species can be made.

In the direct spray of the analyte peptide mixture via positive nESI, the mass spectrum (Figure 5.5(a)) showed multiple charge states of each of the peptide analytes, which makes the mass spectrum a bit complicated. Extracted CV ionograms of the doubly protonated peaks of the four peptide components demonstrated well separation of the four ion species by DMS separation, (Figure 5.5(b)) and this is confirmed by the mass spectra at each of the climax transmission CV voltages (data not shown).

In the normal DMS separation of the reagent periodate ion (IO_4^-) via negative nESI, the climax transmission CV voltage for periodate ion is -11.3V (Figure 5.5(d)). With a fixed CV voltage at -11.3V , the mass spectrum for the periodate ion (Figure 5.5(c)) is much cleaner and contains only the periodate ion, so no isolation was performed after the DMS separation.

The 1.5D DMS-Ion/Ion experiment was performed as described in Section 5.3.1, with the CV ramp for the peptide analytes in the positive mode and a fixed CV value of -11.3V for the transmission and separation of the periodate ion in the negative mode. After the mutual storage step, ion/ion reaction products are formed and detected by the TOF. For ARAAHA and AKAAKA, the ion/ion reaction generated $[\text{M}+\text{H}]^+$ proton transfer products (data not shown). For K(AG)₄K, $[\text{M}+\text{H}]^+$ of proton transfer reaction and an electrostatic complex of $[\text{M}+\text{IO}_4+2\text{H}]^+$ was observed (data not shown). For GRGMGRGMGRL, only the electrostatic complex of $[\text{M}+\text{IO}_4+2\text{H}]^+$ was observed (data not shown). A broadband activation of all the ion/ion reaction

products via DDC CID was performed to see what species was oxidized by the periodate. Their corresponding MS² mass spectra are shown in Figure 5.5(e)-(h). For ARAAKA (Figure 5.5(g)) and AHAAHA (Figure 5.5(h)), their proton transfer product [M+H]⁺ remained with almost no fragmentation. For K(AG)₄K, the complex [M+IO₄+2H]⁺ all transformed into proton transfer product [M+H]⁺, and no oxidized product was observed (Figure 5.5(f)). For antioxidant residue containing peptide GRGMGRGMGRL (Figure 5.5(e)), the oxidized product [M+H+O]⁺ was formed with full conversion, which is as expected since methionine is a residue readily to be oxidized.

In summary, the 1.5D DMS-Ion/Ion experiment was successfully applied to the peptide mixture system with periodate. DDC CID is very useful in 1.5D DMS-Ion/Ion experiment as it provides broadband excitation on all the ion/ion reaction products. The fixed DMS voltage applied to the reagent ion not only helps stabilize the SV voltage by not having to turning off the SV voltage, but also filters the reagent ions with reduced background noise. The possibility of reagent ion loss after the application of DMS still remains, though in this example the amount of reagent periodate ion is sufficient enough that the ion loss is not that obvious.

5.4 Conclusions

A method of combining DMS with ion/ion reaction is discussed here. With the different DMS application to the reagent ions, the DMS-Ion/Ion experiment can be done through either 1D mode or 1.5D mode. The 1D DMS-Ion/Ion experiment was successfully applied to the system of KAGK(AG)₃ and K(AG)₄K mixture, with the isomeric peptides well separated by the DMS and clearly identified with ion/ion reaction and tandem MS. The 1.5D DMS-Ion/Ion experiment was tested with the peptide mixture and the periodate reagent to show its application in simplification of post-ion/ion results. The DMS-Ion/Ion method could also be used in other systems, such as

proteins and lipids. Future work would focus on more complicated systems, like lipid isomers that differs by double bond locations or by cis- and trans-conformation of the double bond, protein mixture, or even larger and trickier systems. Besides, the extension of 1D and 1.5D DMS-Ion/Ion modes to 2D DMS-Ion/Ion modes can be tuned in hope of better component analysis for complicated systems.

5.5 References

1. Aebersold, R.; Mann, M. Mass Spectrometry-Based Proteomics. *Nature* 422, 198-207 (2003).
2. Yang, K.; Han, X. Lipidomics: Techniques, Applications, and Outcomes Related to Biomedical Sciences. *Trends Biochem. Sci.* 41, 954-969 (2016).
3. Johnson, C. H.; Ivanisevic J.; Siuzdak, G. Metabolomics: Beyond Biomarkers and Towards Mechanisms. *Nat. Rev. Mol. Cell Biol.* 17, 451-459 (2016).
4. Leney, A. C.; Heck, A. J. R. Native Mass Spectrometry: What is in the Name? *J. Am. Soc. Mass Spectrom.* 28, 5-13 (2017).
5. De Hoffmann, E.; Stroobant, Vincent. *Mass Spectrometry: Principles and Applications* (3rd ed.). John Wiley & Sons, Chichester, UK (2007).
6. Fenn, J. B. Electrospray Wings for Molecular Elephants (Nobel Lecture). *Angew. Chem. Int. Ed.* 42, 3871-3894 (2003).
7. Panuwet, P.; Hunter, R. E., Jr.; D'Souza, P. E.; Chen, X.; Radford, S. A.; Cohen, J. R.; Marder, M. E.; Kartavenka, K.; Ryan, P. B.; Barr, D. B. Biological Matrix Effects in Quantitative Tandem Mass Spectrometry-Based Analytical Methods: Advancing Biomonitoring. *Crit. Rev. Anal. Chem.* 46, 93-105 (2016).
8. Sterling, H. J.; Batchelor, J. D.; Wemmer, D. E.; Williams, E. R. Effects of Buffer Loading for Electrospray Ionization Mass Spectrometry of a Noncovalent Protein Complex that Requires High Concentrations of Essential Salts. *J. Am. Soc. Mass Spectrom.* 21, 1045-1049 (2010).
9. Information retrieved from <https://www.uniprot.org/uniprot/?query=reviewed%3Ayes>.
10. Leblebici, P.; Leblebici, M. E.; Ferreira-da-Silva, F.; Rodrigues, A. E.; Pais, L. S. Separation of Human Immunoglobulin G Subclasses on a Protein A Monolith Column. *J. Chromatogr. B* 962, 89-93 (2014).
11. Pappin, D. J. C.; Hojrup, P.; Bleasby, A. J. Rapid Identification of Proteins by Peptide-Mass Fingerprinting. *Curr. Biol.* 3, 327-332 (1993).
12. Chandramouli, K.; Qian, P. Proteomics: Challenges, Techniques and Possibilities to Overcome Biological Sample Complexity. *Hum. Genom. Proteom.* 2009, 239204 (2009).
13. Pitt, J. J. Principles and Applications of Liquid Chromatography-Mass Spectrometry in Clinical Biochemistry. *Clin. Biochem. Rev.* 30, 19-34 (2009).
14. Niessen, W. *Liquid Chromatography – Mass Spectrometry* (3rd ed.). CRC Press, Boca Raton, FL (2006).

15. Kolakowski, B. M.; Mester, Z. Review of Applications of High-Field Asymmetric Waveform Ion Mobility Spectrometry (FAIMS) and Differential Mobility Spectrometry (DMS). *Analyst*, 132, 842-864 (2007).
16. Cumeras, R.; Figueras, E.; Davis, C. E.; Baumbach, J. I.; Gràcia, I. Review on Ion Mobility Spectrometry. Part 1: Current Instrumentation. *Analyst* 140, 1376-1390 (2015).
17. Campbell, J. L.; Le Blanc, J. C.; Kibbey, R. G. Differential Mobility Spectrometry: A Valuable Technology for Analyzing Challenging Biological Samples. *Bioanalysis* 7, 853-856 (2015).
18. Chouinard, C. D.; Wei, M. S.; Beekman, C. R.; Kemperman, R. H. J.; Yost, R. A. Ion Mobility in Clinical Analysis: Current Progress and Future Perspectives. *Clin. Chem.* 62, 124-133 (2016).
19. Levin, D. S.; Miller, R. A.; Nazarov, E. G.; Vouros, P. Rapid Separation and Quantitative Analysis of Peptides Using a New Nanoelectrospray-Differential Mobility Spectrometer-Mass Spectrometer System. *Anal. Chem.* 78, 5443-5452 (2006).
20. Cooper, H. J. To What Extent is FAIMS Beneficial in the Analysis of Proteins? *J. Am. Soc. Mass Spectrom.* 27, 566-577 (2016).
21. Shvartsburg, A. A.; Isaac, G.; Leveque, N.; Smith, R. D.; Metz, T. O. Separation and Classification of Lipids Using Differential Ion Mobility Spectrometry. *J. Am. Soc. Mass Spectrom.* 22, 1146-1155 (2011).
22. Shvartsburg, A. A.; Creese, A. J.; Smith, R. D.; Cooper, H. J. Separation of Peptide Isomers with Variant Modified Sites by High-Resolution Differential Ion Mobility Spectrometry. *Anal. Chem.* 82, 8327-8334 (2010).
23. Zhu, S.; Campbell, J. L.; Chernushevich, I.; Le Blanc, J. C. Y.; Wilson, D. J. Differential Mobility Spectrometry-Hydrogen Deuterium Exchange (DMS-HDX) as a Probe of Protein Conformation in Solution. *J. Am. Soc. Mass Spectrom.* 27, 991-999 (2016).
24. Waridel, P.; Wolfender, J.; Ndjoko, K.; Hobby, K. R.; Major, H. J.; Hostettmann, K. Evaluation of Quadrupole Time-of-Flight Tandem Mass Spectrometry and Ion-Trap Multiple-Stage Mass Spectrometry for the Differentiation of C-Glycosidic Flavonoid Isomers. *J. Chromatogr. A* 926, 29-41 (2001).
25. McLuckey, S. A.; Mentinova, Marija. Ion/Neutral, Ion/Electron, Ion/Photon, and Ion/Ion Interactions in Tandem Mass Spectrometry: Do We Need Them All? Are They Enough? *J. Am. Soc. Mass Spectrom.* 22, 3-12 (2011).
26. Reid, G. E.; McLuckey, S. A. 'Top Down' Protein Characterization via Tandem Mass Spectrometry. *J. Mass Spectrom.* 37, 663-675 (2002).
27. McLuckey, S. A.; Huang, T. Ion/Ion Reactions: New Chemistry for Analytical MS. *Anal. Chem.* 81, 8669-8676 (2009).

28. Stephenson, J. L.; McLuckey, S. A. Ion/Ion Reactions in the Gas Phase: Proton Transfer Reactions Involving Multiply-Charged Proteins. *J. Am. Chem. Soc.* 118, 7390-7397 (1996).
29. Stephenson, J. L.; McLuckey, S. A. Ion/Ion Proton Transfer Reactions for Protein Mixture Analysis. *Anal. Chem.* 68, 4026-4032 (1996).
30. Pitteri, S. J.; Chrisman, P. A.; Hogan, J. M.; McLuckey, S. A. Electron Transfer Ion/Ion Reactions in a Three-Dimensional Quadrupole Ion Trap: Reactions of Doubly and Triply Protonated Peptides with SO_2^- . *Anal. Chem.* 77, 1831-1839 (2005).
31. Newton, K. A.; McLuckey, S. A. Generation and Manipulation of Sodium Cationized Peptides in the Gas Phase. *J. Am. Soc. Mass Spectrom.* 15, 607-615 (2004).
32. Prentice, B. M.; McLuckey, S. A. Gas-Phase Ion/Ion Reactions of Peptides and Proteins: Acid/Base, Redox, and Covalent Chemistries. *Chem. Commun.* 49, 947-965 (2013).
33. Xia, Y.; Wu, J.; McLuckey, S. A.; Londry, F. A.; Hager, J. W. Mutual Storage Mode Ion/Ion Reactions in a Hybrid Linear Ion Trap. *J. Am. Soc. Mass Spectrom.* 16, 71-81 (2005).
34. Rojas-Betancourt, S.; Stutzman, J. R.; Londry, F. A.; Blanksby, S. J.; McLuckey, S. A. Gas-Phase Chemical Separation of Phosphatidylcholine and Phosphatidylethanolamine Cations via Charge Inversion Ion/Ion Chemistry. *Anal. Chem.* 87, 11255-11262 (2015).
35. Campbell, J. L.; Le Blanc, J. C.; Schneider, B. B. Probing Electrosprya Ionization Dynamics Using Differential Mobility Spectrometry: The Curious Case of 4-Aminobenzoic Acid. *Anal. Chem.* 84, 7857-7864 (2012).
36. SCIEX. *Analyst® 1.6.3 Software. SelexION® Technology for 5500 and 5600 Series Systems and SelexION®+ Technology for 6500+ Series Systems User Guide* [PDF file] (2015). Retrieved from <https://sciex.com/Documents/manuals/selexion-selexion-plus-5500-6500-6500plus-user-guide-en.pdf>
37. Han H.; McLuckey, S. A. Selective Covalent Bond Formation in Polypeptide Ions via Gas-Phase Ion/Ion Reaction Chemistry. *J. Am. Chem. Soc.* 131, 12884-12885 (2009).
38. Pilo, A. L.; Bu, J.; McLuckey, S. A. Gas-Phase Oxidation of Neutral Basic Residues in Polypeptide Cations by Periodate. *J. Am. Soc. Mass Spectrom.* 27, 1979-1988 (2016).
39. Pilo, A. L.; McLuckey, S. A. Selective Gas-Phase Ion/Ion Reactions: Enabling Disulfide Mapping via Oxidation and Cleavage of Disulfide Bonds in Intermolecularly-Linked Polypeptide Ions. *Anal. Chem.* 88, 8972-8979 (2016).
40. Pilo, A. L.; Zhao, F.; McLuckey, S. A. Gas-Phase Oxidation via Ion/Ion Reactions: Pathways and Applications. *J. Am. Soc. Mass Spectrom.* 28, 991-1004 (2017).

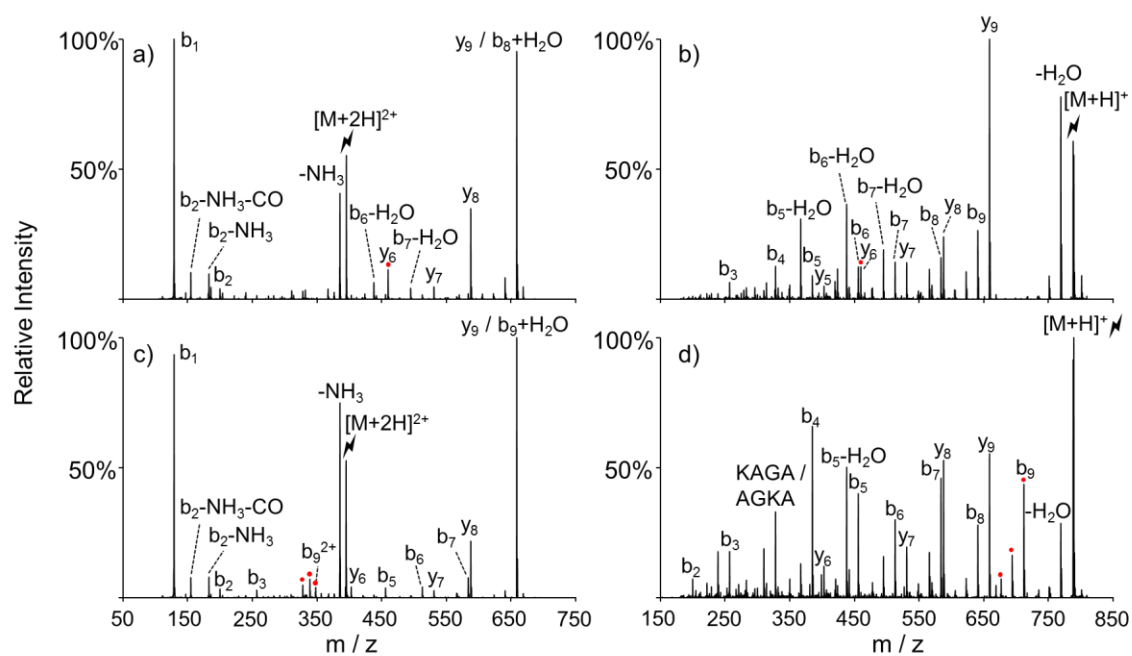


Figure 5.1 CID on $[M+2H]^{2+}$ and $[M+H]^+$ of $K(AG)_4K$ and $KAGK(AG)_3$. Top: $K(AG)_4K$; Bottom: $KAGK(AG)_3$; Left: CID of $[M+2H]^{2+}$; Right: CID of $[M+H]^+$. The red dot labels the unique peaks that distinguish the two peptides.

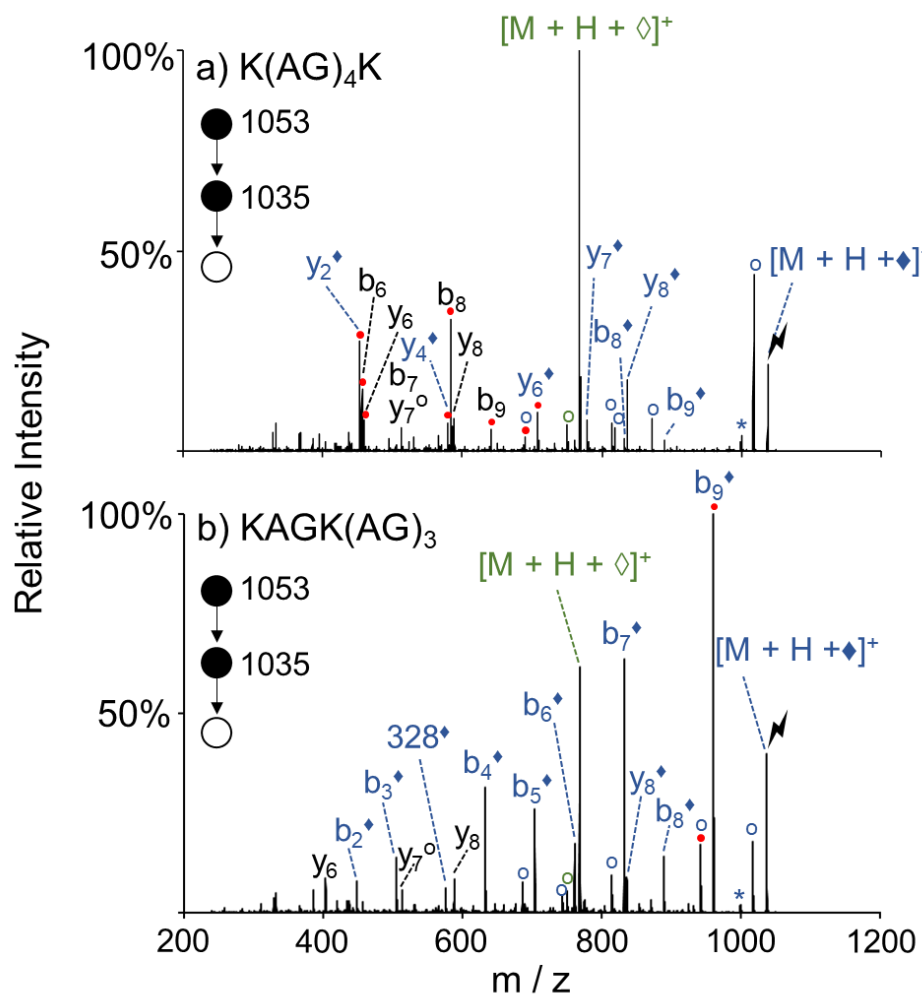


Figure 5.2 CID spectra of FBDSA-modified (a) K(AG)₄K and (b) KAGK(AG)₃. Degree symbols (°) denote water losses (−18 Da). Asterisks (*) denote ammonia losses (−17 Da). Solid diamonds (◆) denote ion mass shift with Schiff base modification (+248 Da) and all Schiff-base modified ions are labeled in blue. Hollow diamonds (◊) denote the rearrangement products (−19 Da) and all products in the Schiff base rearrangement pathway are labeled in green. The red dot labels the unique peaks that distinguish the two peptides.

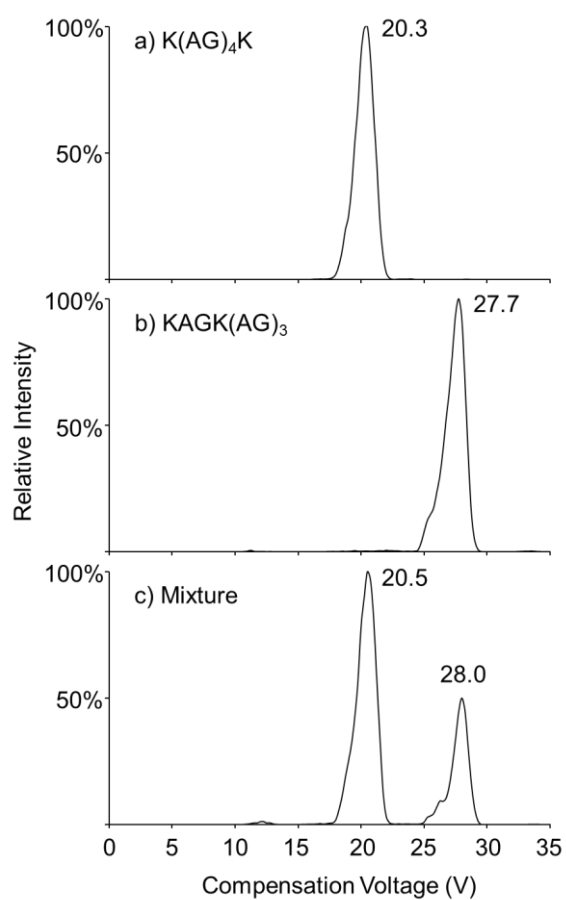


Figure 5.3 Compensation Voltage (CV) of $[M+2H]^{2+}$ ion in a DMS CV scan. Solution: a) K(AG)₄K, b) KAGK(AG)₃, and c) mixture of the two peptides.

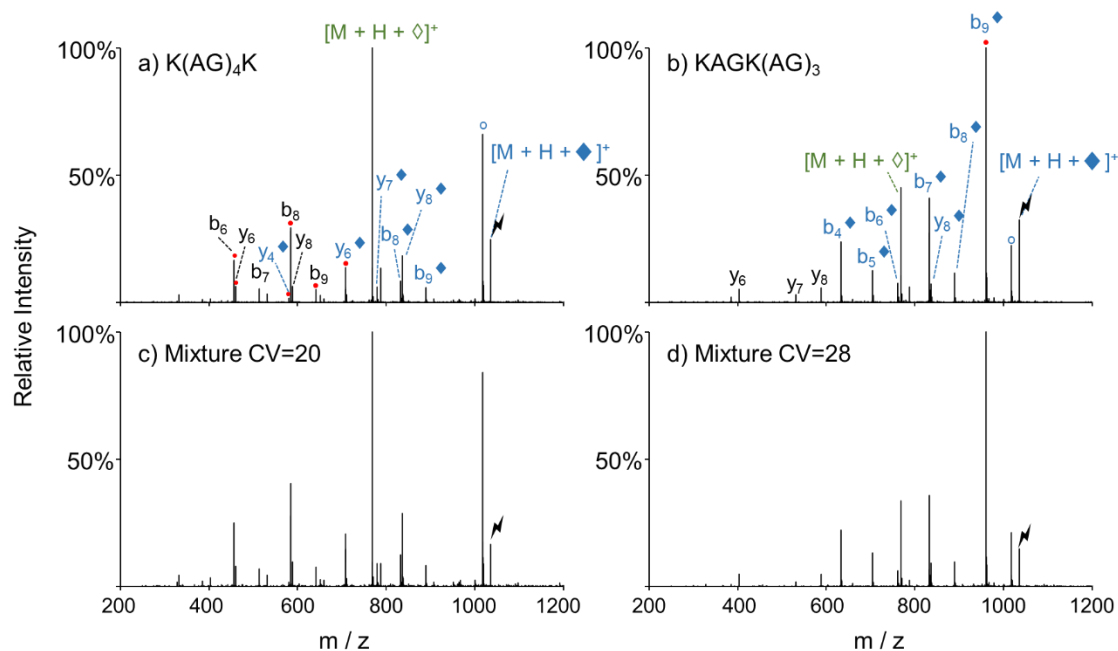


Figure 5.4 CID on Schiff bases formed by $K(AG)_4K$ and $KAGK(AG)_3$ with FBDSA. a) $K(AG)_4K$, CV=20.3V. b) $KAGK(AG)_3$, CV=27.7V. c) Mixture, CV=20.0. d) Mixture, CV=28.0. Degree symbols (°) denote water losses (-18 Da). Solid diamonds (◆) denote ion mass shift with Schiff base modification ($+248$ Da) and all Schiff-base modified ions are labeled in blue. Hollow diamonds (◊) denote the rearrangement products (-19 Da) and all products in the Schiff base rearrangement pathway are labeled in green. The red dot labels the unique peaks that distinguish the two peptides.

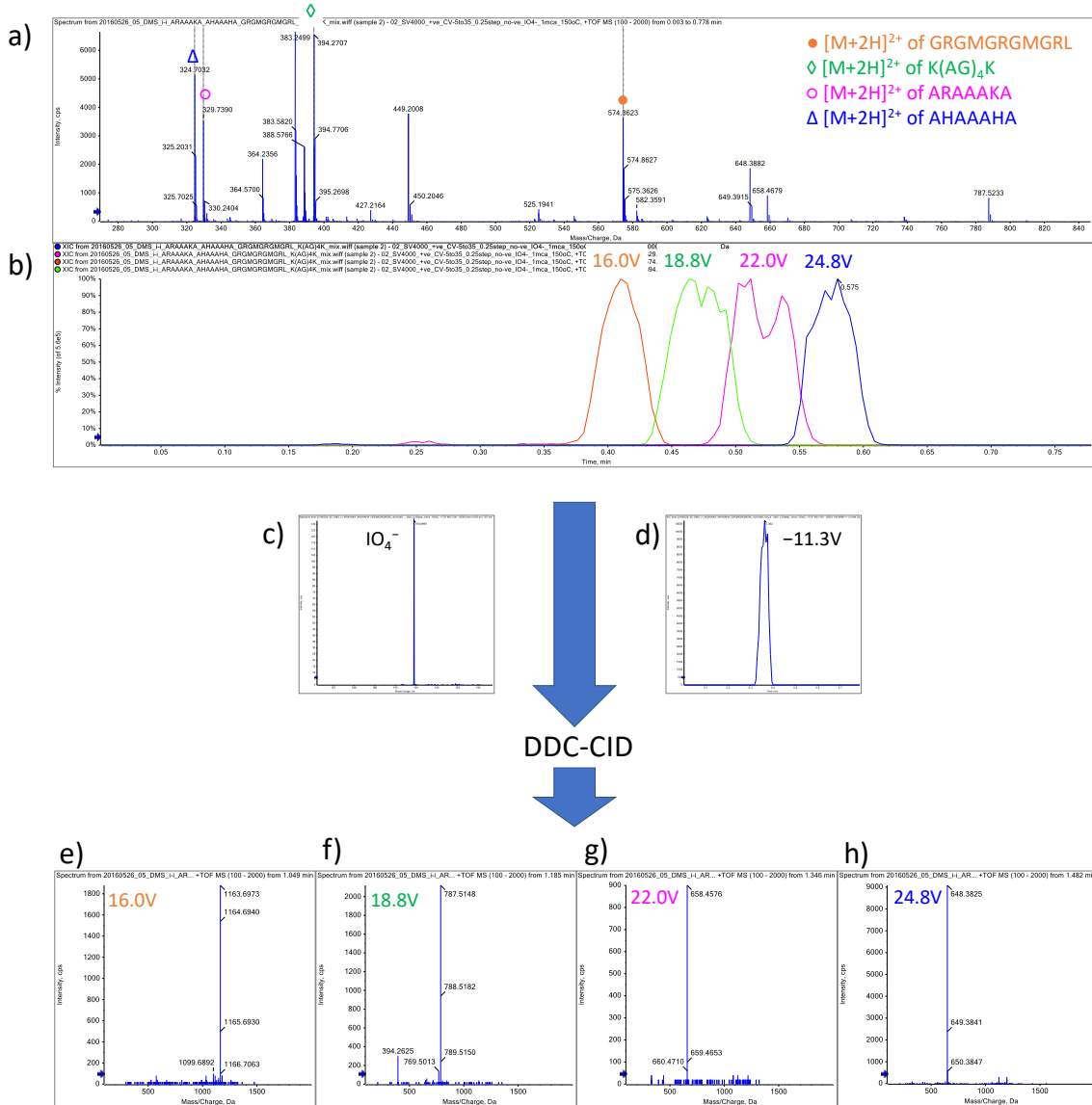


Figure 5.5 The application of 1.5D DSM-Ion/Ion method on the peptide mixture of ARAAKA, AHAAAA, GRGMGRGMGRL, and $K(AG)_4K$. (a) Averaged mass Spectrum of direct spray of the peptide mixture with a DMS CV ramp of $-5V$ to $35V$. (b) Extracted CV ionograms of the doubly protonated peptides, with their corresponding climax CV voltage labeled with the same color coding as the legend in panel (a). (c) Mass spectrum of the periodate ion with a DMS CV ramp of $-25V$ to $5V$. (d) Extracted CV ionogram of the periodate ion. (e)-(h) Post-ion/ion and DDC-CID ($35V$ DDC) mass spectra at the respective climax CV voltage for each analyte peptide ion, with their climax CV voltages labeled using the same color coding as the legend in panel (a). All the DMS experiments are done with an SV setting of $4000V$ and at a DMS temperature of $150^\circ C$. The x-axis of DMS CV ionograms are shown in time (min) due to the software limitation of recording CV voltages in the DMS-Ion/Ion mode, but the CV voltages can be converted from the time using the CV voltage ramp range.

Table 5.1 Fragment ion mass of KAGK(AG)₃ and K(AG)₄K

KAGK(AG) ₃					K(AG) ₄ K				
Seq	#	B	Y	# (+1)	Seq	#	B	Y	# (+1)
K	1	129.1028	787.4427	10	K	1	129.10283	787.44267	10
A	2	200.14	659.3477	9	A	2	200.13995	659.34771	9
G	3	257.1614	588.3106	8	G	3	257.16141	588.31059	8
K	4	385.2564	531.2891	7	A	4	328.19852	531.28913	7
A	5	456.2935	403.1942	6	G	5	385.21999	460.25202	6
G	6	513.315	332.1571	5	A	6	456.2571	403.23055	5
A	7	584.3521	275.1356	4	G	7	513.27856	332.19344	4
G	8	641.3735	204.0985	3	A	8	584.31568	275.17197	3
A	9	712.4106	147.077	2	G	9	641.33714	204.13486	2
G	10	769.4321	76.0399	1	K	10	769.4321	147.1134	1

Note: Red shade means they have the exact mass. Yellow shade means their mass is so close that on the spectrum they may not be distinguishable. Green shade means even though it is not b or y fragment ion for the other peptide, the other peptide could still go through a certain fragmentation pathway and get the same mass fragment.

PUBLICATION

Wang, N.; Pilo, A. L.; Zhao, F.; Bu, J.; McLuckey, S. A. Gas-Phase Rearrangement Reaction of Schiff-Base-Modified Peptide Ions. *Rapid Commun. Mass Spectrom.* 32, 2166-2173 (2018).

Gas-phase rearrangement reaction of Schiff-base-modified peptide ions

Nan Wang | Alice L. Pilo | Feifei Zhao | Jiexun Bu | Scott A. McLuckey 

Department of Chemistry, Purdue University, West Lafayette, IN 47907-2084, USA

Correspondence

S. A. McLuckey, Department of Chemistry, Purdue University, West Lafayette, 560 Oval Drive, IN 47907-2084, USA.
 Email: mcluckey@purdue.edu

Funding information

National Institute of General Medical Sciences, Grant/Award Number: R37-GM045372

Rationale: Schiff base modification of peptides has been shown to facilitate their primary structural characterization via tandem mass spectrometry. However, we have discovered a novel rearrangement reaction via ion trap collisional activation involving the imine of the Schiff base and one of several functional groups, particularly the side chains of the basic residues lysine, arginine, and histidine, in the peptide.

Methods: Gas-phase ion/ion reactions involving an aldehyde-containing reagent were used to generate Schiff-base-modified model peptides in a hybrid triple quadrupole/linear ion trap tandem mass spectrometer. Subsequent ion trap collisional activation was used to study the rearrangement reaction.

Results: Schiff-base-modified peptide ions were found to undergo a rearrangement reaction that was observed to be either a major or minor contributor to the product ion spectrum, depending upon a variety of factors that include, for example, ion polarity, identity of the nucleophile in the peptide (e.g., side chains of lysine, histidine, and arginine), and the position of the nucleophile relative to the imine.

Conclusions: Relatively low-energy rearrangement reactions can occur in Schiff-base-modified peptide ions that involve the imine of the Schiff base and a nucleophile present in the polypeptide. While this rearrangement process does not appear to compromise the structural information that can be generated via collisional activation of Schiff-base-modified peptide ions, it can siphon away signal from the structurally diagnostic processes in some instances.

1 | INTRODUCTION

Tandem mass spectrometry is widely used to probe ion structures by generating informative product ions via fragmentation.¹⁻³ Fragmentation patterns can be highly sensitive to ion type (e.g., protonated molecule versus radical cation) such that complementary information can be obtained by interrogating different analyte ion types.^{4,5} As an approach to the transformation of an analyte from one ion type to another within the mass spectrometer, gas-phase ion/ion reactions have been developed.^{6,7} Small particle transfer ion/ion reactions, e.g., proton and electron transfer reactions, change the analyte charge state, which can open up different fragmentation pathways.^{8,9} Gas-phase covalent modification ion/ion reactions are functional-group-specific reactions that selectively target particular functional groups and thereby alter fragmentation pathways.^{6,7} Moreover,

unique chemistries have been observed via gas-phase ion/ion reactions compared to the solution phase.^{7,10} Examples of gas-phase covalent modification reactions include the reactions between *N*-hydroxysuccinimide (NHS) esters and nucleophiles like primary amines,¹¹ guanidine groups¹² and carboxylates;¹³ gas-phase oxidation of peptides with periodate¹⁴ or persulfate derivatives;¹⁵ carboxylic acid group labelling with carbodiimide reagents;¹⁶ and the Schiff base formation between formyl-benzenesulfonic acids and primary amines.¹⁷

The gas-phase modification of bio-ions via Schiff base formation was first described in 2009.¹⁷ Formation of the Schiff base is achieved by the reaction between a primary amine (i.e., the *N*-terminus or ϵ -amine group of a lysine residue) in a peptide analyte ion and the formyl group in the 4-formyl-1,3-benzenedisulfonic acid (FBDSA) reagent. Gas-phase collisional activation of the Schiff-base-modified

analyte ions has been noted to result in a higher sequence coverage compared to the unmodified peptides in several scenarios.¹⁷⁻²⁰ Cotham et al. took advantage of the benzene chromophore in FBDSA and modified the analyte peptide in solution with this reagent to enhance the ultraviolet photodissociation (UVPD) efficiency.²¹ They also found that the Schiff base modification of phosphopeptides with FBDSA helps retain the phosphate group during the fragmentation process. Fragmentation of the unmodified phosphopeptide often results in loss of the phosphate functionality and thereby precludes identification of the phosphate position. In the case of Schiff-base-modified peptides, on the other hand, the sulfonate group on the reagent disrupts the phosphate neutral loss process and stabilizes the phosphate group when collision-induced dissociation (CID) is applied.²²

Studies of Schiff-base-modified polypeptide ions via tandem mass spectrometry using CID have resulted predominantly in b/y-type fragment ions,¹⁷⁻²² in analogy with unmodified ions.²³ However, in this study, we focus on fragmentation products generated via CID that are unique to the Schiff-base-modified peptide. This work has revealed the existence of a fragmentation pathway that is specific to the Schiff base modification, which should be recognized when using this modification for structural characterization purposes. Possible mechanisms are proposed.

2 | EXPERIMENTAL

2.1 | Materials

HPLC-grade water and methanol were purchased from Fisher Scientific (Waltham, MA, USA). 4-Formyl-1,3-benzenedisulfonic acid (FBDSA) and 2-formylbenzene(mono)sulfonic acid (FBMSA) were purchased from Sigma-Aldrich (St Louis, MO, USA). Model peptides KGAGGKAGGK, RARARAA, AHAAAHA and HAHAAHA were synthesized by NeoBioLab (Cambridge, MA, USA); KAKAKAA was synthesized by Pepnome Ltd (Shenzhen, China). All peptide solutions for electrospray were prepared in 50/50 (v/v) methanol/water (~0.2 mM). The FBDSA and FBMSA reagent solutions for electrospray were prepared in water (~3 mM).

2.2 | Mass spectrometry

All experiments were performed on a QTRAP[®] 4000 hybrid triple quadrupole/linear ion trap mass spectrometer (SCIEX, Concord, ON, Canada) previously modified for ion/ion reactions,²⁴ unless specifically noted. Alternately pulsed nano-electrospray ionization (nESI)²⁵ allowed for sequential injections of reagent and analyte ions, which were sequentially isolated in the Q1 mass filter prior to their injection into the q2 reaction cell. After a defined mutual storage reaction time, the product ions were then transferred to Q3. The ions then underwent further probing via MSⁿ using ion trap collisional activation and mass analysis via mass-selective axial ejection (MSAE).²⁶ The exact mass measurement experiments were performed on a TripleTOF[®] 5600 mass spectrometer (SCIEX, Concord, ON, Canada) previously modified for ion/ion reactions.²⁴

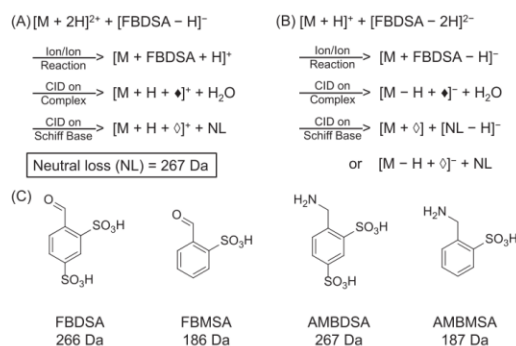
3 | RESULTS AND DISCUSSION

3.1 | Novel fragmentation pathway from Schiff-base-modified lysine-containing peptides

Gas-phase Schiff base formation has been demonstrated as an approach to provide structural information complementary to that derived from unmodified species in the tandem mass spectrometry of polypeptide ions.¹⁷⁻²² It involves the reactivity between a peptide primary amine group, either on the N-terminus or the lysine side chain, and the formyl group on the reagent ion. The reagents used in this study are 4-formyl-1,3-benzenedisulfonic acid (FBDSA) and 2-formylbenzene(mono)sulfonic acid (FBMSA) (structures shown in Scheme 1C). Each reagent contains a benzaldehyde reactive group and one or two sulfonate group(s).

The Schiff base modification and ion trap CID of the Schiff-base-modified peptide ions are illustrated by the spectra provided in Figure 1. Using a model peptide of sequence KAKAKAA, the doubly protonated peptide, $[M + 2H]^{2+}$, was formed via positive nESI and reacted with singly deprotonated FBDSA, $[FBDSA - H]^-$, resulting in an electrostatically bound complex, $[M + FBDSA + H]^+$, and a proton transfer product, $[M + H]^+$, as seen in Figure 1A. Upon CID of the complex (see Figure 1B), a signature water loss from the

SCHEME 1 Reactions for Schiff base modification and fragmentation in (A) positive mode and (B) negative mode with FBDSA as an example. (C) Structures of Schiff base modification reagents (FBDSA, FBMSA) and proposed neutral loss structures (AMBDSA and AMBMSA). Solid diamonds (◆) denote ion mass shift with Schiff base modification (+248 Da for FBDSA). Hollow diamonds (◇) denote the mass shift of the special fragmentation products (-19 Da)



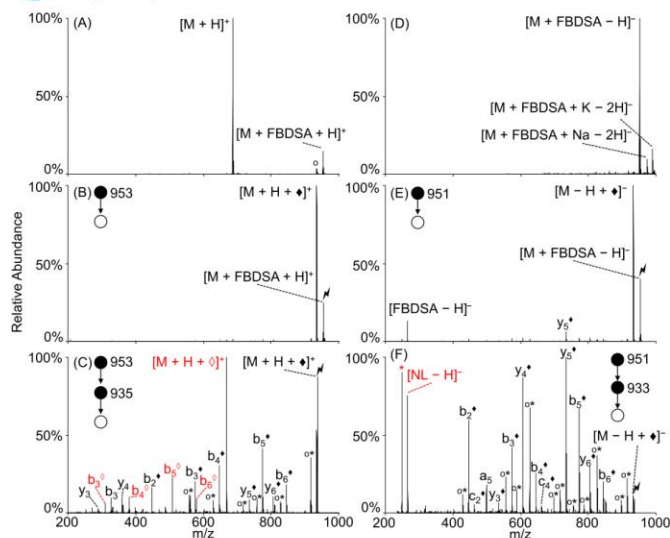


FIGURE 1 Spectra illustrating the gas-phase Schiff base modification of KAKAKAA with FBDSA and its special fragmentation pathway. Positive mode (A) ion/ion reaction between doubly protonated peptide cation $[M + 2H]^{2+}$ and singly deprotonated FBDSA $[FBDSA - H]^-$, (B) CID of the ion/ion complex $[M + FBDSA + H]^+$ forming a Schiff-base-modified peptide $[M + H + \bullet]^+$, (C) ion-trap CID of $[M + H + \bullet]^+$. Negative mode (D) ion/ion reaction between singly protonated peptide cation $[M + H]^+$ and doubly deprotonated FBDSA $[FBDSA - 2H]^{2-}$, (E) CID of the ion/ion complex $[M + FBDSA - H]^-$ forming a Schiff-base-modified peptide $[M - H + \bullet]^-$, (F) ion-trap CID of $[M - H + \bullet]^-$. Degree symbols ($^\circ$) denote water losses (-18 Da). Asterisks ($*$) denote ammonia losses (-17 Da). Solid diamonds (\bullet) denote ion mass shift with Schiff base modification ($+248$ Da). Hollow diamonds (\diamond) denote the special fragmentation products (-19 Da) and all products in the special fragmentation pathway are labeled in red [Color figure can be viewed at wileyonlinelibrary.com]

complex reflects the formation of a Schiff-base-modified peptide cation, $[M + H + \bullet]^+$, where the black diamond (\bullet) depicts the mass shift caused by the modification ($+248$ Da). Further CID of the Schiff-base-modified species (see Figure 1C) gives rise to b/y fragment ions, both modified (e.g., b_6^* and y_6^*) and unmodified (e.g., b_3 and y_4), which implies different Schiff base modification sites, either the N-terminus or any one of the lysine side chains. Besides the b/y fragment ions, a highly abundant peak, labelled as $[M + H + \diamond]^+$, was observed 267 Da lower in mass than the peak of the Schiff-base-modified peptide $[M + H + \bullet]^+$, which is inconsistent with commonly observed neutral losses from peptide ions. The hollow diamond (\diamond) in Figure 1C refers to the mass shift of the novel product, -267 Da from the precursor $[M + H + \bullet]^+$, or an apparent -19 Da from the mass of the protonated peptide, $[M + H]^+$. Similarly, there are peaks that are observed -267 Da lower in mass than the modified b ions (b_6^* , b_5^* , b_4^* , and b_3^*), which are also labeled with the hollow diamond (as in b_6^\diamond , b_5^\diamond , b_4^\diamond , and b_3^\diamond).

Evidence for an analogous reaction is noted in the negative mode (Figures 1D–1F). The singly protonated peptide was charge inverted by the doubly deprotonated FBDSA to form a negatively charged complex, $[M + FBDSA - H]^-$ (Figure 1D). CID of the electrostatically bound complex generates a Schiff-base-modified peptide anion $[M - H + \bullet]^-$ (Figure 1E). As above, the solid diamond (\bullet) indicates the mass shift of the Schiff base modification ($+248$ Da). CID of the Schiff-base-modified peptide anion $[M - H + \bullet]^-$ mainly leads to

backbone fragment ions, including modified b/y and c fragment ions (e.g., b_5^* , y_5^* and c_2^*) and unmodified backbone fragment ions (e.g., a_5) (Figure 1F). In previous negative mode Schiff base modification studies,^{18–20} another common CID fragmentation product from $[M - H + \bullet]^-$ is deprotonated FBDSA $[FBDSA - H]^-$ (m/z 265 Da). The precursor $[M - H + \bullet]^-$ population can consist of both Schiff-base-modified peptides and the unreacted electrostatic complex of FBDSA and peptide with one water loss from somewhere else in the peptide. The latter type of $[M - H + \bullet]^-$ ion can give rise to the $[FBDSA - H]^-$ CID product. In Figure 1F, however, no $[FBDSA - H]^-$ peak (m/z 265) was observed. Rather, there are two dominant singly negatively charged peaks of m/z 266 (i.e., the peak labeled with $[NL - H]^-$ in red) and m/z 249 (the peak labeled with $*$ in red) in the lower mass region. These two fragments are inconsistent with any common peptide fragment pathways. Considering that the neutral loss (NL), i.e., the mass difference between the unidentified peak and the Schiff-base-modified peptide, is 267 Da, the m/z 266 product ion was assigned as $[NL - H]^-$, and the m/z 249 product was assigned as $[NL - H - NH_3]^-$ due to the 17 Da difference. Activation of the m/z 266 Da ion ($[NL - H]^-$) formed in the CID spectrum of the Schiff-base-modified KAKAKAA anion with FBDSA leads exclusively to ammonia loss, as shown in Figure S2C (supporting information), which implies that the neutral loss structure contains an amine group.

Analogous results were obtained using singly deprotonated FBMSA in reaction with doubly protonated KAKAKAA. The Schiff-

base-modified peptide product, $[M+H+\diamond]^+$ ($\diamond=+168$ Da), was directly formed upon ion/ion reaction along with the proton transfer product, $[M+H]^+$ (Figure S1A, supporting information). Upon activation of the $[M+H+\diamond]^+$ product, the resulting product ion spectrum (Figure S1B) contained a dominant $[M+H+\diamond]^+$ product that is -187 Da from the $[M+H+\diamond]^+$ ion, and b/y ions with the same mass shift (b_3^\diamond , b_4^\diamond , b_5^\diamond , and b_6^\diamond), all of which are labeled with the hollow diamond ($\diamond=-19$ Da). Other backbone fragmentation products were observed in the spectrum in relatively low abundances. The 187 Da mass loss in the case of the FBMSA reagent is 80 Da less than that observed from the reactions with the FBDSA reagent, which is consistent with the difference in mass between FBMSA and FBDSA.

The $[M+H+\diamond]^+$ ions generated from Schiff-base-modified KAKA KAA cations with FBDSA and FBMSA were subjected to CID (Figures S2A and S2B, supporting information). The essentially identical dissociation patterns for the two spectra indicate that the $[M+H+\diamond]^+$ ions generated from modified peptides with different reagents are of the same structure or mixture of structures. The fragment peaks with the same mass shift ($\diamond=-19$ Da) are mostly b ions (b_2^\diamond , b_3^\diamond , b_4^\diamond , b_5^\diamond , b_6^\diamond) and some y ions (y_5^\diamond , y_6^\diamond). Their fragmentation sites and abundance ratios are similar to the modified b/y fragment ions (b_2^* , b_3^* , b_4^* , b_5^* , b_6^* , y_5^* , y_6^*) in Figure 1C, which indicates that the mass shift is related to the Schiff base modification. Unmodified b/y fragment ions were also observed.

Experiments analogous to those performed for the KAKAKAA peptide were also performed with the peptide KGAGGKAGGK and reagent FBDSA (see Figures S1C, S1D, S2D, and S2E, supporting information) leading to similar results. For example, the same loss of 267 Da from activation of Schiff-base-modified peptide cation, $[M+H+\diamond]^+$ ($\diamond=+248$ Da), leading to a dominant $[M+H+\diamond]^+$ product ($\diamond=-19$) was noted (Figure S1C, supporting information). Activation of the Schiff-base-modified peptide anion, $[M-H+\diamond]^-$ ($\diamond=+248$ Da), gave rise primarily to modified backbone fragment ions (e.g., b_{11}^* , y_{11}^*), as shown in Figure S1D (supporting information). However, the m/z 266 ion (labeled as $[NL-H]^-$ in red) was also observed, but in much lower relative abundance compared with those in the CID spectrum of the Schiff-base-modified KAKAKAA anion (Figure 1F). The results for the KGAGGKAGGK peptide ions indicate that the unusual products noted here arise from a process with at least some generality.

3.2 | Proposed reaction and mechanism

The general experimental steps and observations in positive mode and negative mode with FBDSA as the reagent are summarized in Schemes 1A and 1B, respectively. The formation of the unusual product ions and the neutral losses imply a previously unidentified reaction and fragmentation pathway when at least some Schiff-base-modified peptides are subjected to ion trap collisional activation. Considering that the neutral losses for Schiff-base-modified KAKA KAA with FBDSA and FBMSA are 267 Da and 187 Da, respectively, which has the same 80 Da mass difference as the two reagents, it is clear that the neutral loss has the partial structure of the reagents. As mentioned above, the existence of singly negatively charged ions

at m/z 266 ($[NL-H]^-$) and m/z 249 ($[NL-H-NH_3]^-$) in the product ion spectra of the modified KAKAKAA and KGAGGKAGGK anions generated with FBDSA (Figure 1F and Figure S1D, supporting information) indicates the presence of a relatively acidic site on the 267 Da species. The loss of 17 Da in the CID of $[NL-H]^-$ (Figure S2C, supporting information) suggests the presence of an amino group. Considering these observations collectively, the neutral loss is proposed to be 4-(aminomethyl)benzene-1,3-disulfonic acid (AMBDSA, 267 Da) for FBDSA or 2-(aminomethyl)benzene(mono)sulfonic acid (AMBMSA, 187 Da) for FBMSA (for structures, see Scheme 1C). An exact mass measurement of the m/z 266 ($[NL-H]^-$) and m/z 249 ($[NL-H-NH_3]^-$) ions using a quadrupole/time-of-flight (QTOF) instrument verified the elemental composition of the proposed product. We note that while the m/z 249 ion can be generated from ammonia loss from deprotonated AMBDSA, a mechanism for the direct formation of the product at m/z 249 (Scheme S1, supporting information) might also contribute to at least some of the m/z 249 signal.

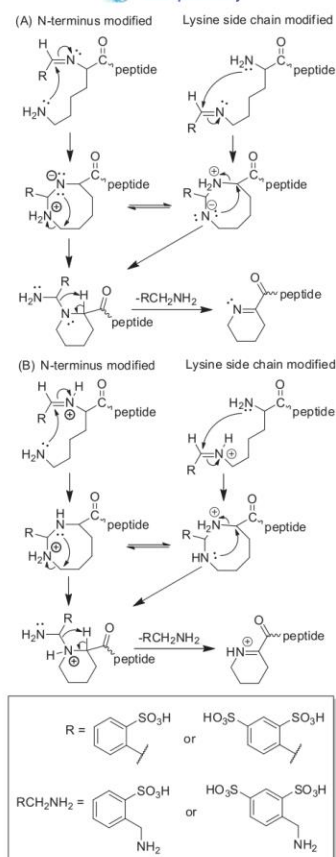
Based on the structures of the neutral loss species, proposed mechanisms for the rearrangement of lysine-containing Schiff-base-modified peptides are shown in Scheme 2. The amino groups on the N-terminus and on the ϵ -amino group of the lysine side chain are used here as an example. Either amino group could be modified with the imine bond. The lone electron pair on the nitrogen of the amine attacks the electrophilic carbon of the imine to form an eight-membered ring. Further proton transfer and ring rearrangements generate a more stable six-membered ring. Finally, the leaving group is eliminated with a proton to form the neutral loss amine and thus the rearranged peptide product with a ring imine.

Based on the proposed mechanism for the rearrangement reaction, the imine (on the N-terminus or the lysine side chains) could react with amino groups (unmodified N-terminus or lysine side chain amino groups), which is consistent with the CID spectra of $[M+H+\diamond]^+$ and $[M-H+\diamond]^-$ ions derived from the peptides KAKAKAA and KGAGGKAGGK (Figure S2, supporting information). Note that analogous experiments with the model peptide AKAAAKA (Figure S3, supporting information) showed the rearrangement reaction taking place at significantly lower levels than with the N-terminal lysine-containing model peptides, which suggests that a lysine at the N-terminal position is particularly reactive.

3.3 | Reactivity of histidine- or arginine-containing Schiff-base-modified peptides

Previous studies have indicated that initial Schiff base formation takes place primarily at neutral primary amines to generate the imine. However, the other common basic residues (i.e., nucleophiles), histidine and arginine, might also be able to engage in a rearrangement process involving the imine via mechanisms analogous to those provided in Scheme 2. To compare with KAKAKAA results, model peptides RARARAA and HAHAAHA were chosen to study the effect of amino acid residue type. The experimental data are summarized in Figure 2.

For positive mode Schiff base modification of RARARAA, doubly protonated RARARAA was subjected to an ion/ion reaction with deprotonated FBDSA anions to generate an ion/ion complex of the



SCHEME 2 Proposed mechanism for the rearrangement of the lysine-containing Schiff-base-modified peptides between an amino group and (A) a neutral imine group or (B) a protonated imine group. N-terminal lysine residue is used here as an example

form $[M+H+FBDSA]^+$. Activation of this complex resulted in the signature water loss to generate the covalently modified product $[M+H+\bullet]^+$. Further activation of this product yielded dominant formation of the rearrangement product, viz., $[M+H+\circ]^+$, indicated in red in Figure 2A, which is similar to the results from Schiff-base-modified peptide KAKAKAA (Figure 1C). Since methanediimine loss from the arginine side chain (labeled with solid square) generates an ornithine residue,²⁷ which contains an amino group, the rearrangement products with ornithine-containing fragments could also arise from reactions with the ornithine side chain. Other fragments derived from neutral losses (e.g., ammonia and water) as well as backbone cleavages (e.g., γ_3 , γ_4 , γ_5 , γ_6 , and b_6^*) were observed at lesser abundances. Furthermore, the presence of the modified b_6^* ion and lack of any modified γ ions indicate that the FBDSA is covalently attached to the N-terminal region of the peptide, which is consistent with Schiff base reactivity at a primary amine. The neutral arginine side chain

could react with the imine bond through a similar mechanism, as shown in Scheme 3A. In the example of arginine in the N-terminus position, the lone pair on the nitrogen of the guanidine group attacks the imine carbon and forms a nine-membered ring. Rearrangement of the ring and further proton transfer lead to the formation of the imine ring structure along with the loss of neutral AMBDSA or AMBMSA. When the arginine side chain is protonated, a similar process could occur, as shown in Scheme 3B.

As for negative mode Schiff base modification, singly protonated RARARAA reacted with doubly deprotonated FBDSA anions to form an electrostatic complex $[M-H+FBDSA]^-$, which upon activation generated the signature water loss peak $[M-H+\bullet]^-$. Activation of $[M-H+\bullet]^-$ species formed mainly neutral loss fragments (e.g., ammonia and methanediimine losses) and deprotonated FBDSA $[FBDSA-H]^-$ (Figure 2B), which indicates that the water loss from the electrostatic complex is partly due to water loss from the peptide itself and not coming from the formation of the imine bond.¹⁸⁻²⁰ The m/z 249 Da peak was also seen (labeled with 249 in red). No abundant peptide rearrangement product ions were seen, which is consistent with the low signal for the m/z 249 ion. The attack from the imine to the guanidinium group in the positive mode may be more facile than that from the neutral guanidine group to the neutral imine group in the negative mode (Scheme 3) but further studies would be required to make such a generalization. We note, however, for the limited set of peptide ions examined in this work, peptide anions generally showed notably less contribution from ions generated by the rearrangement reactions described here than the corresponding positive ions.

The Schiff-base-modified histidine-containing peptides generated by reaction with FBDSA ions showed a different neutral loss associated with a rearrangement (330 Da) than the lysine- and arginine-containing peptides (267 Da) upon activation (Figures 2C and 2D). The doubly protonated peptide HAHAAHA reacted with singly deprotonated FBDSA in the positive mode to form an ion/ion complex $[M+H+FBDSA]^+$, which upon CID gave the signature water loss indicating formation of Schiff base modification product $[M+H+\bullet]^+$. Further activation of the Schiff-base-modified peptide generated backbone cleavages (e.g., b_6^* and γ_5) as well as a peak labeled as $[M+H+\bullet]^+$ ($\bullet = -82$ Da) that is 330 Da lower in mass than the precursor ion $[M+H+\bullet]^+$ (Figure 2C). In the negative mode, mutual storage of the singly protonated peptide HAHAAHA and the doubly deprotonated FBDSA led to the formation of a complex $[M-H+FBDSA]^-$ and upon CID of the complex the signature water loss peak $[M-H+\bullet]^-$ was generated. Activation of the ion generated by water loss (Figure 2D) gave rise predominantly to modified backbone fragment ions (e.g., b_6^*) and neutral losses (e.g., CO_2 losses). $[FBDSA-H]^-$ ions were also observed, along with the m/z 249 Da ion (labeled as 249 in red) and an m/z 329 ion (labeled as $[NL(\bullet)-H]^-$), which presumably is the deprotonated species derived from the 330 Da molecule that was observed to be lost in the positive mode experiment described above. The m/z 249 ion can also be generated from the m/z 329 ion through the mechanism shown in Scheme S1 (supporting information).

The rearrangement reaction between the histidine side chain and the imine bond differs from those of the primary amine and guanidine

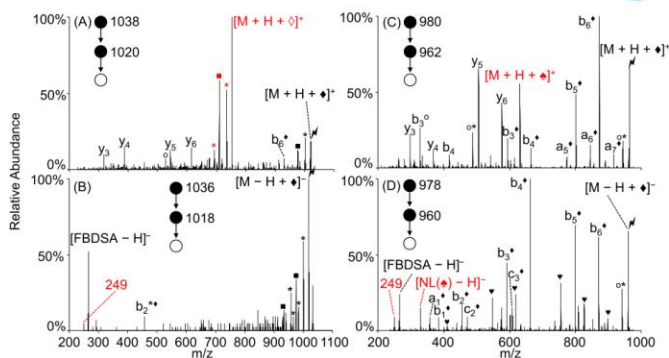
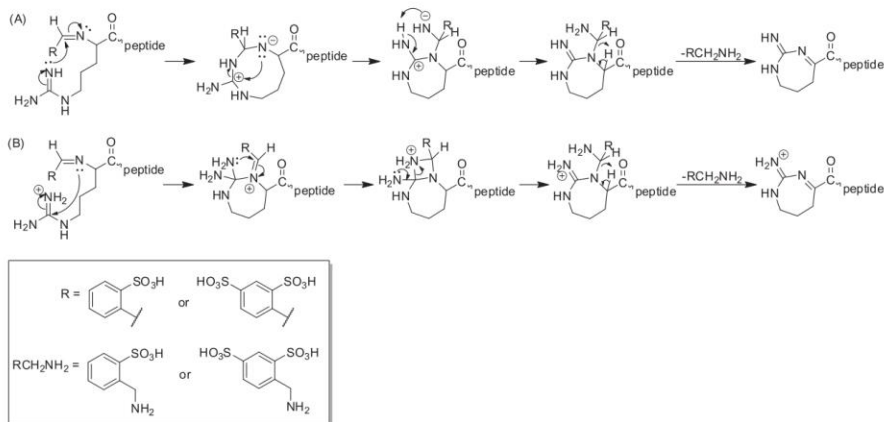


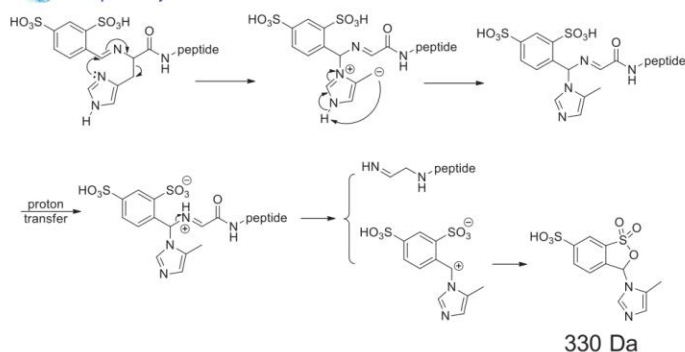
FIGURE 2 Ion trap CID of the gas-phase Schiff-base-modified peptides formed using (A) singly deprotonated FBDSA and doubly protonated RARARAA, (B) doubly deprotonated FBDSA and singly protonated RARARAA, (C) singly deprotonated FBDSA and doubly protonated HAHAAHA, and (D) doubly deprotonated FBDSA and singly protonated HAHAAHA. Degree symbols (°) denote water losses (-18 Da). Asterisks (*) denote ammonia losses (-17 Da). Black solid diamonds (◆) denote ions with Schiff base modification ($+248$ Da). Solid squares (■) denote the arginine side chain methanediimine ($\text{H}_2\text{N}=\text{C}=\text{NH}_2$) losses to form ornithine (-42 Da). Solid hearts (♥) denote carbon dioxide losses (-44 Da). Hollow diamonds (◇) denote peptide rearrangement products (-19 Da) with the formation of the AMBDSA neutral loss. Solid spades (♠) denote histidine-specific rearrangement products (-82 Da) with the formation of the 330 Da neutral loss. All rearrangement related products are labeled in red [Color figure can be viewed at wileyonlinelibrary.com]



SCHEME 3 Proposed mechanism for rearrangement reaction of arginine-containing Schiff-base-modified peptides between an imine group and (A) a neutral guanidine group or (B) a protonated guanidinium group. N-terminal arginine residue is used here as an example

groups because of the ring structure of the imidazole group. The AMBDSA neutral loss observed with lysine and arginine could not form through a similar process for histidine. Instead, the 330 Da neutral loss could be explained by the reaction between the imine bond and the histidine side chain, as shown in Scheme 4. With the rearrangement, the histidine side-chain moiety transfers to the original imine carbon, and the imine bond shifts to the other carbon connected to the imine nitrogen. Further activation of the rearranged structure could lead to the 330 Da neutral loss. This mechanism is especially favored if the histidine residue is located on the N-terminus of the

peptide, since that location enables the rearrangement to occur with a six-membered ring transition state structure. When histidine is not present at the N-terminus, the mechanism just mentioned is apparently not particularly competitive, as indicated by the analogous experiment performed with doubly protonated AHAAAHA. Activation of the Schiff-base-modified peptide AHAAAHA in the positive mode (Figure S4, supporting information) yielded abundant backbone cleavages (e.g., b_6^* and y_4) but no discernable 330 Da neutral loss, in contrast with the modified HAHAAHA ion (Figure 2C). Interestingly, the AMBDSA neutral loss rearrangement product can be seen in low



SCHEME 4 Proposed mechanism for rearrangement reaction of histidine-containing Schiff-base-modified peptides between an imine group and a neutral imidazole group. N-terminal histidine residue is used here as an example

abundance in the spectrum shown in Figure S4 (supporting information), which could implicate the rearrangement reaction involving the imine and amide nitrogen (Scheme S2, supporting information), albeit with lower probability due to the lesser nucleophilicity of an amide nitrogen relative to a primary amine.

4 | CONCLUSIONS

Rearrangement of gas-phase Schiff-base-modified peptides has been observed and characterized using tandem mass spectrometry. Evidence for the reaction is provided by the appearance of a product ion that is nominally 19 Da lower in mass than that of the protonated or deprotonated peptide upon collisional activation of the Schiff-base-modified peptide. Sequence ions with the same -19 Da mass difference may also be observed at relatively low abundance. Upon casual inspection, these products could be mistaken as arising from a water loss but the mass is off by 1 Da. The results are consistent with a nucleophilic attack on the imine site generated via Schiff base formation. The side chains of lysine, arginine, and histidine all show evidence for participation in the rearrangement reaction. Based on the experimental results, Schiff-base-modified peptides of positive polarity more readily undergo the rearrangement reaction compared to the corresponding negatively charged ions. Plausible mechanisms were proposed for the rearrangement reactions between the imine bond and the amine, guanidine and histidine side-chain groups. The possible contribution from this rearrangement reaction, at least under ion trap collisional activation conditions, should be taken into account in any work flow involving the Schiff base modification of polypeptide ions.

ACKNOWLEDGEMENT

The authors acknowledge support for this work by the National Institute of General Medical Sciences under grant R37-GM045372.

ORCID

Scott A. McLuckey <http://orcid.org/0000-0002-1648-5570>

REFERENCES

- McLafferty FW. Tandem mass spectrometry. *Science*. 1981;214(4518):280-287. <https://doi.org/10.1126/science.7280693>
- Santos LS, Pavam CH, Almeida WP, Coelho F, Eberlin MN. Probing the mechanism of the Baylis-Hillman reaction by electrospray ionization mass and tandem mass spectrometry. *Angew Chem Int Ed*. 2004;43(33):4330-4333. <https://doi.org/10.1002/anie.200460059>
- Aebersold R, Mann M. Mass-spectrometric exploration of proteome structure and function. *Nature*. 2016;537(7620):347-355. <https://doi.org/10.1038/nature19949>
- Reid GE, Roberts KD, Simpson RJ, O'Hair RA. Selective identification and quantitative analysis of methionine containing peptides by charge derivatization and tandem mass spectrometry. *J Am Soc Mass Spectrom*. 2005;16(7):1131-1150. <https://doi.org/10.1016/j.jasms.2005.03.015>
- Kinter M, Sherman NE. *Protein Sequencing and Identification Using Tandem Mass Spectrometry*. New York, NY: John Wiley & Sons; 2005.
- McLuckey SA, Mentinova M. Ion/neutral, ion/electron, ion/photon, and ion/ion interactions in tandem mass spectrometry: Do we need them all? Are they enough? *J Am Soc Mass Spectrom*. 2011;22(1):3-12. <https://doi.org/10.1007/s13361-010-0004-9>
- Prentice BM, McLuckey SA. Gas-phase ion/ion reactions of peptides and proteins: Acid/base, redox, and covalent chemistries. *Chem Commun*. 2013;49(10):947-965. <https://doi.org/10.1039/c2cc36577d>
- Stephenson JL Jr, McLuckey SA. Ion/ion proton transfer reactions for protein mixture analysis. *Anal Chem*. 1996;68(22):4026-4032. <https://doi.org/10.1021/ac9605657>
- Syka JE, Coon JJ, Schroeder MJ, Shabanowitz J, Hunt DF. Peptide and protein sequence analysis by electron transfer dissociation mass spectrometry. *Proc Natl Acad Sci U S A*. 2004;101(26):9528-9533. <https://doi.org/10.1073/pnas.0402700101>
- Pilo AL, McLuckey SA. Selective gas-phase ion/ion reactions: Enabling disulfide mapping via oxidation and cleavage of disulfide bonds in intermolecularly-linked polypeptide ions. *Anal Chem*. 2016;88(18):8972-8979. <https://doi.org/10.1021/acs.analchem.6b01043>
- Mentinova M, McLuckey SA. Covalent modification of gaseous peptide ions with N-hydroxysuccinimide ester reagent ions. *J Am Chem Soc*. 2010;132(51):18248-18257. <https://doi.org/10.1021/ja107286p>
- McGee WM, Mentinova M, McLuckey SA. Gas-phase conjugation to arginine residues in polypeptide ions via N-hydroxysuccinimide ester-based reagent ions. *J Am Chem Soc*. 2012;134(28):11412-11414. <https://doi.org/10.1021/ja304778j>
- Peng Z, McGee WM, Bu J, Barefoot NZ, McLuckey SA. Gas phase reactivity of carboxylates with N-hydroxysuccinimide esters. *J Am*

- Soc. Mass Spectrom. 2015;26(1):174-180. <https://doi.org/10.1007/s13361-014-1002-0>
14. Pilo AL, Bu J, McLuckey SA. Gas-phase oxidation of neutral basic residues in polypeptide cations by periodate. *J Am Soc Mass Spectrom.* 2016;27(12):1979-1988. <https://doi.org/10.1007/s13361-016-1491-0>
 15. Pilo AL, Bu J, McLuckey SA. Transformation of $[M+2H]^{2+}$ peptide cations to $[M-H]^+$, $[M+H+O]^+$, and M^{*+} cations via ion/ion reactions: Reagent anions derived from persulfate. *J Am Soc Mass Spectrom.* 2015;26(7):1103-1114. <https://doi.org/10.1007/s13361-015-1125-y>
 16. Prentice BM, Gilbert JD, Stutzman JR, Forrest WP, McLuckey SA. Gas-phase reactivity of carboxylic acid functional groups with carbodiimides. *J Am Soc Mass Spectrom.* 2013;24(1):30-37. <https://doi.org/10.1007/s13361-012-0506-8>
 17. Han H, McLuckey SA. Selective covalent bond formation in polypeptide ions via gas-phase ion/ion reaction chemistry. *J Am Chem Soc.* 2009;131(36):12884-12885. <https://doi.org/10.1021/ja904812d>
 18. Hassell KM, Stutzman JR, McLuckey SA. Gas-phase bioconjugation of peptides via ion/ion charge inversion: Schiff base formation on the conversion of cations to anions. *Anal Chem.* 2010;82(5):1594-1597. <https://doi.org/10.1021/ac902732v>
 19. Stutzman JR, Luongo CA, McLuckey SA. Covalent and non-covalent binding in the ion/ion charge inversion of peptide cations with benzene-disulfonic acid anions. *J Mass Spectrom.* 2012;47(6):669-675. <https://doi.org/10.1002/jms.2968>
 20. Stutzman JR, Hassell KM, McLuckey SA. Dissociation behavior of tryptic and intramolecular disulfide-linked peptide ions modified in the gas phase via ion/ion reactions. *Int J Mass Spectrom.* 2012;312:195-200. <https://doi.org/10.1016/j.ijms.2011.07.002>
 21. Cotham VC, Shaw JB, Brodbelt JS. High-throughput bioconjugation for enhanced 193 nm photodissociation via droplet phase initiated ion/ion chemistry using a front-end dual spray reactor. *Anal Chem.* 2015;87(18):9396-9402. <https://doi.org/10.1021/acs.analchem.5b02242>
 22. Cotham VC, McGee WM, Brodbelt JS. Modulation of phosphopeptide fragmentation via dual spray ion/ion reactions using a sulfonate-incorporating reagent. *Anal Chem.* 2016;88(16):8158-8165. <https://doi.org/10.1021/acs.analchem.6b01901>
 23. Brodbelt JS. Ion activation methods for peptides and proteins. *Anal Chem.* 2016;88(1):30-51. <https://doi.org/10.1021/acs.analchem.5b04563>
 24. Xia Y, Wu J, McLuckey SA, Londry FA, Hager JW. Mutual storage mode ion/ion reactions in a hybrid linear ion trap. *J Am Soc Mass Spectrom.* 2005;16(1):71-81. <https://doi.org/10.1016/j.jasms.2004.09.017>
 25. Liang X, Xia Y, McLuckey SA. Alternately pulsed nanoelectrospray ionization/atmospheric pressure chemical ionization for ion/ion reactions in an electrodynamic ion trap. *Anal Chem.* 2006;78(9):3208-3212. <https://doi.org/10.1021/ac052288m>
 26. Londry FA, Hager JW. Mass selective axial ion ejection from a linear quadrupole ion trap. *J Am Soc Mass Spectrom.* 2003;14(10):1130-1147. [https://doi.org/10.1016/S1044-0305\(03\)00446-X](https://doi.org/10.1016/S1044-0305(03)00446-X)
 27. McGee WM, McLuckey SA. Gas phase dissociation behavior of acyl-arginine peptides. *Int J Mass Spectrom.* 2013;354-355:181-187. <https://doi.org/10.1016/j.ijms.2013.05.022>

SUPPORTING INFORMATION

Additional supporting information may be found online in the Supporting Information section at the end of the article.

How to cite this article: Wang N, Pilo AL, Zhao F, Bu J, McLuckey SA. Gas-phase rearrangement reaction of Schiff-base-modified peptide ions. *Rapid Commun Mass Spectrom.* 2018;32:2166-2173. <https://doi.org/10.1002/rcm.8298>